



MATEMATICKO-FYZIKÁLNÍ FAKULTA Univerzita Karlova

DIPLOMOVÁ PRÁCE

Jan Střeleček

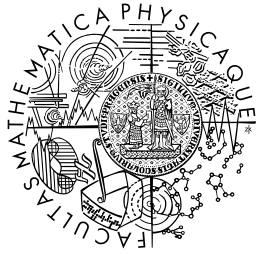
Geometrický přístup k externě vedeným kvantovým systémům

Vedoucí diplomové práce: prof. RNDr. Pavel Cejnar, Dr., DSc.

Studijní program: Fyzika

Studijní obor: Teoretická fyzika

Praha 2022



**FACULTY
OF MATHEMATICS
AND PHYSICS**
Charles University

MASTER THESIS

Jan Střeleček

**Geometric approach to externally
driven quantum systems**

Supervisor of the master thesis: prof. RNDr. Pavel Cejnar, Dr., DSc.

Study programme: Physics

Study branch: Theoretical physics

Prague 2022

I declare that I carried out this master thesis independently, and only with the cited sources, literature and other professional sources. It has not been used to obtain another or the same degree.

I understand that my work relates to the rights and obligations under the Act No. 121/2000 Sb., the Copyright Act, as amended, in particular the fact that the Charles University has the right to conclude a license agreement on the use of this work as a school work pursuant to Section 60 subsection 1 of the Copyright Act.

In date
Author's signature

Huge thanks go to my supervisor prof. Pavel Cejnar, who was willing to discuss the results and theory anytime my mind needed some guidance. It is also worth mentioning here the long consultation I had with my friends, concerning quantum mechanics or differential geometry. I hereby thank Michal Grňo, Jakub Novotný and Martin Zika for allowing me to sort my thoughts in this way.

Title: Geometric approach to externally driven quantum systems

Author: Jan Střeleček

Institute: Institute of Particle & Nuclear Physics

Supervisor: prof. RNDr. Pavel Cejnar, Dr., DSc.

Abstract: The theory of quantum driving is presented and reformulated using the language of differential geometry. The general fidelity driving in a two level Hamiltonian system is then analyzed with special importance of the fidelity time dependence. For the Lipkin-Meshkov-Glick model the geometrical structure of its energy state manifolds is calculated, with aim to analyze adiabatic and close adiabatic drivings.

Keywords: adiabaticity driving fidelity Lipkin-Meshkov-Glick quench

Contents

Some notes to the notation	3
Introduction	5
1 Mathematical introduction	7
1.1 Essentials	7
1.2 Fiber bundle	9
1.3 Riemannian geometry	10
1.4 Geometry in 2 dimensions	11
2 Introduction to quantum geometry	13
2.1 Space of all states	13
2.2 Rays and bare states	14
2.3 Sectioning the space	15
2.4 Transporting states on state manifolds	16
2.5 Fidelity	19
2.6 Metric and geometric tensor	20
3 Quantum state driving	24
3.1 Counter-diabatic driving	25
3.1.1 Classical gauge potential	26
3.1.2 Quantum gauge potential	27
3.2 Driving on the ground state manifold	28
3.2.1 Minimizing the distance on state manifolds	28
3.2.2 Minimizing the energy variance	29
3.2.3 Transport using quenches	30
3.3 Adiabatic perturbation theory	31
4 Two level system	33
4.1 Hamiltonian	33
4.2 Harmonic oscillator correspondence	34
4.3 Energy variance for two level system	34
4.4 Geodesic driving	35
4.4.1 Derivation of the fidelity	36
4.4.2 Analysis of the infidelity formula	37
4.4.3 Energy variance	39
4.5 Linear driving	41
4.5.1 Dependence on time	42
4.5.2 Final fidelity	43
4.5.3 Summary of linear driving	48
4.5.4 Energy variance	49
5 Lipkin-Meshkov-Glick model	50
5.1 Geometry for fixed dimension	50
5.1.1 3-dimensional Hamiltonian	51
5.1.2 5-dimensional Hamiltonian	57

5.1.3	Infinite dimension limit	60
5.2	General spectrum behavior	61
Conclusion		67
Bibliography		68
List of Figures		70
A Geometrization of quantum mechanics		73
A.1	From the projective Hilbert space to state manifolds	73
A.2	Restriction to eigenstate manifolds	74
B Eigenvalues for Lipkin-Meshkov Glick model		76
C Attachments		78
C.1	Computing the metric tensor	78
C.2	Computing the Geodesics	78
C.3	Computing the driving fidelity	78

Some notes to the notation

Symbol	Meaning	Characterizing formula
\mathcal{A}_μ	Calibrational (gauge) potential	$\mathcal{A}_\mu := i\hbar\partial_\mu$
A_μ	Berry connection	$A_\mu := \langle o \mathcal{A}_\mu o \rangle$
\mathcal{C}^k	k -times continuously differentiable function	
\mathbb{C}	complex numbers	
γ_s	geometrical phase induced by s^{th} energy level	
D_μ	covariant derivative	
E_s	s^{th} energy level of Hamiltonian	
F	fidelity	$F(\psi\rangle, \phi\rangle) = \langle\psi \phi\rangle ^2$
F^*	infidelity	$F^* := 1 - F$
f	fidelity amplitude	$ f ^2 := F$
$g_{\mu\nu}$	metric tensor	$g_{\mu\nu} = \text{Re}\chi_{\mu\nu}$
$\hat{H}(\boldsymbol{\lambda})$	parameter controlled Hamiltonian	
\mathcal{H}	Hilbert space	
$\mathcal{H}(\boldsymbol{\lambda})$	Hilbert space for $\hat{H}(\boldsymbol{\lambda})$	
Ind_a	winding number around point a	
\mathcal{J}	driving curve in parametric space	
$\boldsymbol{\lambda}$	n -dimensional real parameter of Hamiltonian	$\boldsymbol{\lambda} \in \mathcal{U} \subset \mathbb{R}^n$
\mathcal{M}	manifold	
\mathcal{M}_s	s^{th} energy state manifold	$\mathcal{M}_s := \cup_{\boldsymbol{\lambda} \in \mathcal{U}, \varphi \in [0, 2\pi)} e^{i\varphi} s(\boldsymbol{\lambda})\rangle$
N	dimension of the Hamiltonian	
\mathbb{N}	natural numbers (excluding zero)	
$ o(\boldsymbol{\lambda})\rangle$	ground state of Hamiltonian $\hat{H}(\boldsymbol{\lambda})$	
\mathcal{O}	order of the function (Big O notation)	
\mathcal{PM}_s	s^{th} energy projective state manifold	$\mathcal{PM}_s := \cup_{\boldsymbol{\lambda} \in \mathcal{U}} s(\boldsymbol{\lambda})\rangle$
φ_B	Berry phase	
\mathbb{R}	Real numbers	
$R^\alpha_{\mu\nu\kappa}$	Riemann tensor	
$R_{\mu\nu}$	Ricci tensor	$R_{\mu\nu} := R^\alpha_{\mu\alpha\nu}$
$R \equiv \text{Ric}$	Ricci scalar, or Ricci curvature	$R := R^\mu_\mu$
$\nu_{\mu\nu}$	Berry curvature	$\nu_{\mu\nu} = \text{Im}\chi_{\mu\nu}$
$ s\rangle$	eigenstate corresponding to energy E_s	$\hat{H} s\rangle = E_s s\rangle$
t	time	
T	final time of driving	
$\mathbb{T}_a \mathcal{M}$	tangent field of \mathcal{M} in $a \in \mathcal{M}$	
$\mathbb{T}_a^* \mathcal{M}$	cotangent field of \mathcal{M} in $a \in \mathcal{M}$	
$\mathbb{T}_q^p \mathcal{M}$	q -times covariant and p -times contravariant tensor field of \mathcal{M}	
\mathcal{U}	parametric space, open subset of \mathbb{R}^n	
$U(k)$	k -parametric unitary transformation group	
$\chi_{\mu\nu}$	geometric tensor	
$(\chi; \lambda)$	LMG model parameters	$(\chi, \lambda) \equiv \boldsymbol{\lambda} \in \mathbb{R}^2$

Shortcut	Full name
APT	adiabatic perturbation theory
LZS	Landau-Zener-Stueckelberg
LMG	Lipkin-Meshkov-Glick

- Quantum operators are denoted with *hat*,
- abstract indices are written in *Greek*, pointer indices in *Latin*.
- If the object is defined by the formula on right, “:=” is used. If the equality holds by definition, “≡” is used.
- Coordinate derivative can be denoted using comma before index and covariant derivative using semicolon.
- The colored text is sometimes used. The text can be understood without the colors, its goal is strictly pedagogical and helps reader to see some underlying connections.

Introduction

One of big unsolved problems of the modern physics is the construction of quantum computer. The implications here are mainly to so-called *adiabatic quantum computers*, where the solution to some mathematical problem is substituted for finding the energy minima in some system of coupled qubits¹. The energy minima can be found by numerous measurements of the specific superposition of qubits. The preparation of such superposed state is complicated process and one method of achieving it is so-called *quantum annealing*². This is the process of changing the state from some simple *initial state* to the required state in superposition (*final state*). The initial state is typically chosen to be the ground state of some easily obtainable configuration, such as *all spins up*. The change in states is called *quantum state transport* or *quantum state driving*.

The point of interest of this thesis is the quantum state driving. This driving usually needs to be performed *adiabatically*, i.e., without excitation of the system. The probability that the state will remain in a ground state during such transport is called *fidelity*. For illustration of this problem see Fig. 1, where two scenarios are drawn. First, the state moves adiabatically (fidelity is one), second, the state excites in the small energy gap area, which in the case of quantum computers devalues the experiment.

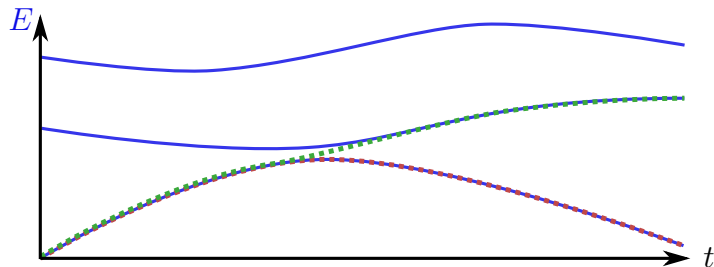


Figure 1: Visualization of the **state adiabatic transport** compared to **transport with excitation** in a system with time varying **energy eigenstates**.

This problem is of course more general. From mathematical point of view, in the example above we have *parameter driven Hamiltonian* $\hat{H}(\boldsymbol{\lambda})$ between qubits (omitting the thermal basis of the environment and other effects), which depends on some vector $\boldsymbol{\lambda}$ from *parameter space*. Change in the driving parameter (for example orientation of a magnetic field, or strength of qubit coupling) influences the qubits and *drives* them to some final state in superposition.

The question of interest is: “How to achieve the better *final fidelity*, meaning *how to prepare the final ground state with the higher probability?*” During the driving one might add some energy to the qubit, which leads to its excitation and possibly destroys the superposition. This can be improved by many methods. From the theory of *quantum state driving* three methods are emphasized here — *adiabatic driving*, *counter-diabatic driving*, or *choosing better driving path*. Adiabatic driving can be performed by infinitely slow drivings, making it unsuitable

¹As qubits one might use for example quantum dots [Loss and DiVincenzo, 1998], or Josephson junctions [Makhlin et al., 2000].

²The name comes from the resemblance to annealing in metallurgy.

for practical applications. Counter-diabatic driving requires adding another element to the Hamiltonian, which leads to *unit fidelity protocols* (the system does not excite), making it a good candidate for practical applications. The method of finding better driving path can be combined with all other methods, and means that different paths in parameter space lead to different fidelity. Because these trajectories are influenced by energy spectra, one might be interested in the *quantum state manifolds*. These are especially important for some drivings, such as driving using small *quenches* (quick, but small changes in driving parameter), or close-adiabatic driving, where the fidelity is almost one.

To understand the geometry of quantum state driving, the basics of differential geometry are presented in Chapter 1. It does not serve the full theory, only some basic intuition is build and useful definitions are provided here. The theory of quantum driving itself is described in Chapter 2. First the geometrical space is constructed, then the concept of *quantum state driving*, *fidelity* and *metric tensor* are introduced. The driving methods are described in Chapter 3. Especially *counter-diabatic*, *adiabatic* and *close-adiabatic* drivings are introduced, along with reformulation of theorems about fidelity. Special importance is played by the *ground state manifold* and geodesics, for which some applications are proposed.

To understand the general fidelity driving, a simple two level system is analyzed in Chapter 4. Driving fidelity and energy variance are calculated for two special drivings — *linear* and *geodesic*. This demonstrates some basic phenomena which occur in quantum state driving in general. Finally, the more convoluted Lipkin-Meshkov-Glick model is analyzed in Chapter 5. The analysis is first performed in specific dimensions, from which some general formulas in arbitrary dimension are derived. Focus is especially on the ground state manifold and geometrical structures on it. This can help to understand drivings with unit or almost unit fidelity.

1. Mathematical introduction

The modern approach to the closed system dynamics is using *differential geometry* formalism. Before we get to the quantum mechanics itself, let's introduce this formalism and recapitulate some definitions of this branch of mathematics. It is important to realize basic definitions and construction, so the mathematical formalism can be used rigorously. More detailed notes can be found for example in Krtouš [2013], Loring [2017], or Fecko [2006]. This chapter should lead the reader to better understanding of the physical theory in following chapters, but is not essential for performing the analysis of driving in Hamiltonian systems.

1.1 Essentials

Consider manifold \mathcal{M} over the field of complex numbers \mathbb{C} . Curves on this manifold are parametrized by some real interval:

$$\mathcal{J} : \mathbb{R} \supset (P_i, P_f) \rightarrow \mathcal{M}, \quad \xi \mapsto \mathcal{J}(\xi) \text{ for } \xi \in (P_i, P_f).$$

The space of functions is $\mathcal{FM} \equiv \{f : \mathcal{M} \rightarrow \mathbb{C}\}$.

To define *vectors* on \mathcal{M} , we need to make sense of the *direction*. The direction is defined using curves \mathcal{J}_i satisfying

$$\mathcal{J}_1(0) = \mathcal{J}_2(0) \equiv P$$

$$\frac{d}{dt}x^i(\mathcal{J}_1(t))\Big|_{t=0} = \frac{d}{dt}x^i(\mathcal{J}_2(t))\Big|_{t=0}.$$

Taking the equivalence class created by these two rules, sometimes noted as $[\mathcal{J}] = v$, we have an element of the tangent space to \mathcal{M} . We use standard notation for the *tangent space of \mathcal{M}* in some point $P \in \mathcal{M}$ as $\mathbb{T}_P\mathcal{M}$. Cotangent space is denoted as $\mathbb{T}_P^*\mathcal{M}$. Unifying all *tangent*, resp. cotangent spaces over all x we get tangent and cotangent bundle, $\mathcal{T}\mathcal{M}$ and $\mathcal{T}^*\mathcal{M}$ respective. To generalize this notation to higher tensors, we denote $\mathbb{T}_P\mathcal{M} \in \mathcal{T}_P^1\mathcal{M}$, $\mathbb{T}_P^*\mathcal{M} \in \mathcal{T}_{P1}\mathcal{M}$. This gives us the possibility to increase the order, leading to p -times *contravariant* and q -times *covariant* tensors. These are usually denoted $\mathcal{T}_q^p\mathcal{M}$. Tensor space in point $P \in \mathcal{M}$ is denoted $\mathcal{T}_q^p\mathcal{M}$. Using the congruence of curves on \mathcal{M} , the expression

$$\frac{d}{d\xi}f \circ \mathcal{J}(\xi)\Big|_{\xi=0} \tag{1.1}$$

has a good meaning, and we can define the *vector* in some $P \in \mathcal{M}$ as

$$v : \mathcal{FM} \rightarrow \mathbb{C} \quad f \mapsto v[f] \equiv \frac{df(\mathcal{J}(\xi))}{d\xi}\Big|_P \equiv \partial_\xi\Big|_P f. \tag{1.2}$$

It holds that $v \in \mathbb{T}_P\mathcal{M}$ and can be expressed as the *derivative in direction*, which can be understood in coordinates as

$$v[f] = \frac{d}{dv}f \circ \mathcal{J}(\xi)\Big|_{\xi=0} = v^k \frac{d}{dx^k}f(x)\Big|_P. \tag{1.3}$$

The directional derivative is denoted ∇_v and in basis $\mathbf{e}_i \equiv \partial/\partial x^i$ it becomes

$$\nabla = (\mathbf{e}_1, \mathbf{e}_2, \mathbf{e}_3).$$

During the whole thesis, the *abstract indices* (written by Greek letters) and *pointer indices* (written using Latin letters) is differentiated. Abstract indices show the rank of the tensor, meaning *how many empty slots for contraction the tensor has*. Pointer indices extract specific number from the tensor. For example

$$t_{\nu\kappa}^\mu \in \mathcal{T}_2^1 \mathcal{M}, \quad \text{whilst for some } i, j, k \in \mathbb{N} : t_{jk}^i \in \mathbb{C}.$$

For *Tensor contraction*, the index notation is used. When it is clear what type of tensors we are operating with, the object notation can be used, for example $t(\mathbf{u}, \mathbf{v}) \equiv t_{\mu\nu} \mathbf{u}^\mu \mathbf{v}^\nu$. The contraction can also be noted using contraction operator \mathbf{C} , when it is clear which indices are contracted, or when it does not matter which of them are.

Now we have the notation to define one strong structure on manifolds – *metric tensor*.

Definition 1 (Metric tensor). *If the 2-form $g_{\mu\nu} \in \mathcal{T}_2^0 \mathcal{M}$ is*

- *linear in second argument:* $\forall \alpha, \beta \in \mathbb{C}; \mathbf{u}, \mathbf{v}, \mathbf{w} \in \mathcal{T}^1 \mathcal{M} : g(\mathbf{u}, \alpha \mathbf{v} + \beta \mathbf{w}) = \alpha g(\mathbf{u}, \mathbf{v}) + \beta g(\mathbf{u}, \mathbf{w})$,
- *hermitian:* $\forall \mathbf{v}, \mathbf{w} \in \mathcal{T}^1 \mathcal{M} : g(\mathbf{v}, \mathbf{w}) = g(\mathbf{w}, \mathbf{v})^*$,
- *non-degenerate:* $\forall \mathbf{v} \in \mathcal{T}^1 \mathcal{M}$ the function $\mathbf{w} \mapsto g(\mathbf{v}, \mathbf{w})$ is not identically zero,

we call $g_{\mu\nu}$ a metric tensor. The $*$ marks complex conjugation.

We often require *differentiable metric tensor*, or at least almost everywhere¹. That assures that *covariant derivatives* and *parallel transport* are well-defined almost everywhere.

Vectors of tangent space to some manifold can be compared only within one such space. To perform some tensor operations we need to transport them to some common tangent space. This can be done using the *parallel transport* which is connected to the notion of *covariant derivative*.

Definition 2 (Covariant derivative). $D_{\mathbf{v}}$ is called the covariant derivative in a direction $\mathbf{v} \in \mathbb{T}_P \mathcal{M}$, if $\forall f \in \mathcal{F} \mathcal{M}$, $\mathbf{A}, \mathbf{B} \in \mathcal{T}_q^p \mathcal{M}$, $\alpha \in \mathbb{C}$:

- $D_{\mathbf{v}} : \mathcal{T}_q^p \mathcal{M} \rightarrow \mathcal{T}_{P_q}^p \mathcal{M}$
- $D_{f\mathbf{v}} \mathbf{A} = f D_{\mathbf{v}} \mathbf{A}$ (*ultralocality in a direction*)
- $D_{\mathbf{v}}(\mathbf{A} + \alpha \mathbf{B}) = D_{\mathbf{v}} \mathbf{A} + \alpha D_{\mathbf{v}} \mathbf{B}$ (*linearity in argument*)
- $D_{\mathbf{v}}(\mathbf{AB}) = (D_{\mathbf{v}} \mathbf{A}) \mathbf{B} + \mathbf{A} (D_{\mathbf{v}} \mathbf{B})$ (*Leibniz rule*)
- $D_{\mathbf{v}}(\mathbf{CA}) = \mathbf{C} D_{\mathbf{v}}(\mathbf{A})$ (*commutation with contraction*)

¹Almost everywhere means with an exception to the submanifold of zero measure.

- $\mathbf{D}_v f = v[f] \equiv v^\beta \mathbf{d}_\beta f$ (*operation on functions*)

Definition 3 (Parallel transport). *Parallel transport of tensors in tensor field $\mathbf{A} \in \mathcal{T}_{q^P}^p \mathcal{M}$ along some path \mathcal{J} going from $P_i \in \mathcal{M}$ to $P_f \in \mathcal{M}$ is denoted*

$$\begin{aligned} par_{\mathcal{J}} : \mathcal{T}_{P_i} \mathcal{T}_{q^P}^p \mathcal{M} &\rightarrow \mathcal{T}_{P_f} \mathcal{T}_{q^P}^p \mathcal{M} \\ \mathbf{A}|_{P_i} &\mapsto (par_{\mathcal{J}} \mathbf{A})|_{P_f}. \end{aligned}$$

This means that the parallel transport takes a tensor at some $\mathcal{T}_{P_i} \mathcal{T}_{q^P}^p \mathcal{M}$ and transports it to $\mathcal{T}_{P_f} \mathcal{T}_{q^P}^p \mathcal{M}$. Those two tensors belong to the same tensor field, but are essentially different. One cannot simply add or subtract them. For that they need to be parallel transported into the same tensor space $\mathcal{T}_{q^P}^p \mathcal{M}$.

Another object which is needed for computing the covariant derivative is *affine connection*. It is generally defined as the difference of covariant and coordinate derivative $\Gamma := \mathbf{D} - \partial$. Because this definition requires some additional theory, only the *connection on metric spaces* is provided here.

Definition 4 (Connection and Christoffel symbols). *The Affine connection on metric spaces can be defined as*

$$\Gamma_{\mu\nu}^\alpha := \frac{1}{2} g^{\alpha\beta} (g_{\beta\mu,\nu} + g_{\nu\beta,\mu} - g_{\mu\nu,\beta}), \quad (1.4)$$

where we used comma notation for the coordinate derivative. Its elements are called the Christoffel symbols.

The covariant derivative of a vector $\mathbf{a} \in \mathbb{T}_P \mathcal{M}$ for manifold with coordinates x^μ can be expressed as

$$\frac{D\mathbf{a}^\mu}{dx^\nu} = \mathbf{a}_{,\nu}^\mu - \Gamma_{\alpha\beta}^\mu x^\alpha \mathbf{a}^\beta \quad (1.5)$$

and for $\boldsymbol{\alpha} \in \mathbb{T}_P^* \mathcal{M}$ it is

$$\frac{D\boldsymbol{\alpha}_\mu}{dx^\nu} = \boldsymbol{\alpha}_{\mu,\nu} - \Gamma_{\mu\beta}^\alpha x^\beta \boldsymbol{\alpha}_\alpha \quad (1.6)$$

The vector $v \in \mathbb{T}_P \mathcal{M}$ is said to be parallel transported along curve $\mathcal{J}(\lambda)$, if its covariant derivative vanishes along $\mathcal{J}(\xi)$, meaning

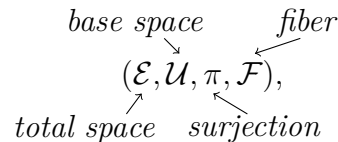
$$\frac{Dv^\mu}{d\xi} = 0. \quad (1.7)$$

1.2 Fiber bundle

Sometimes one needs to add additional structure to every point on manifold. These structures are usually imagined like fibers going from the manifold, similarly to the hair going from your head.

At every point of the manifold we introduced a tensor space. This structure can be described by so-called *fiber bundles*.

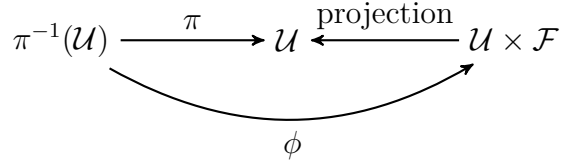
Definition 5 (Fiber bundle). *Structure*



for topological spaces \mathcal{E} , \mathcal{U} , \mathcal{F} and continuous surjection $\pi : \mathcal{E} \rightarrow \mathcal{U}$ satisfying a local triviality, is called a Fiber bundle. The local triviality means that \mathcal{U} is connected² and for every $x \in \mathcal{U}$, there is an open neighborhood $\mathcal{N} \subset \mathcal{U}$ (trivializing neighborhood) such that there exists a homeomorphism from \mathcal{N} to so-called product space

$$\phi : \pi^{-1}(\mathcal{N}) \rightarrow \mathcal{N} \times \mathcal{F},$$

such that $\pi^{-1} \circ \pi(\mathcal{N}) = \mathcal{N}$. Plus there exist natural projection from $\mathcal{N} \times \mathcal{F}$ to \mathcal{N} , setting the coordinate in fibers to zero. The structure can be visualized as follows:



Because the projections of products are open maps, $\pi : \mathcal{E} \rightarrow \mathcal{N}$ must be an open map. The manifolds at every point $x \in \mathcal{F}$ are all locally diffeomorphic to each other.

With the analogy to the hair on your head, one can say that \mathcal{N} is the head, \mathcal{F} is the hair, π applied on the any point on hair returns the point on your head and \mathcal{E} is the head with all the hairs. This analogy holds only if all of your hairs are the same.

1.3 Riemannian geometry

Some Riemannian geometry theorems have implications in theory of quantum driving on ground state manifolds. First, some basic definitions are needed.

Definition 6 (Riemannian manifold). *Manifold is called Riemannian, iff it's equipped with positive definite metric tensor.*

Definition 7 (Connected manifold). *Manifold is connected, iff the distance between two points is infimum of the lengths of curves joining the two points.*

Definition 8 (Compact manifold). *Manifold is said to be compact if its every open cover has a finite subcover.*

Definition 9 (Geodesical completeness). *A manifold is said to be geodesically complete if its every geodesic can be extended to infinite values of their affine parameter.*

This condition holds if the space does not contain any singularities. It is a coordinate-independent notion.

Definition 10 (Geodesic maximality). *A manifold is said to be geodesically maximal if it is either geodesically complete, or every non-complete geodesic (such that cannot be extended to infinite values of their affine parameter) ends in a singularity.*

²Connected mean, it can't be represented as a union of two and more disjoint sets

Geodesic maximality is coordinate dependent notion, only if the manifold is geodesically complete.

Theorem 1 (Von Neumann-Wigner). [Landau and Lifshitz, 1981][page 305]

This, sometimes called the Non-Crossing Theorem, states that the eigenvalues of Hermitian matrix driven by N continuous real parameters forms at maximum $(N - 2)$ -dimensional submanifold.

Theorem 2 (Hopf-Rinow Theorem). [Petersen, 1998][page 125]

For connected Riemannian manifold \mathcal{M} with the metric g , following are equivalent:

- (\mathcal{M}, g) is geodesically complete, i.e. all geodesics are infinite
- (\mathcal{M}, g) is geodesically complete at some point P , i.e. geodesics going through P are infinite
- (\mathcal{M}, g) satisfies the Heine-Borel property, i.e. every closed bounded set is compact
- (\mathcal{M}, g) is complete as a metric space.

Theorem 3 (Modified Hopf-Rinow Theorem). [Gorodski, 2012][Chapter 3]

For connected Riemannian manifold \mathcal{M} with the metric g , any two points on \mathcal{M} can be joined with a minimizing geodesic.

This generally means that in a space with singularity exists such points, which cannot be connected with the rest of the manifold using geodesics. In General relativity, this area is for example below the event horizon of black holes.

Theorem 4. [Gorodski, 2012][Chapter 3]

A compact Riemannian manifold is geodesically complete.

1.4 Geometry in 2 dimensions

An important tensor in differential geometry is the *Riemann tensor*

$$R^\alpha_{\beta\gamma\delta} := \Gamma^\alpha_{\beta\delta,\gamma} - \Gamma^\alpha_{\beta\gamma,\delta} + \Gamma^\mu_{\beta\delta}\Gamma^\alpha_{\mu\gamma} - \Gamma^\mu_{\beta\gamma}\Gamma^\alpha_{\mu\delta}. \quad (1.8)$$

Ricci tensor can be defined as its contraction

$$R_{\alpha\gamma} := R^\mu_{\alpha\mu\gamma}, \quad (1.9)$$

which is second order symmetric tensor. *Ricci scalar*, describing the curvature on manifold, is defined as contraction of the Ricci tensor

$$R := R^\mu_\mu. \quad (1.10)$$

This can be simplified for 2-dimensional manifold as

$$R = \frac{2}{g_{22}} \left(\Gamma^1_{22,1} - \Gamma^1_{12,2} + \Gamma^1_{11}\Gamma^1_{22} + \Gamma^1_{12}\Gamma^2_{22} - \Gamma^1_{21}\Gamma^1_{12} - \Gamma^1_{22}\Gamma^2_{12} \right). \quad (1.11)$$

Another possibility to express the Ricci tensor in two dimensions, see Gutiérrez-Ruiz et al. [2021, eq. 6,7], is

$$R = \frac{1}{\sqrt{|g|}}(\mathcal{S} + \mathcal{T}), \quad (1.12)$$

for

$$\mathcal{S} := \left(\frac{g_{12}}{g_{11}\sqrt{|g|}}g_{11,2} - \frac{1}{\sqrt{|g|}}g_{22,1} \right)_{,1} \quad (1.13)$$

$$\mathcal{T} := \left(\frac{2}{\sqrt{|g|}}g_{12,1} - \frac{1}{\sqrt{|g|}}g_{11,2} - \frac{g_{12}}{g_{11}\sqrt{|g|}}g_{11,1} \right)_{,2}. \quad (1.14)$$

2. Introduction to quantum geometry

This chapter depends on the mathematical formalism developed in Chapter 1 and some basic knowledge of quantum mechanics is required. Most parts are inspired by Kolodrubetz et al. [2017] and original notes by Berry [1984], Berry [1989], Berry [2009] with attempt to give them more rigorous meaning in the language of differential geometry.

The aim of this chapter is the construction of space on which the *driving of quantum states* (changing the states by controlling the Hamiltonian parameter) is performed and introducing some basic concepts needed. There may be many geometrical constructions of the space, because usually only some sections of the full space are used. Different constructions require different mathematical formalism. One might choose the way of *vector bundles*, or *fiber bundles* (our case), or just sectioning one Hilbert space in different ways, constructing the needed physical spaces. The reason for choosing the way of fiber bundles is that from the Hamiltonian with free parameter $\hat{H}(\lambda)$ we get one Hilbert space for every value of the parameter. The fiber structure then gives the natural formalism for connecting these spaces and embeds the space with natural geometry due to changing eigenbasis during the driving. In addition, the fiber space holds the information about driving parameter λ .

Even though the theory below depends on differential geometry, it does not reformulate the whole quantum mechanics into this language. This is rather complicated task and for introduction into this approach see Appendix A.

From now on we use natural units, so $\hbar = 1$.

2.1 Space of all states

Assume parameter $\boldsymbol{\lambda} \in \mathcal{U} \subset \mathbb{R}^N$ for \mathcal{U} open set. This parameter controls some finite-dimensional Hamiltonian $\hat{H}(\boldsymbol{\lambda})$, which is bounded from below and has discrete spectrum. From this we can construct the fiber bundle, such that at every point of the base manifold $\boldsymbol{\lambda} \in \mathcal{U}$, we construct fiber as a Hilbert space $\mathcal{H}(\boldsymbol{\lambda})$. The fiber structure can be according to Def. 5 written as

$$\left(\mathcal{H}_{full} := \bigcup_{\boldsymbol{\lambda} \in \mathcal{U}} \mathcal{H}(\boldsymbol{\lambda}), \quad \mathcal{U} \subset \mathbb{R}^N, \quad \pi, \quad \mathcal{H}(\boldsymbol{\lambda}) := \bigcup_{states} |\psi(\boldsymbol{\lambda})\rangle \right).$$

The projection is defined as $\pi(\boldsymbol{\lambda}) : |\psi(\boldsymbol{\lambda})\rangle \mapsto \boldsymbol{\lambda}$ and $\mathcal{H}(\boldsymbol{\lambda})$ is a Hilbert space containing all pure states of $\hat{H}(\boldsymbol{\lambda})$. Geometric intuition is displayed in Fig. 2.1.

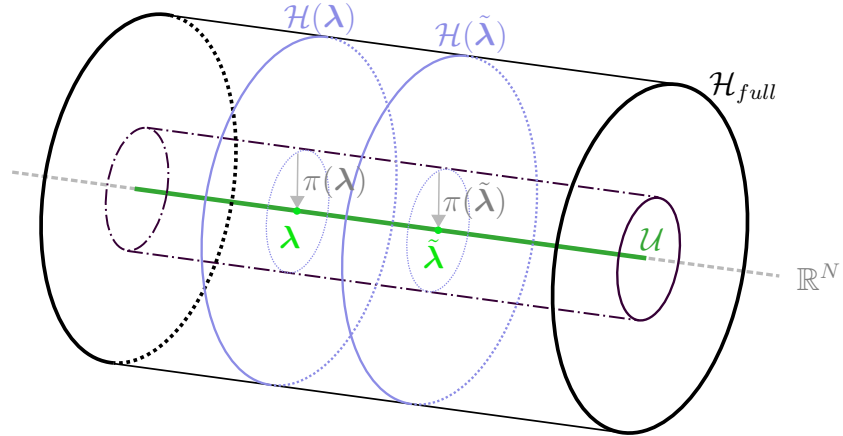


Figure 2.1: Base manifold $\mathcal{U} \subset \mathbb{R}^N$ is visualized as a line. For every point $\lambda \in \mathcal{U}$ one Hilbert space $\mathcal{H}(\lambda)$ (blue disk) is constructed as a fiber. The union of all these fibers creates the full Hilbert space \mathcal{H}_{full} (hollow cylinder) and from every Hilbert space there exist projection π onto the base manifold.

2.2 Rays and bare states

Physical observables in quantum mechanics are related to the *space of rays* or *projective Hilbert space*, defined as $\mathcal{PH} := \mathcal{H}/U(1)$, where elements of $U(1)$ are unitary transformations $e^{i\varphi}$ for $\varphi \in [0, \pi]$. This defines the *global* gauge symmetry between quantum states. The phase φ is chosen the same for every vector and can be chosen arbitrarily. We cannot alter the phase of individual vectors, meaning there is no local gauge symmetry.

This resembles the fiber structure

$$(\mathcal{H}, \mathcal{PH}, \pi_{rays}, \{e^{i\varphi} | \varphi \in [0, 2\pi)\}),$$

where π_{rays} is just rule setting phase φ to arbitrary value. The geometrical intuition is drawn on Fig. 2.2.

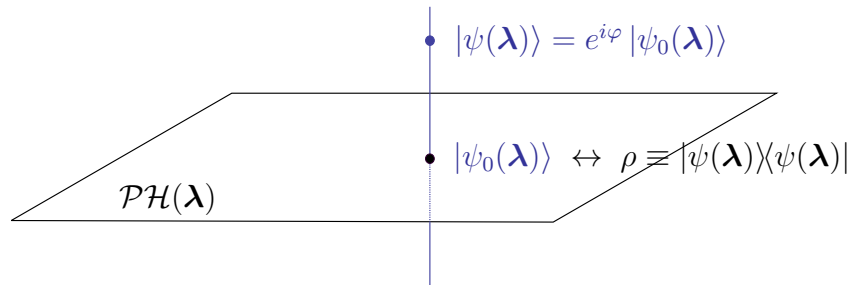


Figure 2.2: For every λ we have the projective Hilbert space $\mathcal{PH}(\lambda)$ containing physical states $|\psi(\lambda)\rangle$ corresponding to density matrix $\rho \equiv |\psi(\lambda)\rangle\langle\psi(\lambda)|$. Every state can be multiplied by phase factor $e^{i\varphi}$, extending it to Hilbert space $\mathcal{H}(\lambda)$.

2.3 Sectioning the space

Consider initial state $|\psi_0\rangle \in \hat{H}(\boldsymbol{\lambda}_0)$. The state then evolves along some path

$$\mathcal{J} := \{\boldsymbol{\lambda}(t) | t \in [0, T], \boldsymbol{\lambda} \in \mathcal{U}\} \subset \mathbb{R}^N, \quad \boldsymbol{\lambda}(0) = \boldsymbol{\lambda}_0 \quad (2.1)$$

parametrized by time t , according to the Schrödinger equation

$$i\hbar \frac{d}{dt} |\psi(\boldsymbol{\lambda}(t))\rangle = \hat{H}(\boldsymbol{\lambda}(t)) |\psi(\boldsymbol{\lambda}(t))\rangle. \quad (2.2)$$

For eigenstates $\{|s\rangle\}_{s=0}^{N-1}$ of instantaneous Hamiltonian it reads as a Schrödinger energy equation

$$\hat{H}(\boldsymbol{\lambda}) |s(\boldsymbol{\lambda})\rangle = E_s(\boldsymbol{\lambda}) |s(\boldsymbol{\lambda})\rangle. \quad (2.3)$$

Notice that these states are independent on the trajectory \mathcal{J}_t . For every $\hat{H}(\boldsymbol{\lambda})$ its energies can be sorted from the smallest, defining the *Hamiltonian spectrum*

$$\sigma(\hat{H}(\boldsymbol{\lambda})) := \{E_0, \dots, E_{N-1}\}. \quad (2.4)$$

In this set degeneracies are not unified into one element, therefore every $\sigma(\boldsymbol{\lambda})$ has N elements. From this there exists an isomorphism between all σ -sets, and we can define *section*

$$\sec_s : |s(\boldsymbol{\lambda})\rangle \mapsto \mathcal{U} \subset \mathbb{R}^N, \quad \text{for } s \in \{0, \dots, N-1\}.$$

This maps eigenstates corresponding to energy E_s to the base manifold. This mapping is similar to previously introduced π , except it is an isomorphism, not a projection. The isomorphism is showed later on, when introducing the metric structure on these spaces.

Now we have constructed N sections of the full Hilbert space, which are isomorphic to the base manifold. Because \mathcal{U} is a Riemannian manifold, these so-called *projective state manifolds*

$$\mathcal{PM}_s := \left\{ \bigcup_{\boldsymbol{\lambda} \in \mathcal{U}} |s(\boldsymbol{\lambda})\rangle \right\}, \quad (2.5)$$

must be also Riemannian. Of special importance is the *projective ground state manifold* \mathcal{PM}_0 , which is used later on for adiabatic transports of ground states. Geometrical intuition for state manifolds is drawn on Fig. 2.3.

The reason for calling the manifolds *projective* is the gauge symmetry of the Schrödinger equation. We can change the phase of vector $|s\rangle \mapsto e^{i\varphi} |s\rangle$ by any $\varphi \in \mathbb{R}$. If all the possible \mathcal{PM} are unified over all phases (only interval $[0, 2\pi]$ is used to avoid degeneracy), we get *state manifolds*

$$\mathcal{M}_s := \left\{ \bigcup_{\varphi \in [0, 2\pi]} \bigcup_{\boldsymbol{\lambda} \in \mathcal{U}} e^{i\varphi} |s(\boldsymbol{\lambda})\rangle \right\} \quad (2.6)$$

Because these manifolds were created by sectioning, they are considered to be vector spaces in a geometrical sense. This was expected, because they contain quantum states, which themselves are vectors.

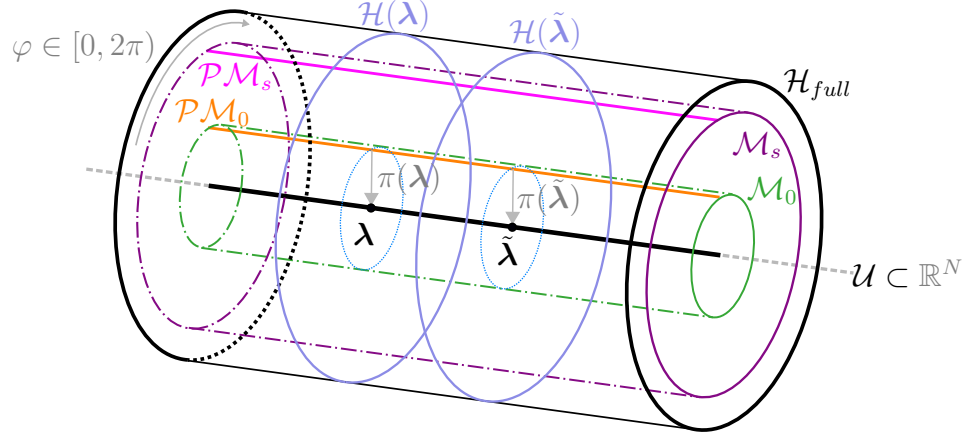


Figure 2.3: From the full Hilbert space \mathcal{H}_{full} (the biggest hollow cylinder) we identified eigenstates and unified them into state manifolds \mathcal{M}_s . These are drawn as inner cylinders of \mathcal{H}_{full} , especially see the ground state manifold \mathcal{M}_0 as the inner cylinder. The phase φ introduces gauge symmetry $e^{i\varphi}$. If it is fixed, we get projective state manifolds \mathcal{PM}_s , especially see \mathcal{PM}_0 . Projective state manifolds are isomorphic to the base manifold \mathcal{U} .

The Hilbert spaces in different points λ have the same finite dimension, so the natural question is if we really need the fiber structure and if we could understand the projection π as a surjection from one Hilbert space to the base manifold $\pi : \mathcal{H} \rightarrow \mathcal{M}$. This can surely be done, but we would lose some generality. For example, the natural choice for basis in the Hilbert space is the eigenbasis. This basis is different for every $\mathcal{H}(\lambda)$ and this opens up two different approaches to a wave-function collapse.

1. In the fiber structure, we can imagine changing the parameter λ as moving between $\mathcal{H}(\lambda)$ subspaces of \mathcal{H}_{full} , in which the eigenbasis can be embedded geometrically. The space structure can be precalculated, and every driving can be performed in this space.
2. If we imagine only one Hilbert space, the eigenbasis varies in time and the driving is performed in a changing space in time.

Another reason is that the coordinate in fiber space holds the value of driving parameter λ . In one simple Hilbert space this information needs to be held separately.

2.4 Transporting states on state manifolds

This chapter is inspired by Berry [1984]. The decomposition of \mathcal{H}_{full} to different state manifolds \mathcal{M}_s is performed as displayed on Fig. 2.4.

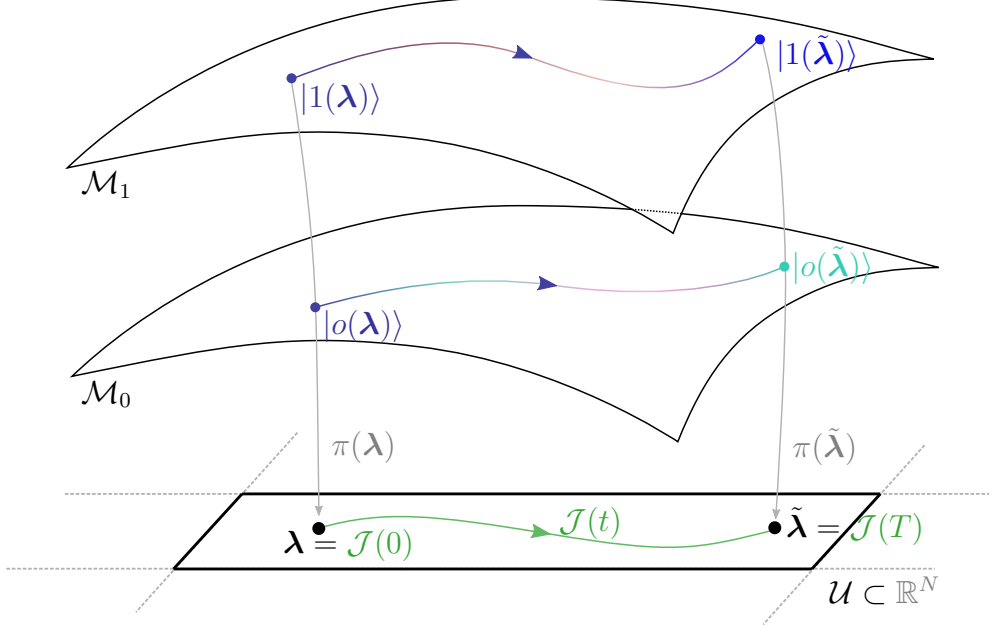


Figure 2.4: The cylinders from Fig. 2.3 are now displayed as two-dimensional sheets. The [transport of states](#) on state manifolds \mathcal{M}_s along the [path](#) $\mathcal{J}(t)$. The information about gauge phase φ is represented by color (see the changing color on the paths in \mathcal{M}_s).

Changing the state from eigenstate $|s(\lambda)\rangle$ to $|s(\tilde{\lambda})\rangle$ on \mathcal{M}_s during some time period is unitary transformation and can be thought of as *parallel transport on fiber bundle* between two states. Assuming the transport goes along \mathcal{J} defined by Eq. 2.1, the transported state can be written at any time as

$$|s(\lambda(t))\rangle = \text{par}_{\gamma_s(t)} |s(\lambda(0))\rangle = \exp\left(-i \int_0^t E_s(\tau) d\tau\right) \exp(i\gamma_s(t)) |s(\lambda(0))\rangle. \quad (2.7)$$

Let's describe the meaning of two exponentials in this transport.

Dynamical phase

The first exponential in Eq. 2.7, the *dynamical phase*, is well known solution to the energy Schrödinger equation 2.3 and depends only on time and Hamiltonian spectrum during the transport. This dynamical phase changes the states only within the projective state manifold \mathcal{PM}_s .

Geometrical phase

The complication arises with the fact that our playground is a state manifold \mathcal{M}_s and some element $\varphi = \gamma_s(t)$, called *geometrical phase* needs to be included. This phase is generally non-integrable, meaning it depends on the whole path and cannot be written simply as $\gamma_s(\lambda)$. For a closed curve

$$C = \{\lambda(t) | t \in [0, T], \text{ such that } \lambda(0) = \lambda(T)\} \subset \mathcal{U} \quad (2.8)$$

we generally get $\text{par}_C |\psi(\lambda)\rangle \neq |\psi(\lambda)\rangle$. This property is sometimes called an *anholonomy* and can be imagined on Fig. 2.4 as change of the path color after

circulating around some closed path on \mathcal{M}_s . Without anholonomy the path does not change the color. On Fig. 2.3, the change of phase means the curve goes around the inner cylinder \mathcal{M}_s and without anholonomy it gets restricted to $\textcolor{orange}{P}\mathcal{M}_s$ line.

Substituting general solution 2.7 to Eq. 2.2 yields¹

$$\hat{H}(\boldsymbol{\lambda}(t)) |\psi(t)\rangle = i \frac{d}{dt} |\psi(t)\rangle \quad (2.9)$$

$$E_s(\boldsymbol{\lambda}(t)) |s(\boldsymbol{\lambda}(t))\rangle = E_s(\boldsymbol{\lambda}(t)) |s(\boldsymbol{\lambda}(t))\rangle - \frac{d\gamma_s(t)}{dt} |s(\boldsymbol{\lambda}(t))\rangle + \frac{d}{dt} |s(\boldsymbol{\lambda}(t))\rangle \quad (2.10)$$

$$\frac{d\gamma_s(t)}{dt} = i \langle s(\boldsymbol{\lambda}(t)) | \frac{d}{dt} |s(\boldsymbol{\lambda}(t))\rangle. \quad (2.11)$$

Separating the dependence of vectors on driving parameter and time, we get

$$\frac{d\gamma_s(\boldsymbol{\lambda}(t))}{dt} = i \langle s(\boldsymbol{\lambda}(t)) | \partial_j s(\boldsymbol{\lambda}) \rangle \dot{\boldsymbol{\lambda}}^j(\lambda), \quad (2.12)$$

for partial derivative along \mathcal{U} coordinates ∂_j and dot as time derivative. Integrating this equation around some closed curve C and assuming the dynamical phase to be zero, we get

$$\gamma_s(C) = i \oint_C \langle s(\boldsymbol{\lambda}) | \partial_j s(\boldsymbol{\lambda}) \rangle d\boldsymbol{\lambda}^j. \quad (2.13)$$

This equation implies that the geometric phase does not depend on energy or time, only on the sequence of Hamiltonians, which means it depends only on the path \mathcal{J} and spectrum $\sigma(\hat{H}(\boldsymbol{\lambda}))$.

Restriction to 3-dimensional parametric space

The problem in integration in Eq. 2.13 lies in the derivative $\partial_{\boldsymbol{\lambda}} s(\boldsymbol{\lambda})$, which locally requires knowledge of single-valued basis $\{|0\rangle, \dots, |N-1\rangle\}$. This can be avoided in 3-dimensions using Stokes's theorem for S as the surface with boundary $\partial S = C$, for coordinate gradient ∇

$$\begin{aligned} \gamma_s(C) &= -\text{Im} \iint_C \mathbf{d}S \cdot \nabla \times \langle s(\boldsymbol{\lambda}) | \nabla n(\boldsymbol{\lambda}) \rangle \\ &= -\text{Im} \iint_C \mathbf{d}S \cdot \langle \nabla s(\boldsymbol{\lambda}) | \times | \nabla s(\boldsymbol{\lambda}) \rangle \\ &= -\text{Im} \iint_C \mathbf{d}S \cdot \sum_{m \neq s} \langle \nabla s(\boldsymbol{\lambda}) | m(\boldsymbol{\lambda}) \rangle \times \langle m(\boldsymbol{\lambda}) | \nabla s(\boldsymbol{\lambda}) \rangle \\ &= - \iint_C \mathbf{d}S \cdot \mathbf{V}_s(\boldsymbol{\lambda}), \end{aligned} \quad (2.14)$$

for

$$\mathbf{V}_s(\boldsymbol{\lambda}) = \sum_{m \neq s} \text{Im} \frac{\langle s(\boldsymbol{\lambda}) | \nabla \hat{H}(\boldsymbol{\lambda}) | m(\boldsymbol{\lambda}) \rangle \times \langle m(\boldsymbol{\lambda}) | \nabla \hat{H}(\boldsymbol{\lambda}) | s(\boldsymbol{\lambda}) \rangle}{(E_m(\boldsymbol{\lambda}) - E_s(\boldsymbol{\lambda}))^2}. \quad (2.15)$$

The element of summation $m = s$ in third step of derivation 2.14 is real, therefore has no influence on γ_s and can be omitted.

¹Here the derivation along upper bound $F(x) := \int_0^{g(x)} f(t) dt \Rightarrow F'(x) = f(g(x))g'(x)$ for $f(t) \in L^1(0, g(x))$ and differentiable function g , is used.

Comparing the first expression in Eq. 2.14 with its last one and extending it to real numbers, we get

$$\mathbf{V}_s(\boldsymbol{\lambda}) = \nabla \times \langle s(\boldsymbol{\lambda}) | \nabla m(\boldsymbol{\lambda}) \rangle, \quad (2.16)$$

defining *vector potential* $\mathbf{V}_s(\boldsymbol{\lambda})$.

Proof of Eq. 2.14. All steps are simple algebraic operations, except for the last equivalence. This can be shown by differentiating the Schrödinger equation 2.3. For any $|s(\boldsymbol{\lambda})\rangle \in \mathcal{M}_s$, $|m(\boldsymbol{\lambda})\rangle \in \mathcal{M}_m$ (the dependence on $\boldsymbol{\lambda}$ in notation is omitted), we get

$$\begin{aligned} \nabla(\underbrace{\hat{H}|s\rangle}_{E_s|s\rangle}) &= (\nabla \hat{H})|\nabla s\rangle + \hat{H}|\nabla s\rangle \\ \langle m|E_s|s\rangle &= \langle m|\nabla \hat{H}|s\rangle + \underbrace{\langle m|\hat{H}}_{\langle m|E_m}|\nabla s\rangle \\ \langle m|\nabla s\rangle &= \frac{\langle m|\nabla \hat{H}|s\rangle}{E_s - E_m}, \quad s \neq m, \end{aligned} \quad (2.17)$$

where we used $|\nabla s\rangle := \nabla|s\rangle$. \square

As was mentioned, the above procedure from Eq. 2.13 was performed only for three-dimensional space. Proper generalization to k-dimensional space would yield

$$\gamma_s(C) = - \iint_C (\mathbf{d}S)^{\alpha\beta} \cdot \text{Im} \frac{\overbrace{\langle s(\boldsymbol{\lambda}) | \mathbf{d}_\alpha \hat{H}(\boldsymbol{\lambda}) | m(\boldsymbol{\lambda}) \rangle}^{\in \mathcal{T}_1 \mathcal{M}} \wedge \overbrace{\langle m(\boldsymbol{\lambda}) | \mathbf{d}_\beta \hat{H}(\boldsymbol{\lambda}) | s(\boldsymbol{\lambda}) \rangle}^{\in \mathcal{T}_1 \mathcal{M}}}{(E_m(\boldsymbol{\lambda}) - E_s(\boldsymbol{\lambda}))^2}, \quad (2.18)$$

for exterior derivative \mathbf{d} .

2.5 Fidelity

The *fidelity* measures “closeness” of two quantum states. It is generally defined for two density operators $\hat{\rho}, \hat{\sigma}$ as

$$\begin{aligned} \mathcal{F} : \text{End}(\mathcal{H}) \times \text{End}(\mathcal{H}) &\mapsto \mathbb{R}, \\ \mathcal{F}(\hat{\rho}, \hat{\sigma}) &:= \left(\text{Tr} \sqrt{\sqrt{\rho}\sigma\sqrt{\rho}} \right)^2 = (\text{Tr} \sqrt[4]{\rho\sigma\sigma\rho})^2 = \left(\text{Tr} \sqrt[4]{\rho\sigma(\rho\sigma)^+} \right)^2, \end{aligned} \quad (2.19)$$

where last equality holds due to hermiticity of density matrices. The usefulness of this definition can be shown in three special cases.

- If both states are pure, $\hat{\rho} =: |\rho\rangle\langle\rho|$, $\hat{\sigma} =: |\sigma\rangle\langle\sigma|$, the fidelity formula reduces to

$$\begin{aligned} F : \mathcal{H} \times \mathcal{H} &\mapsto \mathbb{R}, \\ \mathcal{F}(\hat{\rho}, \hat{\sigma}) &=: F(|\rho\rangle, |\sigma\rangle) = |\langle\rho|\sigma\rangle|^2. \end{aligned} \quad (2.20)$$

- For pure state $\hat{\rho} = |\rho\rangle\langle\rho|$, the fidelity is

$$\mathcal{F}(\hat{\rho}, \hat{\sigma}) = \langle \rho | \hat{\sigma} | \rho \rangle \left(\text{Tr} \sqrt{|\rho\rangle\langle\rho|} \right)^2 = \langle \rho | \hat{\sigma} | \rho \rangle. \quad (2.21)$$

- Commuting density matrices have a meaning of probability distributions. The commutativity implies that $\hat{\rho}, \hat{\sigma}$ can be diagonalized in the same eigenbasis. For $\hat{\rho} = \sum_i p_i |i\rangle\langle i|$, $\hat{\sigma} = \sum_i s_i |i\rangle\langle i|$ we get

$$\sqrt{\hat{\rho}\hat{\sigma}} = \text{Tr} \left(\sum_k \sqrt{p_k s_k} |i\rangle\langle i| \right) = \sum_k \sqrt{p_k s_k} \quad (2.22)$$

and inserting into the definition 2.19 gives

$$F(\hat{\rho}, \hat{\sigma}) = \left(\sum_k \sqrt{p_k s_k} \right)^2. \quad (2.23)$$

The physical meaning of fidelity can be also seen on the state manifolds, imagining *quantum quench between two states* (rapid change of some Hamiltonian parameters). In this case F is the probability that system prepared in some initial ground state $|\rho\rangle$, is found in the new ground state $|\sigma\rangle$. $1-F$ is then the probability of exciting the system during this quench.

Before moving to the practical usage of fidelity, let's look at some general properties.

Theorem 5 (The fidelity properties). *For any two density matrices $\hat{\rho}, \hat{\sigma}$*

- $\mathcal{F}(\hat{\rho}, \hat{\sigma}) \in [0, 1]$ (*normalization*),
- $\mathcal{F}(\hat{\rho}, \hat{\sigma}) = \mathcal{F}(\hat{\sigma}, \hat{\rho})$ (*symmetry*),
- $\mathcal{F}(\hat{\rho}, \hat{\sigma}) = 1 \Leftrightarrow \hat{\rho} = \hat{\sigma}$.

Proof. First statement is a consequence of Cauchy-Schwarz inequality. Second and third goes from Uhlmann's theorem, see for example Uhlmann [1976]. \square

2.6 Metric and geometric tensor

As a playground for this chapter, we choose the projective ground state manifold \mathcal{PM}_0 , but it can be easily generalized to any \mathcal{PM}_s . This means the geometrical phase is neglected, because the states are considered to be the physical states from the projective Hilbert space.

To obtain restriction on metric tensor definition, the local gauge dependence needs to be suppressed. This means the distance on \mathcal{PM}_0 cannot depend on coordinate dependent gauge phase $\varphi(\lambda)$. This phase induces the change in a ground state $|o(\lambda)\rangle$ of the Hamiltonian $\hat{H}(\lambda)$ ²

$$|o(\lambda)\rangle \mapsto e^{i\varphi(\lambda)} |o(\lambda)\rangle, \quad (2.24)$$

²Note that we can also write $|o(\lambda)\rangle \in \mathcal{PM}_0 \cap \mathcal{H}(\lambda)$, which is the set containing exactly one vector – the ground state of $\hat{H}(\lambda)$.

which implies

$$\langle o(\boldsymbol{\lambda}) | \nabla o(\boldsymbol{\lambda}) \rangle \mapsto \langle o(\boldsymbol{\lambda}) | \nabla o(\boldsymbol{\lambda}) \rangle + i \nabla \varphi(\boldsymbol{\lambda}) \quad (2.25)$$

For twice differentiable function $\varphi(\boldsymbol{\lambda}) \in \mathcal{C}^2$, the gauge independent function f would be for infinitesimal change for example

$$f := \langle o(\boldsymbol{\lambda} + \delta\boldsymbol{\lambda}) | o(\boldsymbol{\lambda}) \rangle, \quad (2.26)$$

sometimes referred to as the *fidelity amplitude of a ground state*, because for pure states we get the fidelity $F = |f|^2$. The meaning of fidelity as a probability transition between the states during some quench, leads to the definition of *distance on \mathcal{M}_0*

$$ds^2 \equiv 1 - F(|o(\boldsymbol{\lambda} + \delta\boldsymbol{\lambda})\rangle, |o(\boldsymbol{\lambda})\rangle) = 1 - |\langle o(\boldsymbol{\lambda} + \delta\boldsymbol{\lambda}) | o(\boldsymbol{\lambda}) \rangle|^2. \quad (2.27)$$

We can easily check, that the axioms for metric distance holds:

- identity of indiscernibles $s(|\psi\rangle, e^{i\alpha}|\phi\rangle) = 0 \Leftrightarrow |\psi\rangle = |\phi\rangle, \alpha \in \mathbb{R}$,
- symmetry for any two states $|\psi\rangle, |\phi\rangle$ is implied by $|\langle \psi | \varphi \rangle| = |\langle \varphi | \psi \rangle|$
- triangle inequality: $s(|\psi\rangle, |\psi_2\rangle) < s(|\psi\rangle, |\psi_1\rangle) + s(|\psi_1\rangle, |\psi_2\rangle)$ for any $|\psi\rangle, |\psi_1\rangle, |\psi_2\rangle$.

If we take the fidelity between two parameter dependent states, the infidelity $1 - F(|\psi(\boldsymbol{\lambda})\rangle, |\psi(\boldsymbol{\lambda} + \Delta)\rangle) > 0$ and the first term of Taylor expansion in Δ is zero, implying it can be used for the metric tensor definition.

Definition 11 (Metric tensor on projective state manifolds). *Because the projective state manifolds \mathcal{PM}_s are isomorphic to the base manifold \mathbb{R}^N , we can define*

$$g_{\mu\nu} : \textcolor{red}{\mathbb{T}\mathcal{U}} \times \textcolor{red}{\mathbb{T}\mathcal{U}} \rightarrow \mathbb{R} \\ g_{jk} d\boldsymbol{\lambda}^j d\boldsymbol{\lambda}^k + \mathcal{O}(\lambda^3) \equiv ds^2 := 1 - |\langle o(\boldsymbol{\lambda} + \delta\boldsymbol{\lambda}) | o(\boldsymbol{\lambda}) \rangle|^2. \quad (2.28)$$

Even though we call $g_{\mu\nu}$ the metric tensor *on projective state manifolds*, it takes forms from $\textcolor{red}{\mathbb{T}\mathcal{U}}$. Using abstract indices this means

$$g^{\mu\nu} d_\mu \boldsymbol{\lambda} d_\nu \boldsymbol{\lambda}. \quad (2.29)$$

This whole procedure can be made more rigorous using so-called *vector bundles*, see Loring [2017][Chap. 7]. In our case we can use the isomorphism of $\textcolor{red}{\mathbb{T}\mathcal{U}} \times \textcolor{red}{\mathbb{T}\mathcal{U}}$ and $\textcolor{blue}{\mathbb{T}\mathcal{M}} \times \textcolor{blue}{\mathbb{T}\mathcal{M}}$ and simply write

$$g_{jk} d\boldsymbol{\lambda}^j d\boldsymbol{\lambda}^k = g_{jk} \frac{\partial \boldsymbol{\lambda}^j}{\partial \mathbf{v}^l} \frac{\partial \boldsymbol{\lambda}^k}{\partial \mathbf{v}^m} d\mathbf{v}^l d\mathbf{v}^m =: G_{lm} d\mathbf{v}^l d\mathbf{v}^m. \quad (2.30)$$

Practically only g_{jk} is used, thus what should have been called *the metric tensor on state manifolds* $G_{\mu\nu}$ leaves forgotten. “And some things that should not have been forgotten were lost.” [Tolkien, 1977]

Because the metric tensor is a real analytical function of coordinates, its analytical continuation into complex numbers can be performed. For the motivation behind following definition, see Cheng [2013].

Definition 12 (Geometric tensor). *On the ground state manifold \mathcal{M}_0 , the geometric tensor can be defined as*

$$\chi_{jk} := \langle \partial_j o | \partial_k o \rangle_c \equiv \langle \partial_j o | \partial_k o \rangle - \langle \partial_j o | o \rangle \langle o | \partial_k o \rangle, \quad (2.31)$$

where shortened notation $\partial_k := \frac{\partial}{\partial \lambda^k}$ is used. The subscript c means connected and is defined by the formula.

This definition is in fact gauge independent and can be extended onto any state manifold.

Real part of geometric tensor is symmetric, and it is the metric tensor from Def. 11. The imaginary part is antisymmetric and is called the *curvature tensor*, or *Berry curvature*. The metric tensor can then be expressed as

$$g_{jk} = \text{Re}\chi = \frac{1}{2}(\chi_{jk} + \chi_{kj}) = \text{Re} \sum_{o \neq s} \frac{\langle o | \frac{\partial \mathcal{H}}{\partial \lambda^j} | s \rangle \langle s | \frac{\partial \mathcal{H}}{\partial \lambda^k} | o \rangle}{(E_o - E_s)^2}. \quad (2.32)$$

The Berry curvature is

$$\nu_{jk} = \text{Im}\chi = \frac{i}{2}(\chi_{jk} - \chi_{kj}) = -\text{Im} \sum_{o \neq s} \frac{\langle o | \frac{\partial \mathcal{H}}{\partial \lambda^j} | s \rangle \langle s | \frac{\partial \mathcal{H}}{\partial \lambda^k} | o \rangle}{(E_o - E_s)^2}. \quad (2.33)$$

Proof of the metric tensor definitions correspondence.

To prove the correspondence of geometric tensor, defined by Eq. 2.31, to distance on \mathcal{M}_0 in Eq. 2.27, we start with the state $|o(\lambda)\rangle \in \mathcal{M}_s \cap \mathcal{H}(\lambda)$, which is the ground state of $\hat{H}(\lambda)$. Changing parameter λ to $\lambda + \delta\lambda$ results in a state, which is a linear combination of eigenstates $|s(\lambda + \delta\lambda)\rangle \in \mathcal{M}_s \cap \mathcal{H}(\lambda + \delta\lambda)$, meaning the state is no longer eigenstate. Its collapse to any new eigenstate has a probability amplitude

$$\begin{aligned} a_s &= \langle s(\lambda + \delta\lambda) | o(\lambda) \rangle \approx \delta\lambda^j \langle \partial_j s(\lambda) | o(\lambda) \rangle \\ &= -\delta\lambda^j \langle s(\lambda) | \partial_j | o(\lambda) \rangle. \end{aligned} \quad (2.34)$$

If we introduce the *gauge potential*, sometimes called the *calibration potential*, as³

$$\hat{\mathcal{A}}_j := i\partial_j, \quad (2.35)$$

the probability amplitude can be expressed as

$$a = i \langle s(\lambda) | \hat{\mathcal{A}}_j | o(\lambda) \rangle \delta\lambda^j, \quad (2.36)$$

which has a meaning of gauge potential matrix elements. Probability of the excitation, i.e. the transition to any state $s > 0$ from ground state is then (omitting the λ dependence in notation)

$$\begin{aligned} \sum_{s \neq 0} |a_s|^2 &= \sum_{s \neq 0} \delta\lambda^j \delta\lambda^k \langle o | \hat{\mathcal{A}}_j | s \rangle \langle s | \hat{\mathcal{A}}_k | o \rangle + \mathcal{O}(|\delta\lambda^3|) \\ &= \delta\lambda^j \delta\lambda^k \langle o | \hat{\mathcal{A}}_j \hat{\mathcal{A}}_k | o \rangle_c + \mathcal{O}(|\delta\lambda^3|) =: \delta\lambda^j \delta\lambda^k \chi_{jk} + \mathcal{O}(|\delta\lambda^3|), \end{aligned} \quad (2.37)$$

where last term defines the *geometric tensor*. □

³In SI units, the gauge potential is $\hat{\mathcal{A}}_j := i\hbar\partial_j$

To understand why the gauge potential generates some calibrational invariance, let's define the Berry connection.

Definition 13 (Berry connection). *On the ground state manifold \mathcal{M}_0 , the Berry connection is defined as the mean value of gauge potential*

$$A_j(\boldsymbol{\lambda}) := \langle o(\boldsymbol{\lambda}) | \hat{\mathcal{A}}_j | o(\boldsymbol{\lambda}) \rangle = -i \langle o(\boldsymbol{\lambda}) | \partial_j | o(\boldsymbol{\lambda}) \rangle. \quad (2.38)$$

This empowers us to take derivatives in any direction and the expression for geometric tensor on \mathcal{M}_0

$$\chi_{jk}(\boldsymbol{\lambda}) = \partial_j A_k(\boldsymbol{\lambda}) - \partial_k A_j(\boldsymbol{\lambda}). \quad (2.39)$$

This formula can be directly proven by comparing with 2.31. Here we see that the calibrational invariance is

$$A_j \mapsto A_j + \partial_j \alpha(\boldsymbol{\lambda}), \quad \alpha \in \mathcal{C}^2, \quad (2.40)$$

meaning any twice differentiable function can be added to the gauge potential, leaving the geometric tensor unchanged.

Definition 14 (Berry phase). *The Berry phase, as an integral of the Berry connection along some closed curve \mathcal{C} ⁴*

$$\varphi_B := - \oint_{\mathcal{C}} A_j(\boldsymbol{\lambda}) d\boldsymbol{\lambda}^j = \int_{\mathcal{S}} \chi_{jk}(\boldsymbol{\lambda}) d\boldsymbol{\lambda}^j \wedge d\boldsymbol{\lambda}^k, \quad (2.43)$$

where we used the Stokes theorem for some area \mathcal{S} with boundary $\partial\mathcal{S} = \mathcal{C}$.

Berry phase is zero, when the curve does not go around some geometric tensor singularity. This can be formally written using the *winding number*, which counts *how many times the curve goes counterclockwise around some point of interest*. In our case the points of interest are singularities a , and we have:

$$\text{Ind}_a \mathcal{J}(\boldsymbol{\lambda}) = 0 \Rightarrow \varphi_B = 0.$$

These singularities appear in the system due to energy spectrum degeneracies, in the case of ground state manifold, when $E_1 - E_0 = 0$. These points are called *diabolic*, because of the energy spectrum shape in the $\boldsymbol{\lambda}$ parameter space.⁵

⁴The reasonability of this definition can be seen, if we assume the ground state of a free particle $\langle \mathbf{x} | i(\boldsymbol{\lambda}) \rangle \equiv i(\mathbf{x}, \boldsymbol{\lambda}) = |i(\mathbf{x})| e^{i\varphi(\boldsymbol{\lambda})}$, then the Berry connection is

$$A_j = - \int d\mathbf{x} |i(\mathbf{x}, \boldsymbol{\lambda})|^2 \partial_j \varphi(\boldsymbol{\lambda}) = -\partial_j \varphi(\boldsymbol{\lambda}) \quad (2.41)$$

and Berry phase

$$\varphi_B = \oint_{\mathcal{C}} \partial_j \varphi d\boldsymbol{\lambda}^j, \quad (2.42)$$

which represents total phase accumulated by the wave function. It is really the analogy for Berry phase in classical mechanics, which for example in the case Foucault pendulum on one trip around the Sun makes $\varphi_B = 2\pi$

⁵<https://en.wikipedia.org/wiki/Diabolo>

3. Quantum state driving

The concept of quantum state driving was introduced in the previous chapter. In this chapter the initial state is chosen as eigenstate $|s(\lambda)\rangle$. The driving parameter λ is changed along path parametrized by time t

$$\mathcal{J} := \{\lambda(t) | t \in [0, T], \lambda \in \mathcal{U}\} \subset \mathbb{R}^N, \quad \lambda(0) = \lambda_0, \quad \lambda(T) = \tilde{\lambda}, \quad (3.1)$$

inducing the change in Hamiltonian $\hat{H}(\lambda)$ and consequently in $|\psi(\lambda)\rangle$, according to the Schrödinger equation. This leads to solving the system of N first order differential equations with initial condition $|\psi(\lambda)\rangle = |s(0)\rangle$.

Often needs to achieve as high fidelity as possible during the driving, meaning avoiding the state excitation. If $F = 1$, we speak about *unit fidelity driving* or *adiabatic driving* and \mathcal{J} is called the *unit fidelity protocol*. Higher fidelity can be achieved by many methods, three of them with special importance are

- close adiabatic driving – changing the driving parameters λ slowly, so the system has plenty of time to collapse into the ground state,
- path variation – varying the driving trajectory \mathcal{J} , avoiding the topological defects on manifolds, which would excite the system,
- counter-diabatic driving – countering the excitation by adding some element to the Hamiltonian, making the fidelity precisely 1.¹

Before going through individual methods, let's define the meaning of adiabaticity properly.

Definition 15 (Adiabaticity). *Slow change of the driving parameters of the Hamiltonian $H(\lambda)$ in a sense, that it does not excite the system and allows the system to return to the same energetic state after circulation around any closed path on the ground state manifold with fidelity $F = 1$.*

This means that adiabatic transport is an endomorphism of \mathcal{M}_s . The meaning of the word “slow” clears up next theorem. It defines when the distance between two states can be considered zero.

Theorem 6 (Adiabatic theorem). *For slowly varying Hamiltonian \hat{H} in the time range $(0, T)$, the solution of the Schrödinger equation*

$$\hat{H}(\lambda) |\psi_s(\lambda)\rangle = E_s(\lambda) |\psi_s(\lambda)\rangle$$

with initial condition in x -representation $\langle x|\psi(t=0)\rangle = \psi(x, 0)$ can be approximated as

$$||\psi(\lambda) - \psi_{ad}(\lambda)|| \approx o\left(\frac{1}{T}\right) \quad (3.2)$$

¹There is a nice analogy with driving a toy car (a quantum state) in a curved terrain (a Hilbert space). To avoid the car jumping on the hills (the state excitation), you can either drive slowly (close adiabatic driving), or you can go around the hills (vary the path), or you can alter the space for a specific driving (add a counter-diabatic element), such that it exactly copies the jumping trajectory, therefore the car does not leave the ground.

for the adiabatic state evolved according to Eq. 2.7

$$|\psi_{ad}\rangle = e^{\omega_s(\lambda)} e^{\gamma_s(\lambda)} |\psi(\lambda)\rangle, \quad (3.3)$$

for dynamical phase

$$\omega_s(\lambda) \equiv - \int_0^t E_s(\tau) d\tau$$

and geometrical phase

$$\gamma_s(\lambda) \equiv \int_0^t i \langle \psi_s(\tau) | \partial_t \psi_s(\tau) \rangle d\tau.$$

Proof. The proof can be found in Sakurai and Napolitano [2020][chap. 6]. \square

3.1 Counter-diabatic driving

Assume differentiable and non-singular Hamiltonian $\hat{H}(\boldsymbol{\lambda})$ with non-degenerate eigenbasis $\{|s, \boldsymbol{\lambda}\rangle\}_{s=0}^{N-1}$ called the *adiabatic basis*. This is generally the family of adiabatically connected eigenstates² The transition amplitude between states for adiabatic change is

$$0 = \langle m(\boldsymbol{\lambda}) | \hat{H} | s(\tilde{\boldsymbol{\lambda}}) \rangle \quad \text{for } s \neq m, \forall \boldsymbol{\lambda}, \forall \tilde{\boldsymbol{\lambda}}. \quad (3.4)$$

Differentiation by ∂_t yields

$$\begin{aligned} 0 &= \langle \partial_t m(\boldsymbol{\lambda}) | \hat{H}(\tilde{\boldsymbol{\lambda}}) | s(\tilde{\boldsymbol{\lambda}}) \rangle + \langle m(\boldsymbol{\lambda}) | \overbrace{\partial_t \hat{H}(\tilde{\boldsymbol{\lambda}})}^{\approx \partial_t \hat{H}(\boldsymbol{\lambda})} | s(\tilde{\boldsymbol{\lambda}}) \rangle + \langle m(\boldsymbol{\lambda}) | \hat{H}(\tilde{\boldsymbol{\lambda}}) | \partial_t s(\tilde{\boldsymbol{\lambda}}) \rangle \\ &= E_s(\lambda) \langle \partial_t m(\boldsymbol{\lambda}) | s(\tilde{\boldsymbol{\lambda}}) \rangle + E_m(\lambda) \langle m(\boldsymbol{\lambda}) | \partial_t s(\tilde{\boldsymbol{\lambda}}) \rangle + \langle m(\boldsymbol{\lambda}) | \partial_t \hat{H}(\tilde{\boldsymbol{\lambda}}) | s(\tilde{\boldsymbol{\lambda}}) \rangle \quad (3.5) \\ &= (E_m(\lambda) - E_s(\lambda)) \underbrace{\langle m | \partial_t s(\tilde{\boldsymbol{\lambda}}) \rangle}_{-\frac{i}{\hbar} \langle m | \hat{\mathcal{A}}_t | s(\tilde{\boldsymbol{\lambda}}) \rangle} + \langle m | \partial_t \hat{H} | s(\tilde{\boldsymbol{\lambda}}) \rangle, \end{aligned}$$

which can be rewritten in matrix form as

$$i\hbar \partial_t \hat{H} = [\hat{\mathcal{A}}_t, \hat{H}] - i\hbar \hat{M}_t \quad \text{for } \hat{M}_t \equiv - \sum_s \frac{\partial E_s(\lambda)}{\partial t} |s(\lambda)\rangle \langle s(\lambda)|. \quad (3.6)$$

\hat{M} is diagonal in energetic basis and its elements has meaning of *generalized force*. We can see that $[\hat{H}, \hat{M}] = 0$, implying

$$[\hat{H}, i\hbar \partial_t \hat{H} - [\hat{\mathcal{A}}_t, \hat{H}]] = 0. \quad (3.7)$$

This equation is essentially the system with constraint $\hat{\mathcal{A}}_t$. Its strength lies in fact that it finds the counter-diabatic potential without Hamiltonian diagonalization. For more, see Kolodrubetz et al. [2017][chap. 2.3].

²In the case of energy level crossing, the eigenstates are not unified, because transition between them is not adiabatic.

In section 2.6 we introduced the gauge potential and stated its correspondence to transition probability, see Eq. 2.36. *Gauge transformations*, in classical mechanics called *canonical*, can be defined such that they *preserve Lagrangian of the system under local transformations from some Lie group*. This implies that Hamiltonian $\hat{H}(\boldsymbol{\lambda})$ commutes with its canonically transformed version.³

To understand the meaning of gauge symmetries, let's first consider classical system and then move to quantum mechanics.

3.1.1 Classical gauge potential

This part is inspired by Kolodrubetz et al. [2017][chap. 2.1]. In the Hamiltonian classical mechanics, the manifold \mathcal{M} is assumed to be a subset of the phase space defined by Hamiltonian $H = H(q^i, p_i)$, where momentum p_i and position q^i are assumed to form the orthogonal basis of the phase space

$$\{q^i, p_j\} = \delta_j^i, \quad (3.8)$$

which also defines *calibrational freedom* in their choice. *Canonical transformations* then by definition preserve this formula. Using the *Poisson bracket*, defined on observables as

$$\{A, B\} := \frac{\partial A}{\partial q^j} \frac{\partial B}{\partial p_j} - \frac{\partial B}{\partial q^j} \frac{\partial A}{\partial p_j}, \quad (3.9)$$

we examine continuous canonical transformations generated by gauge potential \mathcal{A}_λ

$$q^j(\lambda + \delta\lambda) = q^j(\lambda) - \frac{\partial \mathcal{A}_\lambda(\mathbf{p}, \mathbf{q})}{\partial p_j} \delta\lambda \Rightarrow \frac{\partial q^j}{\partial \lambda} = -\frac{\partial \mathcal{A}_\lambda}{\partial p_j} = \{\mathcal{A}_\lambda, q^j\} \quad (3.10)$$

$$p_j(\lambda + \delta\lambda) = p_j(\lambda) - \frac{\partial \mathcal{A}_\lambda(\mathbf{p}, \mathbf{q})}{\partial q^j} \delta\lambda \Rightarrow \frac{\partial p_j}{\partial \lambda} = -\frac{\partial \mathcal{A}_\lambda}{\partial q^j} = \{\mathcal{A}_\lambda, p_j\}. \quad (3.11)$$

Substituting this to relations of orthogonality 3.8, we get

$$\{q^j(\lambda + \delta\lambda), p_j(\lambda + \delta\lambda)\} = \delta_j^i + \mathcal{O}(\delta\lambda^2). \quad (3.12)$$

If λ is time parameter and $\mathcal{A}_t = -H$, equations 3.10,3.11 are identical to the Hamilton equations

$$\begin{aligned} \dot{q}^j &= -\{H, q^j\} = \frac{\partial H}{\partial p_j} \\ \dot{p}_j &= -\{H, p_j\} = -\frac{\partial H}{\partial q^j}. \end{aligned} \quad (3.13)$$

Because the Hamiltonian is generator of the movement in the phase space (\mathbf{q}, \mathbf{p}) , we can interpret \mathcal{A}_t as the generators of the movement on \mathcal{M} . Other specific choice might be $\lambda = q^i$, which gives us the momentum components $\mathcal{A}_{q^i} = p_i$.

³This can be easily reformulated to the world of classical physics, where the commutator is replaced by Poisson bracket.

3.1.2 Quantum gauge potential

This part is inspired by Kolodrubetz et al. [2017][chap. 2.2]. Now the aim is to find some special basis transformations \hat{U} between initial system S and the transformed \tilde{S} . Both of them describe the system with Hamiltonian $\hat{H}(\boldsymbol{\lambda})$ with eigenstates $|s(\boldsymbol{\lambda})\rangle$ on state manifolds \mathcal{PM}_s .

Any state of $\mathcal{H}(\boldsymbol{\lambda})$ for $\forall \boldsymbol{\lambda} \in \mathcal{U}$ can be decomposed as

$$|\psi(\boldsymbol{\lambda})\rangle \equiv \sum_s \psi_s(\boldsymbol{\lambda}) |s\rangle \quad (3.14)$$

for some coordinate independent basis $\{|s\rangle\}_{s=0}^{N-1}$. Then there exist unitary transformation

$$\hat{U}(\boldsymbol{\lambda}) : \tilde{S} \rightarrow S, \quad \hat{U}(\boldsymbol{\lambda}) |m(\boldsymbol{\lambda})\rangle = |s\rangle. \quad (3.15)$$

where scalar parameter $\boldsymbol{\lambda}(t)$ is assumed to be changing along the path \mathcal{J} , therefore we can write the Hamiltonian and states only as functions of t . The unitary transformation then satisfies

$$i\hbar \partial_t \hat{U}(t) = \hat{H}(t) \hat{U}(t) \quad (3.16)$$

for \hat{H} the full Hamiltonian of the system and any point on \mathcal{J} , along which the partial derivative is taken.

The generators of unitary transformations are the adiabatic potentials, which can be defined as

$$i\hbar \partial_\lambda |\tilde{\psi}(\boldsymbol{\lambda})\rangle = i\hbar \partial_\lambda \left(\hat{U}^+(\boldsymbol{\lambda}) |\psi\rangle \right) = \underbrace{i\hbar \left(\partial_\lambda \hat{U}^+(\boldsymbol{\lambda}) \right)}_{-\tilde{\mathcal{A}}_\lambda} \hat{U}(\boldsymbol{\lambda}) |\tilde{\psi}(\boldsymbol{\lambda})\rangle. \quad (3.17)$$

The adiabatic potential $\tilde{\mathcal{A}}_\lambda$ can be transformed to non-tilde system as

$$\begin{aligned} \hat{\mathcal{A}}_\lambda &= \hat{U}(\boldsymbol{\lambda}) \tilde{\mathcal{A}}_\lambda \hat{U}^+(\boldsymbol{\lambda}) = -i\hbar \hat{U}(\boldsymbol{\lambda}) \left(\partial_\lambda \hat{U}^+(\boldsymbol{\lambda}) \right) = \\ &= -i\hbar \partial_\lambda \left(\underbrace{\hat{U}^+(\boldsymbol{\lambda}) \hat{U}(\boldsymbol{\lambda})}_\mathbb{1} \right) - \left(\partial_\lambda \hat{U}(\boldsymbol{\lambda}) \right) \hat{U}^+(\boldsymbol{\lambda}) = i\hbar \left(\partial_\lambda \hat{U}(\boldsymbol{\lambda}) \right) \hat{U}^+(\boldsymbol{\lambda}). \end{aligned} \quad (3.18)$$

Now we have explicit formulas for adiabatic potential in two systems

$$\hat{\mathcal{A}}_\lambda = i\hbar \left(\partial_\lambda \hat{U}(\boldsymbol{\lambda}) \right) \hat{U}^+(\boldsymbol{\lambda}) \quad (3.19)$$

$$\tilde{\mathcal{A}}_\lambda = -i\hbar \left(\partial_\lambda \hat{U}^+(\boldsymbol{\lambda}) \right) \hat{U}(\boldsymbol{\lambda}) \quad (3.20)$$

The adiabatic potentials can be shown to be Hermitian

$$\tilde{\mathcal{A}}_\lambda^+ = i\hbar U(\boldsymbol{\lambda})^+ \left(\partial_\lambda \hat{U}(\boldsymbol{\lambda}) \right) = -i\hbar \left(\partial_\lambda \hat{U}(\boldsymbol{\lambda})^+ \right) \hat{U}(\boldsymbol{\lambda}) = \tilde{\mathcal{A}}_\lambda, \quad (3.21)$$

analogically for non-tilde potential.

Using the eigenbasis of \hat{H} , the matrix elements are

$$\langle s | \tilde{\mathcal{A}}_\lambda | m \rangle = i\hbar \langle s | \hat{U}(\boldsymbol{\lambda})^+ \partial_\lambda \hat{U}(\boldsymbol{\lambda}) | m \rangle = i\hbar \langle s(\boldsymbol{\lambda}) | \partial_\lambda | m(\boldsymbol{\lambda}) \rangle. \quad (3.22)$$

and because

$$\langle s(\boldsymbol{\lambda}) | \hat{\mathcal{A}}_\lambda | m(\boldsymbol{\lambda}) \rangle = \langle s | \tilde{\hat{\mathcal{A}}}_\lambda | m \rangle, \quad (3.23)$$

we get

$$\hat{\mathcal{A}}_\lambda = i\hbar\partial_\lambda. \quad (3.24)$$

Full form of adiabatic potential in the theory of gauge symmetries is

$$\hat{\mathcal{A}}_\lambda = i\hbar(\partial_\lambda \hat{U}(\boldsymbol{\lambda})) \hat{U}^+(\boldsymbol{\lambda}) + \hat{U} \hat{\mathcal{A}} \hat{U}^{-1}. \quad (3.25)$$

The fact that second element is missing implies the zero space curvature

$$\chi_{jk}(\boldsymbol{\lambda}) = \partial_j A_k(\boldsymbol{\lambda}) - \partial_k A_j(\boldsymbol{\lambda}) = 0. \quad (3.26)$$

This formula is the same as Eq. 2.31. This means that adiabatic gauge transformations are class of gauge transformations with fidelity $F = 1$, meaning that if the system is driven by Hamiltonian $\hat{H}(\boldsymbol{\lambda})$ with fidelity $F < 1$, there exists such adiabatic potential \mathcal{A}_λ , that driving of the same system using $\hat{H} - \mathcal{A}_\lambda$ has unit fidelity.

The adiabatic gauge potentials can then be understood as affine connections defining the parallel transport on fiber bundle, if we define covariant derivative as

$$D_j := \partial_j + i\hat{\mathcal{A}}_j, \quad (3.27)$$

which yields $D_j |\psi_n\rangle = 0$ for every eigenstate, meaning the transport of eigenvalues on \mathcal{PM}_0 is parallel. $\hat{\mathcal{A}}_j$ is generally defined by Eq. 3.19, which gives non-zero covariant derivative for states not belonging to \mathcal{PM}_0 .

Calculating these potentials has many practical applications, so let's introduce one computational analytical procedure.

3.2 Driving on the ground state manifold

As was mentioned in the introduction of chapter 3, one method of achieving low driving fidelity is *path variation*. This means *finding the best possible driving path*. One might say that the ground state manifold geodesics are a good candidate for this path, because they minimize the distance. The problem is that general fidelity driving does not happen on any state manifold and this premise cannot be used. The natural question here is: “For which drivings do geodesics minimize the fidelity?”. The full role of geodesics is not yet known, but there are a few known cases in which they have particular meaning and which are demonstrated here.

3.2.1 Minimizing the distance on state manifolds

Let's have path \mathcal{J} defined in Eq. 3.1 and a geodesic $\mathcal{G}(\boldsymbol{\lambda}(t))$ with fixed boundary conditions

$$\mathcal{G}(0) = \mathcal{J}(0), \quad \mathcal{G}(T) = \mathcal{J}(T).$$

The driving on projective ground state manifold \mathcal{PM}_0 then consists of infinitesimal quenches over the distance ds . By integration over this path we get

the distance

$$s_{\mathcal{J}} = \int_{\mathcal{J}} ds = \int_0^T \sqrt{g_{jk} \dot{\lambda}^j \dot{\lambda}^k} dt \quad (3.28)$$

Let's state and prove the theorem demonstrating the importance of geodesics.

Theorem 7. *The distance described by formula 3.28 is minimized if \mathcal{J} is a geodesic.*

Proof. Functional of distance is

$$s = \int_0^T \sqrt{g_{jk} d\lambda^j d\lambda^k} = \int_0^T \sqrt{g_{jk} \frac{d\lambda^j}{dt} \frac{d\lambda^k}{dt}} dt =: \int_0^T \mathcal{L}(t, \lambda^j, \dot{\lambda}^j) dt \quad (3.29)$$

for

$$\mathcal{L} = \sqrt{g_{jk} \dot{\lambda}^j \dot{\lambda}^k}. \quad (3.30)$$

Using Euler-Lagrange equations

$$\frac{d\mathcal{L}}{d\lambda^j} - \frac{d}{dt} \frac{d\mathcal{L}}{d\dot{\lambda}^j} = 0, \quad (3.31)$$

we get for $g_{jk} = g_{jk}(\lambda)$ second order differential equation

$$\ddot{\lambda}^j + \Gamma_{ab}^j \dot{\lambda}^a \dot{\lambda}^b = 0 \quad \Gamma_{ab}^j = \frac{1}{2} g^{jk} (g_{ka,b} + g_{kb,a} - g_{ba,k}), \quad (3.32)$$

which is the Geodesic equation. \square

3.2.2 Minimizing the energy variance

The driving can be restricted to the ground state manifold only in approximation, such that the excited parts of wave-function can be neglected in every step. This fact is used for so-called *close adiabatic drivings*. The first theorem about geodesics is from Bukov et al. [2019].

Theorem 8. *For any fast-forward Hamiltonian⁴ $\hat{H}(\lambda(t))$ driven along one dimensional path $\lambda : \mathbb{R} \mapsto \mathbb{R}$ using time t as parametrization, there exist driving speed, for which the fidelity is close to one, $F(t) \approx 1$, $\forall t \in [0, T]$, and the energy fluctuations δE^2 , averaged along the path, are larger than the geodesic length l_λ*

$$\int_0^T \sqrt{\delta E^2(t)} dt =: l_t \geq l_\lambda := \int_{\lambda_i}^{\lambda_f} \sqrt{g_{\lambda\lambda} d\lambda d\lambda} = \int_0^T \sqrt{g_{\lambda\lambda}} |\dot{\lambda}| dt. \quad (3.33)$$

The length l_λ is defined in parametric space For energy variance it holds

$$\delta E^2 := \langle o(t) | \hat{H}(t)^2 | o(t) \rangle - \langle o(t) | \hat{H}(t) | o(t) \rangle^2 = \langle \partial_t o(t) | \partial_t o(t) \rangle_c = G_{tt}, \quad (3.34)$$

where in second equality the Schrödinger equation was used.

The Metric tensor in parametric space is defined as

$$g_{\lambda\lambda} := \langle \partial_\lambda o(t) | \partial_\lambda o(t) \rangle_c, \quad (3.35)$$

see chapter 2.6

⁴The system is driven to the target state in some fixed final time T .

Proof. The essential realization is

$$\delta E^2 \equiv \langle o(t) | \hat{H}(t)^2 | o(t) \rangle_c = \dot{\lambda}^2 G_{\lambda\lambda} + \mathcal{O}(\dot{\lambda}^4), \quad (3.36)$$

where $\mathcal{O}(\dot{\lambda}^4)$ needs to be positive for any real-valued Hamiltonian. This comes from the fact, that the system has instantaneous time-reversal symmetry. For details see Bukov et al. [2019]. \square

The conjecture can be extended to an arbitrary dimensional path. The main problem of this conjecture is the statement *close unit fidelity protocol*. It is not clear how good the approximation needs to be. This makes the statement much weaker, because it only states that *for any driving, there exist nonzero driving speed for which the energy variance is minimized on geodesics*.

3.2.3 Transport using quenches

Unifying the ground states $|o(\boldsymbol{\lambda})\rangle$ over all points $\boldsymbol{\lambda} \in \mathcal{U}$ in parametric space, we get the ground state manifold. Here the fidelity F and distance s are

$$ds^2 = 1 - F(\boldsymbol{\lambda} + \delta\boldsymbol{\lambda}, \boldsymbol{\lambda}) = 1 - |\langle o(\boldsymbol{\lambda} + \delta\boldsymbol{\lambda}) | o(\boldsymbol{\lambda}) \rangle|^2. \quad (3.37)$$

The final fidelity of transport on \mathcal{M} is then

$$F = \iint_{\mathcal{J}} g_{jk} d\boldsymbol{\lambda}^j d\boldsymbol{\lambda}^k = \int_{t_i}^{t_f} \underbrace{\int_{t_i}^{\tau} g_{jk} \frac{d\boldsymbol{\lambda}^j}{dt} \frac{d\boldsymbol{\lambda}^k}{dt} dt d\tau}_{\mathcal{L}(\boldsymbol{\lambda}, \dot{\boldsymbol{\lambda}}, \tau)}. \quad (3.38)$$

From Euler-Lagrange equations, the fidelity is minimized if \mathcal{J} is geodesic. It is worth mentioning the same problem as was with Theorem 8. It is only stated here that *there exist such slow driving, that the fidelity is minimized on geodesics*. Not how slow this driving needs to be.

Imagine at every point of transport that the fidelity is small enough, so for some small parameters $\Delta_i \in \mathbb{C}$ the transport over distance ds in eigenbasis at time $t = 0$ is

$$|o(\boldsymbol{\lambda}_i)\rangle \equiv \begin{pmatrix} Z_0(\boldsymbol{\lambda}_i) \\ 0 \\ \vdots \\ 0 \end{pmatrix} \xrightarrow{\text{transport } ds} |o(\boldsymbol{\lambda}_i + \delta\boldsymbol{\lambda})\rangle \equiv \begin{pmatrix} Z_0(\boldsymbol{\lambda}_i + \delta\boldsymbol{\lambda}) \\ 0 \\ \vdots \\ 0 \end{pmatrix} + \underbrace{\begin{pmatrix} 0 \\ \Delta_1(\boldsymbol{\lambda}_i + \delta\boldsymbol{\lambda}) \\ \vdots \\ \Delta_n(\boldsymbol{\lambda}_i + \delta\boldsymbol{\lambda}) \end{pmatrix}}_{\Delta(\boldsymbol{\lambda}_i + \delta\boldsymbol{\lambda})},$$

where the last term is neglected, because

$$\langle \Delta(\boldsymbol{\lambda}) | o(\boldsymbol{\lambda} + \delta\boldsymbol{\lambda}) \rangle \approx 0.$$

This might have interesting implication for slow transports, or small distance transports. For slow transports, this condition is hardly fulfilled, because one needs to neglect the sum of many of these terms. One possible way out of this is to reset the state into the ground-state when the fidelity would get too far from 1. This can be achieved by projecting the state $|\psi(t)\rangle$ to the ground state $|0(t)\rangle$

periodically, such that every time the fidelity is almost one. These small jumps are sometimes called *quenches*, and it can be achieved by introducing thermalization to the system.

If we imagine $\delta\lambda$ to be finite (not infinitely small, as the notation suggests), the *transport* means *doing a sequence of quenches and measuring the system after every quench*. This consequently leads to the unit fidelity transport.

3.3 Adiabatic perturbation theory

Until now, our interest was mostly in *unit fidelity protocols*. But how to calculate the case when the fidelity is “almost one”? This is the aim of *adiabatic perturbation theory*.

Following the article from Rigolin and Ortiz [2008], the wave-function can be approximated by series. Because every element is then decomposed into another series, we bear in mind the *locality of variables*, which clarifies the reason for performing this procedure. Let’s call variable $V(t)$ *local* if it does not depend on driving path. These variables are in shades of blue and *non-local* variables, written in shades of red, are usually expressed as an integral over driving path \mathcal{J} .

We are interested in the driving along path \mathcal{J} defined by Eq. 3.1, where t is time and T final time of the driving. Let the initial condition be

$$|\psi(0)\rangle =: |\psi_0\rangle \in \mathcal{PM}_0. \quad (3.39)$$

Solving the Schrödinger equation might seem like a straightforward solution at this point, but if the fidelity is close to 1, the approximate methods are in comparison with numerical methods relatively stable, and second, they can be used to obtain an analytical solution to the problem.

The power series is derived using a small parameter $v := 1/T$

$$|\Psi(t)\rangle = \sum_{p=0}^{\infty} v^p |\Psi^{(p)}(t)\rangle, \quad (3.40)$$

for

$$|\Psi^{(p)}(t)\rangle = \sum_{s=0}^{N-1} e^{-\frac{i}{v}\omega_s(t)} e^{i\gamma_s(t)} b_s^{(p)}(t) |s(t)\rangle. \quad (3.41)$$

Here we have

$$\text{dynamical phase } \omega_s(t) := \frac{1}{\hbar} \int_0^t E_s(\tau) d\tau, \quad (3.42)$$

$$\text{Berry phase } \gamma_s(t) := i \int_0^t \langle s(\tau) | \frac{d}{d\tau} s(\tau) \rangle d\tau \equiv i \int_0^t M_{ss}(\tau) d\tau \quad (3.43)$$

and $|s(t)\rangle$ are solutions to

$$\hat{H}(t) |s(t)\rangle = E_s(t) |s(t)\rangle. \quad (3.44)$$

Variables $\omega_s(t)$ and $\gamma_s(t)$ are defined using integration over the whole protocol, therefore they are *non-local variables*. The problem now lies in determining

$b_s^{(p)}(t)$, which is also **non-local**. Because it depends on its relative **geometric** and **dynamical phase** to other **energy levels**, let's write it as a series

$$b_s^{(p)}(t) = \sum_{m=0}^{N-1} e^{\frac{i}{v}\omega_{sm}(t)} e^{-i\gamma_{sm}(t)} b_{sm}^{(p)}(t), \quad (3.45)$$

where $\omega_{sm} := \omega_m - \omega_s$, $\gamma_{sm} := \gamma_m - \gamma_s$. The reason for **locality** of $b_{sm}^{(p)}(t)$ will be clear soon.

Inserting all to original series 3.40, we get

$$|\Psi(t)\rangle = \sum_{s,m=0}^{N-1} \sum_{p=0}^{\infty} v^p e^{-\frac{i}{v}\omega_m(t)} e^{i\gamma_m(t)} b_{sm}^{(p)}(t) |s(t)\rangle. \quad (3.46)$$

Because the initial state is an eigenstate of the Hamiltonian at time $t = 0$, we get initial condition $b_{sm}^{(0)}(t) = 0$. In addition, one can rewrite equation 3.46 to the iteratively solvable form

$$\frac{i}{\hbar} \Delta_{sm}(t) b_{sm}^{(p+1)}(t) + \dot{b}_{sm}^{(p)}(t) + W_{sm}(t) b_{sm}^{(p)}(t) + \sum_{k=0, k \neq s} M_{sk}(t) b_{km}^{(p)}(t) = 0, \quad (3.47)$$

for $\Delta_{sm}(t) := E_m - E_s$, $W_{sm}(t) := M_{ss}(t) - M_{mm}(t)$, where M_{ms} is defined in Eq. 3.43. We can see that $b_{ms}^{(p)}$, as a solution to Eq. 3.47, only depends on difference between energy levels, eigenstates during the path and their directional derivatives. Not on the path itself. All of those are easily obtained, once the driving path is prescribed.

4. Two level system

Before we move to more complicated Hamiltonian model, we investigate a simple two level system. To understand the general behavior of fidelity on Hamiltonian spectrum, two analytically solvable drivings — *geodesic* and *linear* — is investigated.

4.1 Hamiltonian

Let's have a Hamiltonian

$$\hat{H}(t) = \begin{pmatrix} \Omega(t) & \Delta(t) \\ \Delta(t) & -\Omega(t) \end{pmatrix} \quad (4.1)$$

for $\Omega : \mathbb{R}^+ \rightarrow \mathbb{R}$, $\Delta : \mathbb{R}^+ \rightarrow \mathbb{R}$ and time t . Its spectrum is

$$E_1(t) = -E_0(t) = \sqrt{\Omega^2(t) + \Delta^2(t)} \quad (4.2)$$

and using the eigenbasis

$$\mathcal{B} := \left\{ |0\rangle \equiv \begin{pmatrix} 1 \\ 0 \end{pmatrix}, |1\rangle \equiv \begin{pmatrix} 0 \\ 1 \end{pmatrix} \right\}, \quad (4.3)$$

the eigenvectors can be written as

$$|0(t)\rangle = N_+ \begin{pmatrix} 1 \\ \frac{E_0(t)+\Omega(t)}{\Delta(t)} \end{pmatrix}, \quad |1(t)\rangle = N_- \begin{pmatrix} 1 \\ \frac{E_1(t)+\Omega(t)}{\Delta(t)} \end{pmatrix} \quad (4.4)$$

for normalization constants $N_{\pm} := \left(\left(\frac{\pm E_0(t)+\Omega(t)}{\Delta(t)} \right)^2 + 1 \right)^{-1/2}$. Notice that the eigenbases differ in time, but are described using constant basis \mathcal{B} , which forms an eigenbasis at time $t = 0$.

The goal is to find *fidelity* $F_{\mathcal{J}}(t) := |\langle 0(t)|\psi(t)\rangle|^2$ of different driving protocols

$$\mathcal{J} := \{\boldsymbol{\lambda}(t) | t \in [0, T], \boldsymbol{\lambda} \in \mathcal{U}\} \subset \mathbb{R}^N. \quad (4.5)$$

For this we need to solve time Schrödinger equation

$$\hat{H}(t) |\psi(t)\rangle = i \frac{d}{dt} |\psi(t)\rangle \quad (4.6)$$

with time varying Hamiltonian $\hat{H}(\boldsymbol{\lambda}(t)) =: \hat{H}(t)$ and $\boldsymbol{\lambda}$ on path \mathcal{J} . For 2-dimentional system with

$$|\psi(t)\rangle =: \begin{pmatrix} a(t) \\ b(t) \end{pmatrix}, \quad (4.7)$$

we get the system of *two coupled differentials equations of the first order with non-constant coefficients*

$$\Omega(t)a(t) + \Delta(t)b(t) = i\dot{a}(t) \quad (4.8)$$

$$\Delta(t)a(t) - \Omega(t)b(t) = i\dot{b}(t) \quad (4.9)$$

with normalization

$$a^2(t) + b^2(t) = 1, \quad \forall t \in [0, T]. \quad (4.10)$$

and initial value

$$\begin{pmatrix} a(0) \\ b(0) \end{pmatrix} = |0(0)\rangle. \quad (4.11)$$

4.2 Harmonic oscillator correspondence

Coupled Equations 4.8, 4.9 have no general analytical solution, with an exception to a few easy protocols \mathcal{J} . Before moving to some of these special cases, let's analyze this coupled system of equations generally.

N-dimensional Schrödinger equation can be rewritten to *one differential equation of N^{th} order with non-constant coefficients*. In our two-dimensional case, this equation corresponds to *damped harmonic oscillator without external force*

$$0 = \ddot{a}(t) + \gamma(t)\dot{a}(t) + \omega^2(t)a(t) \quad (4.12)$$

$$\gamma(t) := -\frac{\dot{\Delta}(t)}{\Delta(t)} \quad (4.13)$$

$$\omega^2(t) := i \left(\dot{\Omega}(t) - \frac{\dot{\Delta}(t)}{\Delta(t)} \Omega(t) \right) + \Delta^2(t) + \Omega^2(t). \quad (4.14)$$

Along with normalization condition 4.10 and initial condition

$$\begin{pmatrix} a(0) \\ b(0) \end{pmatrix} = |0(0)\rangle; \quad \dot{a}(0) = -i(\Omega(0)a(0) + \Delta(0)b(0)). \quad (4.15)$$

Note that we used the condition $\Delta \neq 0$. Because the energy spectrum has $\Delta \leftrightarrow \Omega$ symmetry, we can change the driving by interchanging Δ and Ω on any intervals, where the parameters 4.13, 4.14 would diverge.

Classical mechanics correspondence

When solving differential equations, it might be useful to know some analogy to classical mechanics Lagrangian. Even though it is not used any further, let's quickly find it.

From the perspective of classical mechanics, meaning $x(t) := a(t)$ is a position in a phase space (x, p) , we can write classical Lagrangian from Eq. 4.12 as

$$\mathcal{L} = \frac{1}{2} \exp \left(\int_0^t \gamma(s) ds \right) (\dot{x}^2 - \omega^2(t)x^2) \quad (4.16)$$

Proof. The correspondence of Lagrangian 4.16 with Eq. 4.12 can be shown by direct evaluation of Euler-Lagrange equations

$$\begin{aligned} \frac{\partial \mathcal{L}}{\partial x} - \frac{d}{dt} \frac{\partial \mathcal{L}}{\partial \dot{x}} &= 0 \\ \frac{1}{2} \exp \left(\int_0^t \gamma(s) ds \right) (-2\omega^2(t)x) - \frac{d}{dt} \left(\exp \left(\int_0^t \gamma(s) ds \right) \dot{x} \right) &= 0 \\ -\omega^2(t)x - \gamma(t)\dot{x} - \ddot{x} &= 0. \end{aligned} \quad (4.17)$$

□

4.3 Energy variance for two level system

For two level system, the variance of wavefunction at time t

$$\delta E^2(t) := \langle \psi(t) | \hat{H}^2(t) | \psi(t) \rangle - \langle \psi(t) | \hat{H}(t) | \psi(t) \rangle^2 \quad (4.18)$$

can be rewritten inserting identity $\mathbb{1} = |0\rangle\langle 0| + |1\rangle\langle 1|$ around Hamiltonian. Omitting the time dependence of every element we get

$$\begin{aligned}
 \delta E^2 &= \langle \psi | \mathbb{1} \hat{H}^2 \mathbb{1} | \psi \rangle - \langle \psi | \mathbb{1} \hat{H} \mathbb{1} | \psi \rangle^2 \\
 &= \langle \psi | 0 \rangle \langle 0 | \hat{H}^2 | 0 \rangle \langle 0 | \psi \rangle + \langle \psi | 1 \rangle \langle 1 | \hat{H}^2 | 1 \rangle \langle 1 | \psi \rangle \\
 &\quad + \langle \psi | 0 \rangle \langle 0 | \hat{H}^2 | 1 \rangle \langle 1 | \psi \rangle + \langle \psi | 1 \rangle \langle 1 | \hat{H}^2 | 0 \rangle \langle 0 | \psi \rangle \\
 &\quad - \left(\langle \psi | 0 \rangle \langle 0 | \hat{H} | 0 \rangle \langle 0 | \psi \rangle + \langle \psi | 1 \rangle \langle 1 | \hat{H} | 1 \rangle \langle 1 | \psi \rangle \right. \\
 &\quad \left. + \langle \psi | 0 \rangle \underbrace{\langle 0 | \hat{H} | 1 \rangle}_{\propto \langle 0 | 1 \rangle = 0} \langle 1 | \psi \rangle + \langle \psi | 1 \rangle \underbrace{\langle 1 | \hat{H} | 0 \rangle}_{\propto \langle 0 | 1 \rangle = 0} \langle 0 | \psi \rangle \right)^2.
 \end{aligned} \tag{4.19}$$

Using Fidelity definition $F(t) = |\langle 0(t)|\psi(t)\rangle|^2$ and Schrödinger equation $\hat{H}|k\rangle = E_k|k\rangle$ we get a simplified formula for energy variance

$$\delta E^2(t) = F(t)(1 - F(t))(E_0(t) - E_1(t))^2. \tag{4.20}$$

For three level system we have $\mathbb{1} = |0\rangle\langle 0| + |1\rangle\langle 1| + |2\rangle\langle 2|$ and

$$\delta E^2 = \sum_{k=1}^3 E_k^2 F_k (1 - F_k) - 4 \prod_{k=1}^3 E_k F_k - 2F_0 F_1 E_0 E_1 - 2F_0 F_2 E_0 E_2 - 2F_1 F_2 E_1 E_2, \tag{4.21}$$

for $F_k := \langle k | \psi \rangle$, which has no practical simplification.

4.4 Geodesic driving

Some analytically solvable driving protocols are the *Geodesics* of projective ground state manifold.

Define driving in 3-dimensional space

$$d(t) \equiv \begin{pmatrix} \Omega(t) \\ \Xi(t) \\ \Delta(t) \end{pmatrix} := \begin{pmatrix} -s \cos(\omega(T)t) \\ 0 \\ s \sin(\omega(T)t) \end{pmatrix} \tag{4.22}$$

for *speed regulating function* $\omega(T) := \pi/T$. The reason for 3-dimensional driving is the possibility to use Pauli matrix formalism. Such defined drivings are half-spheres in the parametric space, see Fig. 4.1. Note that the driving velocity is constant in the parametric space and on the manifold.

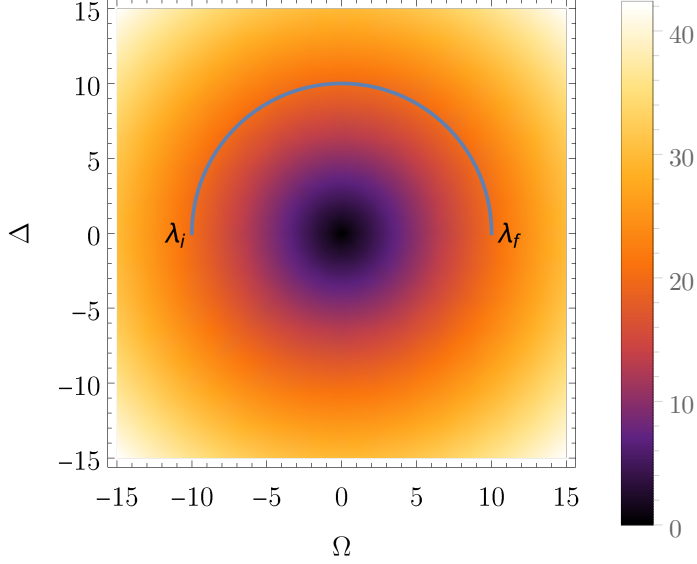


Figure 4.1: Driving along the geodesic. $\lambda_i \equiv (\Omega_i, \Delta_i)$ and $\lambda_f \equiv (\Omega_f, \Delta_f)$ are initial and final parameters respective. Density plot shows the difference between Hamiltonian eigenvalues.

4.4.1 Derivation of the fidelity

Because the Hamiltonian can be rewritten using Pauli matrices

$$\hat{H}(t) = \begin{pmatrix} -s \cos(t\omega) & s \sin(t\omega) \\ s \sin(t\omega) & s \cos(t\omega) \end{pmatrix} = \Delta(t)\sigma_x + \Omega(t)\sigma_z = d(t).\hat{\boldsymbol{\sigma}}, \quad (4.23)$$

for vector $\hat{\boldsymbol{\sigma}} := (\hat{\sigma}_1, \hat{\sigma}_2, \hat{\sigma}_3)^T$.

One can see that changing from the [original frame](#) with function $|\psi\rangle$ to [moving frame of reference](#), with $|\tilde{\psi}\rangle$ (let's omit the final time dependence $\omega = \omega(T)$ for a while) is described as

$$\psi(t) =: e^{\frac{i\omega}{2}\hat{\sigma}_y t} \tilde{\psi}(t). \quad (4.24)$$

This reflects the rotational symmetry of the system. The change of reference frame transforms Schrödinger equation as

$$\begin{aligned} \hat{H}(t)\psi(t) &= i\psi'(t) \\ \hat{H}(t)e^{\frac{i\omega}{2}\hat{\sigma}_y t}\tilde{\psi}(t) &= ie^{\frac{i\omega}{2}\hat{\sigma}_y t} \left(\frac{i\omega\hat{\sigma}_y}{2} \right) \tilde{\psi}(t) + ie^{\frac{i\omega}{2}\hat{\sigma}_y t}\tilde{\psi}'(t) \\ \underbrace{\left(e^{-\frac{i\omega}{2}\hat{\sigma}_y t} \hat{H}(t) e^{\frac{i\omega}{2}\hat{\sigma}_y t} + \frac{\omega}{2}\hat{\sigma}_y \right)}_{\hat{H}(t)} \tilde{\psi}(t) &= i\tilde{\psi}'(t). \end{aligned} \quad (4.25)$$

From this one can equivalently solve the Fidelity problem in this new coordinate system.

Hamiltonian in the moving frame is

$$\tilde{H} = \begin{pmatrix} -s & -i\omega(T)/2 \\ i\omega(T)/2 & s \end{pmatrix}, \quad (4.26)$$

which is time independent and depends only on final time. The Schrödinger equation can now be easily solved using evolution operator

$$\begin{aligned}\hat{U}(t) &= e^{-i\hat{H}t} \\ &= \begin{pmatrix} \cos\left(\frac{t}{2}q\right) + \frac{2is\sin\left(\frac{t}{2}q\right)}{q} & -\frac{\omega\sin\left(\frac{t}{2}q\right)}{q} \\ \frac{\omega\sin\left(\frac{t}{2}q\right)}{q} & \cos\left(\frac{t}{2}q\right) - \frac{2is\sin\left(\frac{t}{2}q\right)}{q} \end{pmatrix},\end{aligned}\quad (4.27)$$

for $q := \sqrt{4s^2 + \omega(T)^2}$.

In the original frame we get the evolution of the state $\psi(0)$

$$\psi(t) = e^{\frac{i\omega}{2}\hat{\sigma}_y t} \hat{U}(t) \tilde{\psi}(0) = \underbrace{e^{\frac{i\omega}{2}\hat{\sigma}_y t} \hat{U}}_{\hat{U}(t)} \underbrace{e^{-\frac{i\omega}{2}\hat{\sigma}_y t} \tilde{\psi}(0)}_{\psi(0)}. \quad (4.28)$$

The evolved wave-function the reads as

$$|\psi(t)\rangle = \begin{pmatrix} \cos\left(\frac{t}{2}q\right) + \frac{2is}{q} \cos(t\omega) \sin\left(\frac{t}{2}q\right) \\ \frac{\omega - 2is \sin(t\omega)}{q} \sin\left(\frac{t}{2}q\right) \end{pmatrix} \quad (4.29)$$

and the ground state

$$|0(t)\rangle = \mathcal{N} \begin{pmatrix} -\cot\left(\frac{t}{2}\omega(T)\right) \\ 1 \end{pmatrix}, \quad (4.30)$$

for a normalization constant $\mathcal{N} := |\langle 0(t) | 0(t) \rangle|^{-1}$. Fidelity during the transport is then¹

$$F = |\langle 0(t) | \psi(t) \rangle|^2. \quad (4.31)$$

Explicit formula for fidelity in time t and geodesic driving with final time T is finally

$$F(t, T) = \frac{\pi^2 \left(\cos\left(t\sqrt{\frac{\pi^2}{T^2} + 4s^2}\right) + 1 \right) + 8s^2 T^2}{2 \sin^4\left(\frac{\pi t}{2T}\right) (4s^2 T^2 + \pi^2) \left(\left| \cot\left(\frac{\pi t}{2T}\right) \right|^2 + 1 \right)^2}. \quad (4.32)$$

The domain can be extended from $t \in (0, T)$ to $[0, T]$ for any $T \in [0, \infty]$, because

$$\lim_{t \rightarrow 0} F = 1, \quad \lim_{T \rightarrow 0} F = 0.$$

Sometimes the *Infidelity*, defined as $F^* := 1 - F$, is used. It has a meaning of *excitation probability during the transport*.

4.4.2 Analysis of the infidelity formula

Infidelity can be calculated by numerical evolution of Schrödinger equation, or from Eq. 4.32. Sometimes both solutions are plotted for comparison between numerical precision.

For some fixed final time, the infidelity is an oscillating curve with values close to 0, see the driving for final time $T = 10$ on Fig. 4.2. The *final infidelity* (fidelity at $t = T$) dependence on final time T can be seen on Fig. 4.3 and 4.4.

¹If we calculated the fidelity in the [comoving frame](#), we would get exactly one. This realization leads to the counter-diabatic driving.

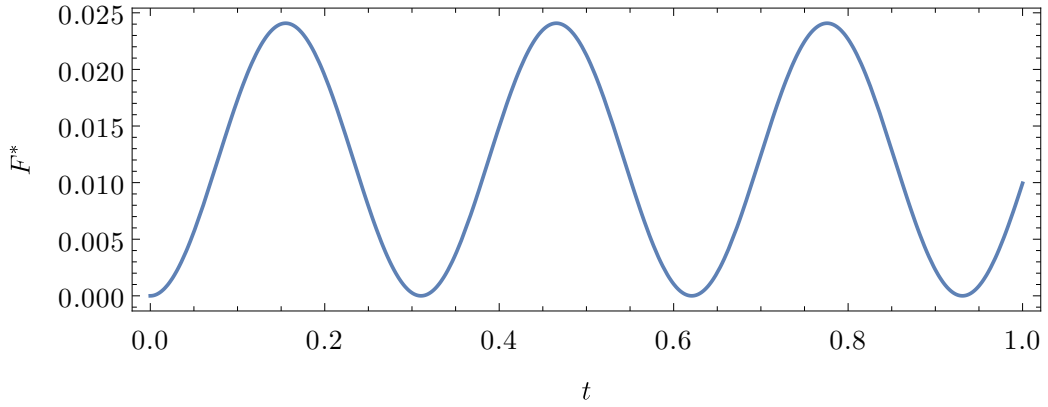


Figure 4.2: Infidelity in time for final time $T = 1$ for geodesical driving.

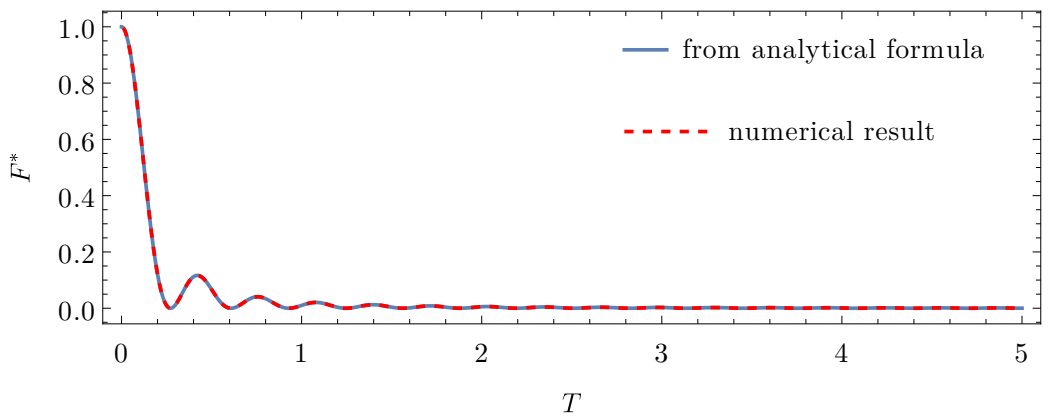


Figure 4.3: Final infidelity dependence on final time T for geodesical driving.

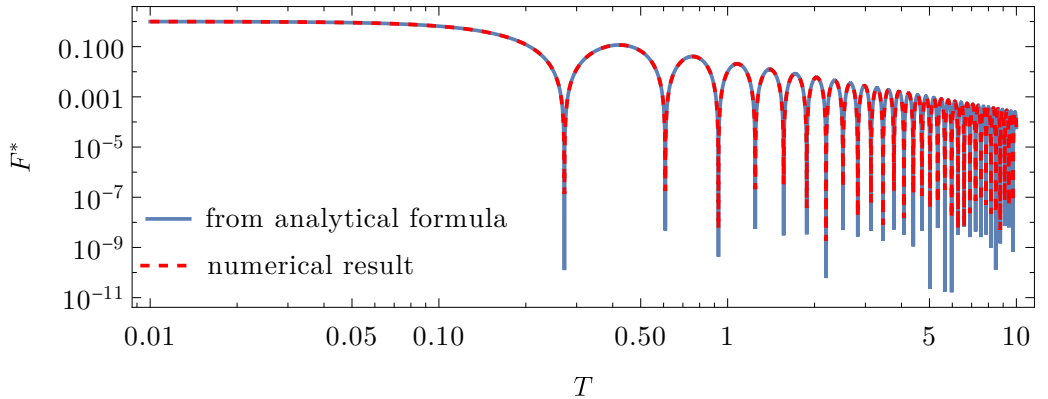


Figure 4.4: Infidelity dependence on final time in logarithmic scale. The difference in numerical precision of both methods can be seen in the spikes height. As it will be shown later, the spikes should go to zero, thus analytical formula has higher numerical precision.

From the fidelity formula 4.32 goes that condition $F = 1$ is equivalent to

$$\cos \left(\sqrt{T_s^2 + \pi^2} \right) = 1, \quad (4.33)$$

for $T_s := 2sT$. The solution to this equation is

$$T_s = \sqrt{(2\pi k)^2 - \pi^2} \text{ for } k \in \mathbb{N}, \quad (4.34)$$

see Fig. 4.5. This implies that spikes on Fig. 4.4 have minimal value $1 - F = 0$. In addition, observe that their density is linear in T .

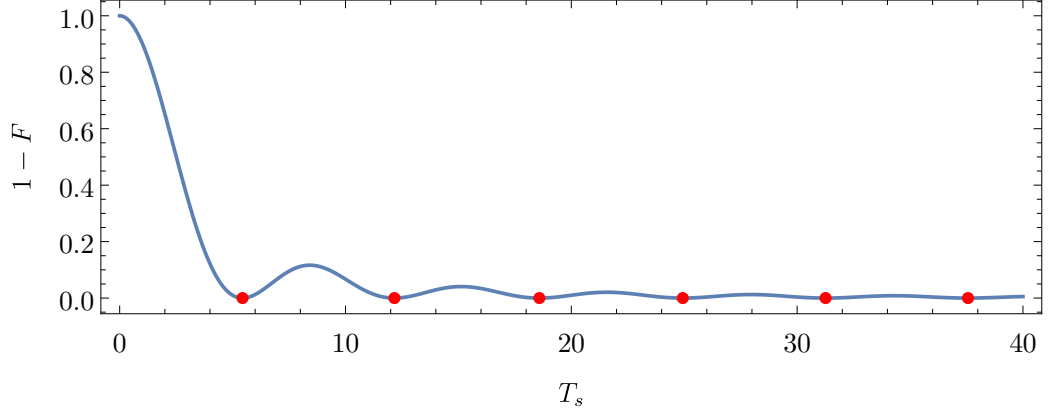


Figure 4.5: Rescaled final infidelity $T_s := 2sT$ dependence on final time. Red points mark the condition $F = 1$.

Fidelity as a function of time and final time can be seen in Fig. 4.6. Note that only $t < T$ has physical meaning.

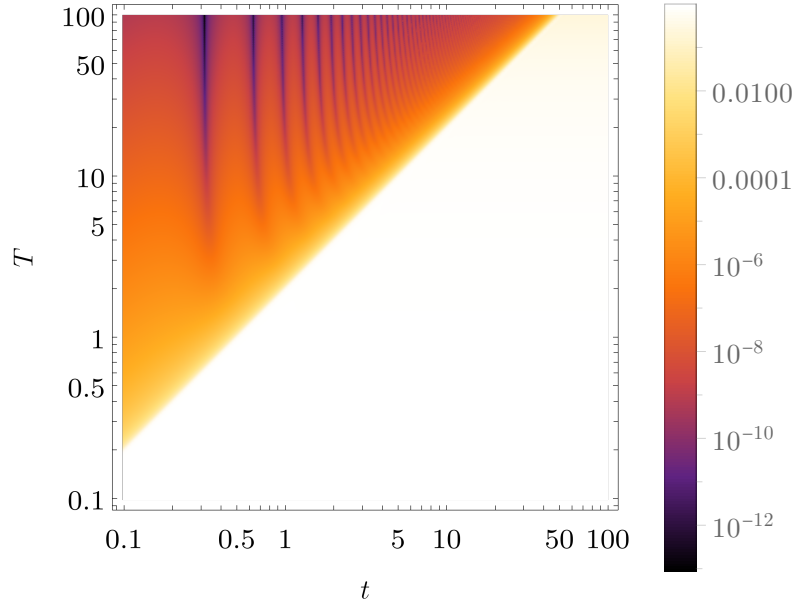


Figure 4.6: Fidelity dependence on time and final time in log-log scale. Note that only $t < T$ has physical meaning.

4.4.3 Energy variance

Another interesting quantity is the energy variance, specially because of Theorem 8. Evaluating the fidelity for geodesical driving gives a function of time t and

final time T

$$\begin{aligned} \delta E^2 = & \frac{s^2}{2q^2} \left[\left[16s^4 + 2s^2 \left((\omega^2 - 8s^2) \cos(2t\omega) - 8\omega^2 \cos^2(t\omega) \cos(t\sqrt{q}) \right) \right. \right. \\ & + 14s^2\omega^2 + \omega^4 \Big] - \omega^2 \left((2s^2 + \omega^2) \cos(2t\omega) - 2s^2 \right) \cos(2tq) \\ & \left. \left. + 8s^2\omega q \sin(2t\omega) \sin(tq) + \omega^3 q \sin(2t\omega) \sin(2tq) \right], \right] \end{aligned} \quad (4.35)$$

see the definition of q under Eq. 4.27. The result of energy variance can be seen on Fig. 4.7. Note that only $t < T$ has a physical meaning, therefore the dependence is smooth along the whole geodesical driving protocols.

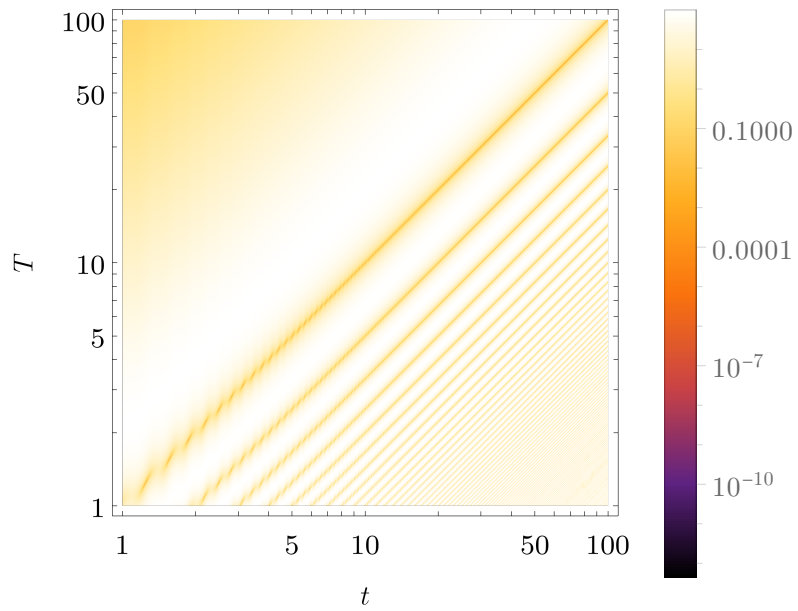


Figure 4.7: Energy variance for geodesical driving protocol, dependent on time t and final time T . Driving occurs only in area $t < T$.

4.5 Linear driving

Another analytically solvable driving is defined using two scaling parameters Ω_{sc} , Δ_{sc} , as

$$\Omega(t) = \Omega_{sc} \left(\frac{2t}{T} - 1 \right), \quad \Delta(t) = \Delta_{sc}, \quad \text{for } \Omega_{sc} = 10, \Delta_{sc} = 1, \quad (4.36)$$

see Fig. 4.8.

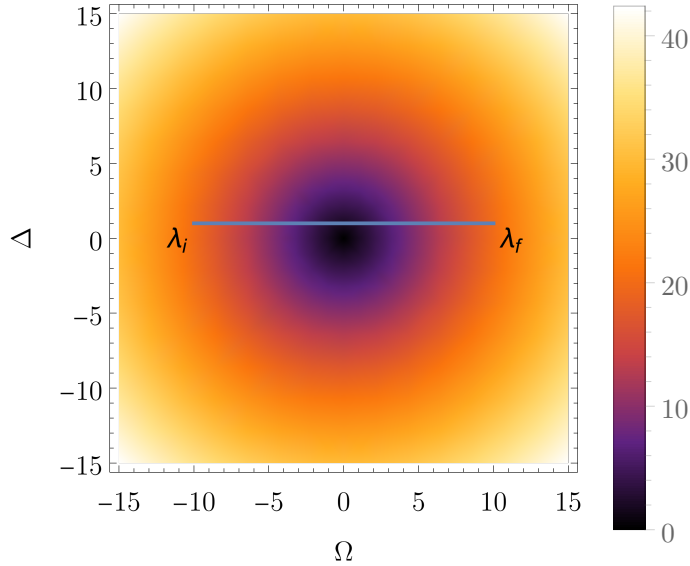


Figure 4.8: Driving along the linear path. $\lambda_i := (-10; 1)$ and $\lambda_f := (10; 1)$ are initial and final parameters respective. Density plot shows the difference between Hamiltonian eigenvalues.

From linear driving definition 4.36 and energy dependence 4.2 we have

$$\dot{\Delta}(t) = 0; \quad \Delta(t) \stackrel{\Delta(t) > 0}{=} \sqrt{\frac{E_{dif}^2(t)}{4} - \Omega^2(t)}; \quad E_{dif} := E_1 - E_0. \quad (4.37)$$

Substituting to Harmonic oscillator damping and frequency functions (Eq. 4.13 and 4.14) we get

$$\gamma(t) = 0 \quad (4.38)$$

$$\omega^2(t) = i \frac{2\Omega_{sc}}{T} + \frac{\Omega_{sc}}{4} \left(\frac{2t}{T} - 1 \right)^2 + \frac{\Delta_{sc}^2}{4} = i \frac{2\Omega_{sc}}{T} + \frac{E_{dif}^2(t)}{4}. \quad (4.39)$$

Corresponding differential equation of second order is

$$a''(t) + \omega^2(t)a(t) = 0, \quad (4.40)$$

which is of *Weber type*² with Parabolic Cylinder functions³ as a solution, see Matus et al. [2022].

²<https://mathworld.wolfram.com/WeberDifferentialEquations.html>

³<https://mathworld.wolfram.com/ParabolicCylinderFunction.html>

4.5.1 Dependence on time

The fidelity in time can be seen on Fig. 4.9. For $t \approx T/2$ Hamiltonian parameters change quickly which leads to fast state excitation. Then the Harmonic oscillator damping gets involved and oscillations are quickly going to zero, never disappearing entirely.

We can see that the final fidelity decreases with longer final time, which correctly leads to adiabatic driving, where $\lim_{T \rightarrow \infty} F^* = 0$. For short final times we can observe so called quench, $\lim_{T \rightarrow 0} F^* = 1$. The interesting phenomenon on this image are the oscillations around $t = T/2$, for which the frequency increases with longer final time.

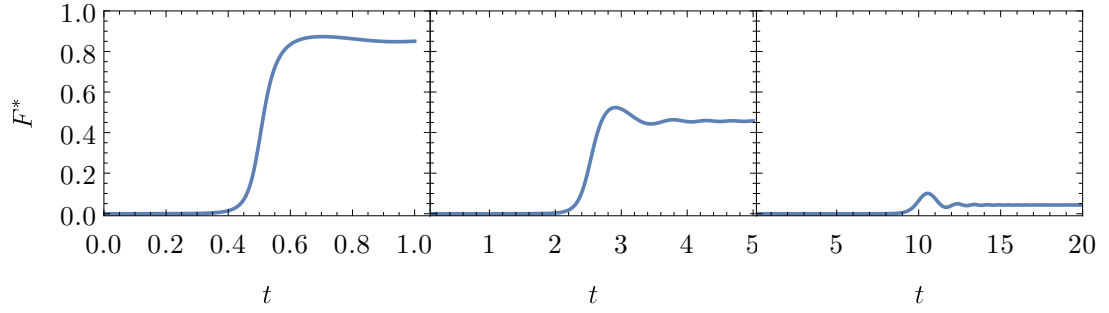


Figure 4.9: Infidelity in time for three final times $T \in \{1, 5, 20\}$ for the linear driving defined in 4.36.

Because in the Harmonic oscillator $\gamma(t) = 0$, the oscillations of $a(t)$ are not damped. What we are observing is infidelity

$$F^*(t) := 1 - |\langle 0(t)|\psi(t)\rangle|^2 = 1 - |\alpha(t)a(t) + \beta(t)b(t)|^2,$$

where the $|\psi(t)\rangle =: (a, b)^T$ represents the evolved state and $|0(t)\rangle =: (\alpha, \beta)^T$ evolved ground state in fixed eigenbasis \mathcal{B} . The ground state is not generally constant. In our case, the ground state described by Eq. 4.4 and is slowly changing its value from the first element α to the second element β , see Fig. 4.10. This means that at the beginning of driving, the projection to the ground state selects $b(t)$. Then it's getting more influenced by $a(t)$ until almost only $a(t)$ influences the fidelity.

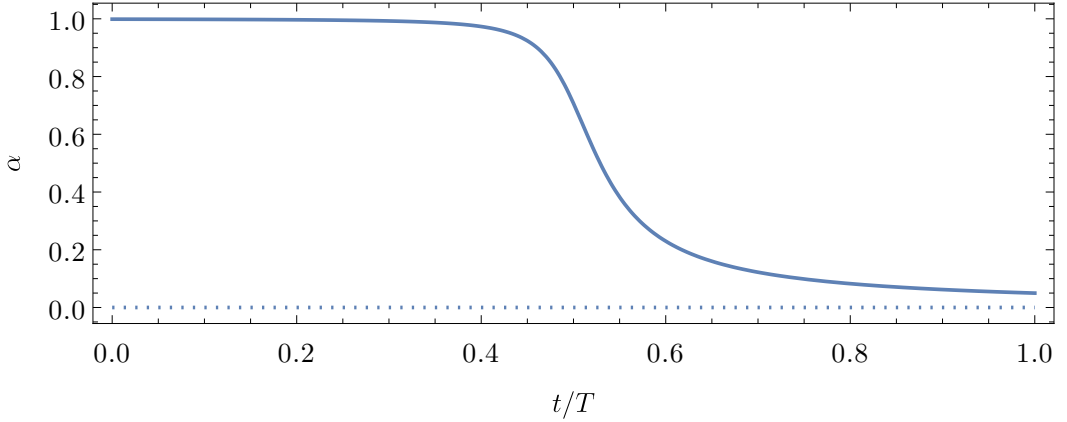


Figure 4.10: Value of first element of the ground state vector $\alpha \equiv |0(t)\rangle^1$ during linear driving.

Because of varying ground state during transport, the oscillations cannot be analyzed only from $\omega^2(t)$ described by Eq. 4.39. At the end of the driving we have

$$\frac{1}{N_+} |0(t)\rangle^1 = \frac{E_0(t) + \Omega(t)}{\Delta(t)} \gg 1 = \frac{1}{N_+} |0(t)\rangle^2, \quad (4.41)$$

leading to the *fidelity at the end of the driving*

$$F_{end} = \left| N_+ \left(\frac{E_0(t) + \Omega(t)}{\Delta(t)} a(t) + b(t) \right) \right|^2 \approx b^2(t), \quad (4.42)$$

therefore when t is getting close to T the fidelity is oscillating with harmonic oscillator frequency 4.14.

4.5.2 Final fidelity

Because the oscillations after fast parameter change in the Hamiltonian never disappear entirely, we must observe these oscillations even at the final time. *Final fidelity* (meaning the fidelity at $t = T$) has dependence on T as can be seen in Fig. 4.11. Because after the final time $T \approx 120$ the values are so small, we can observe some fine structure of the fidelity, along with numerical error artifacts.

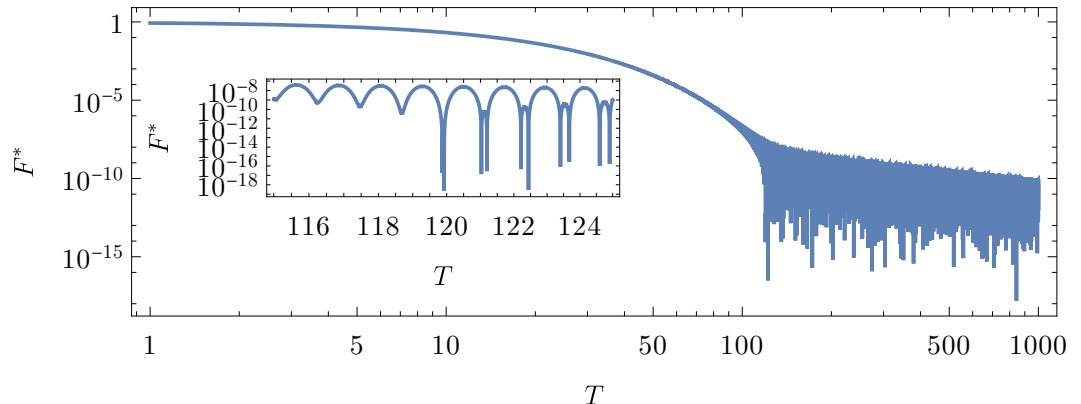


Figure 4.11: Final infidelity as a function of T with zoom on the transitional part.

First, the numerical precision of this calculation was found to be around 10^{-13} . This means that the oscillations we see on Fig. 4.11 are of physical origin with some additional numerical error. In fact these small oscillations are the remnants of the fast excitation during close approach of energy levels, see Fig. 4.9.

Averaged final fidelity

We can eliminate the effect of oscillations by averaging over time. For that we define the *average final infidelity*

$$\langle F^* \rangle_p(T) := \frac{1}{(1-p)T} \int_{(1-p)T}^T F^*(t) dt. \quad (4.43)$$

It turned out that averaging over 1 % ($p = 0.01$) or 10 % ($p = 0.1$) of the driving gave approximately the same results for long enough drivings ($T \gtrsim 10$). The same result can be obtained from analytical continuation of the fidelity formula to $t \rightarrow \infty$. This analytical continuation of harmonic oscillator solution leads to the Fidelity value around which the oscillations occur. The result of averaging can be seen on Fig. 4.12.

Using this we can describe the driving using three regimes⁴.

- *Exponential/fast-driving regime* — $\langle F^* \rangle_p = \exp(-\xi T)$, $\xi \in \mathbb{R}^+$
- *transitional regime* — happens around *critical time* T_c .
- *Polynomial/close-adiabatic regime* — $\langle F^* \rangle_p \propto T^{-\kappa}$ for $\kappa \in \mathbb{R}^+$.

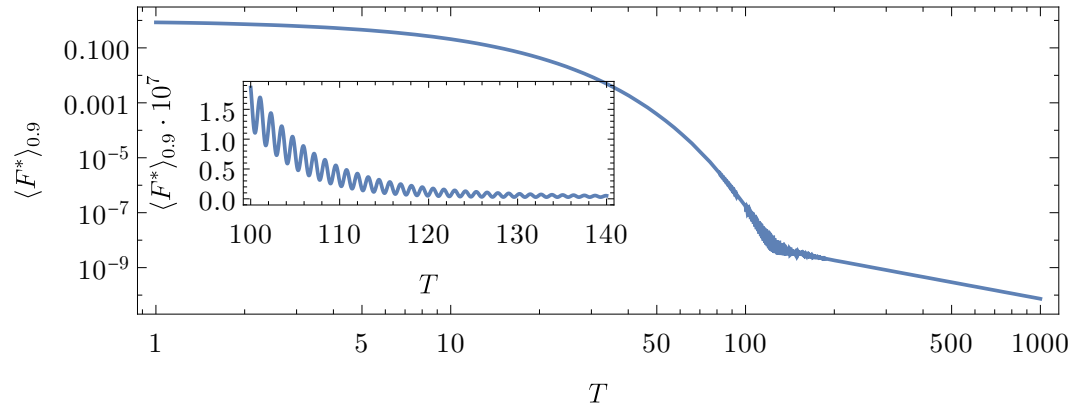


Figure 4.12: Final infidelity as a function of T in log-log scale with linear scaled plot inserted.

The boundary between exponential and linear regime is not strict and can be seen on Fig. 4.13, as transition between *smooth* and *chaotic* regimes. This happens around $t = T_c$. The fine structure, see Fig. 4.14, is caused by the oscillatory

⁴The coefficient p is assumed to be small enough not to cover the biggest oscillations after $t = T/2$ and big enough to average over sufficient number of oscillations. Approximately $p \in [0.6T, 0.999T]$.

character of the final fidelity. This would be smoothed out using the averaged final fidelity. The approximated dependence for final time was numerically estimated as

$$T_c \tilde{\propto} \Delta_{sc}^{-2}. \quad (4.44)$$

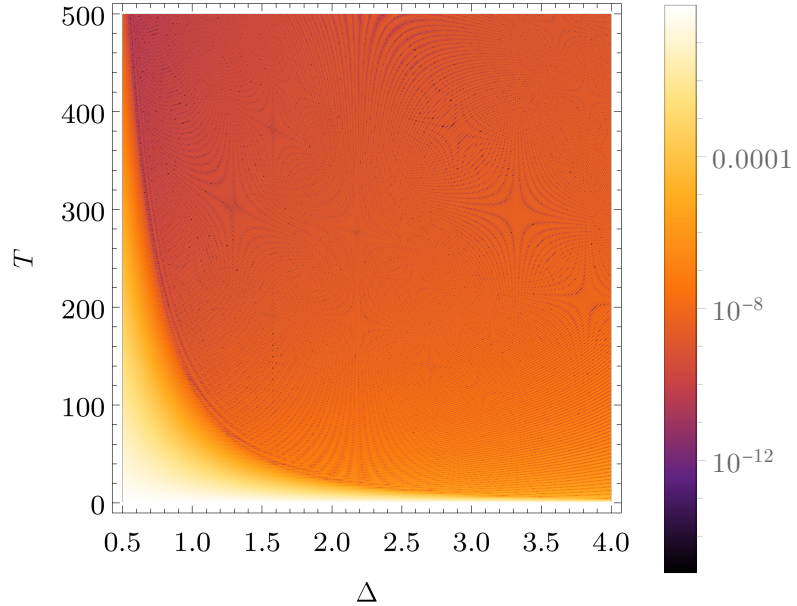


Figure 4.13: Final infidelity as a function of Δ and T and its three regimes. Zoomed boundary between them can be seen on 4.14.

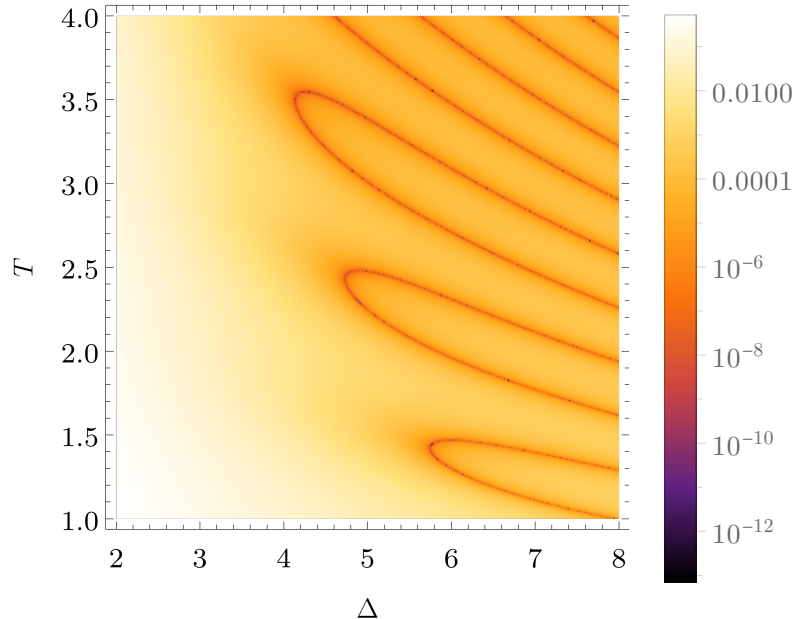


Figure 4.14: Fine structure of the boundary between fast-driving and adiabatic regimes of final infidelity.

To understand the infidelity oscillations, compare Fig. 4.15 with 4.16. Here

we see two regimes, one for $t < T_c$ and on for $T > T_c$. The important observation is that in the first case $F^* \neq 0$ for all $t > 0$ and in the second case it touches zero periodically. The fidelity can be decomposed into a sum of two elements. Small oscillatory part, which can be explained by the theory of APT, and exponentially decreasing fidelity with final time, describable by Landau-Zener formula.

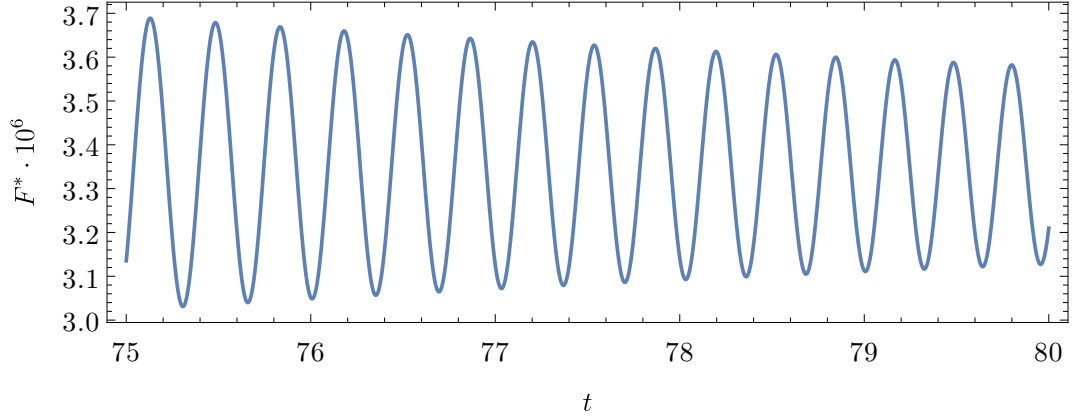


Figure 4.15: Infidelity as function of time for fast-driving regime, $T = 80 < T_c$.

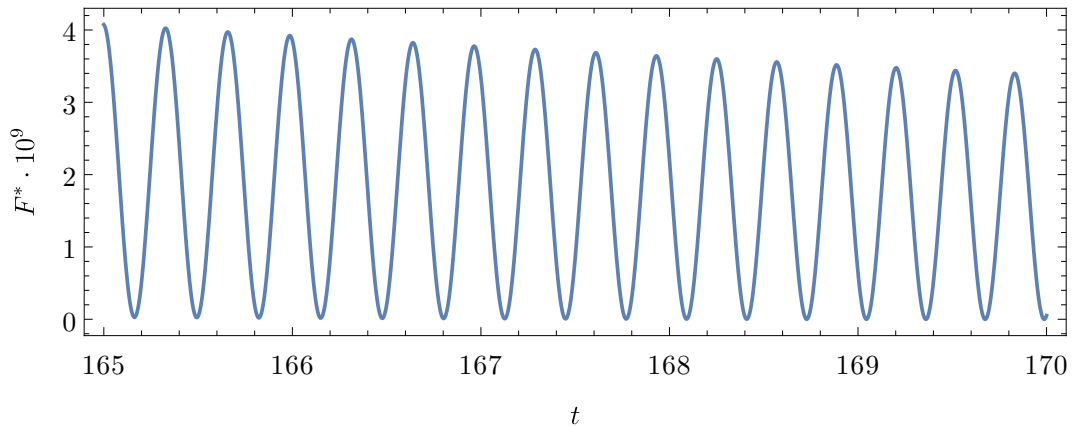


Figure 4.16: Infidelity as function of time for close-adiabatic regime. $T = 170 > T_c$

Exponential and polynomial part, Landau-Zener and APT

Landau-Zener-Stueckelberg theory provides the WKB approximation formula for the fidelity during some transport. Full form can be seen in Nakamura [2012]. In our case, only simplified theorem is needed. First let's review some definitions.

Definition 16 (Diabatic coupling). *Diabatic coupling functions are off-diagonal elements of two-level Hamiltonian. At avoided crossing, it is half of Hamiltonian eigenvalue difference,*

$$A = \frac{E_2 - E_1}{2}. \quad (4.45)$$

Definition 17 (Diabatic potential). *Difference between Hamiltonian eigenvalues can be linearly approximated as*

$$\Delta E \equiv E_1 - E_0 =: \alpha t \quad (4.46)$$

Diabatic potential difference is the ratio

$$|\Delta F| := \left| \frac{\alpha}{t} \right|. \quad (4.47)$$

Theorem 9 (Landau-Zener-Stueckelberg (LZS) for linear driving). *For*

- *two level Hamiltonian*
- *with degeneracy in only one point,*
- *on the linear driving path in a parametric space*

the fidelity can be described for times $t \in (0, T_c)$ as

$$F = \exp \left(-\frac{2\pi A^2}{v|\Delta F|} \right), \quad (4.48)$$

for a diabatic coupling A , and diabatic potential difference $|\Delta F|$.

In our case, we have constant speed $v = 1/T$, off-diagonal elements are also constant $A = \Delta_{sc}$, and the driving path is symmetric along $\Omega = 0$ axis, leading to $|\Delta F| = 2\Omega_i$.

The polynomial, or chaotic regime, can be explained using APT. It holds that

$$\log(F^*) = \log(T^{-2}) + \log \left(\sum_{i=1}^n |b_n^{(1)}(T)|^2 \right), \quad (4.49)$$

for functions $b_n^{(1)}$ from Eq. 3.45. For more details, see Matus et al. [2022].

The LZS approximation can be seen on Fig. 4.17. The LZS and APT approximations give the leading order in corresponding regimes (omitting the oscillations) and intersect at time T_c . In fact these two parts are not only the good approximation on both intervals, but if added together, they represent the whole fidelity curve with very high precision. It might not give a good mathematical meaning to add these two solutions together. But because the APT gives the infidelity of order 10^{-9} , it creates negligible error. The advantage is that by this process one gets suitable approximation for the transitional regime.

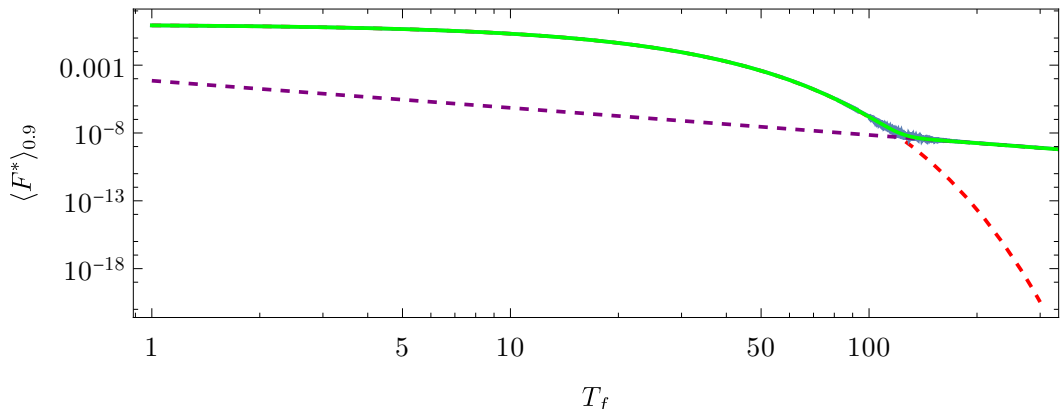


Figure 4.17: Fidelity as a function of driving final time, approximated by the **sum** (green) of Landau-Zener (red, dashed) and APT (purple, dashed)

4.5.3 Summary of linear driving

Now we understand all results separately, let's put it all together. On Fig. 4.18 the most important results can be seen. The difference in the close adiabatic regime and fast regime at the end of the driving is if $F^* = 0$. The chaotic regime is below $t = T$ line for $T < T_c$ and the chaotic cone is crossing this line around $t = T_c$.

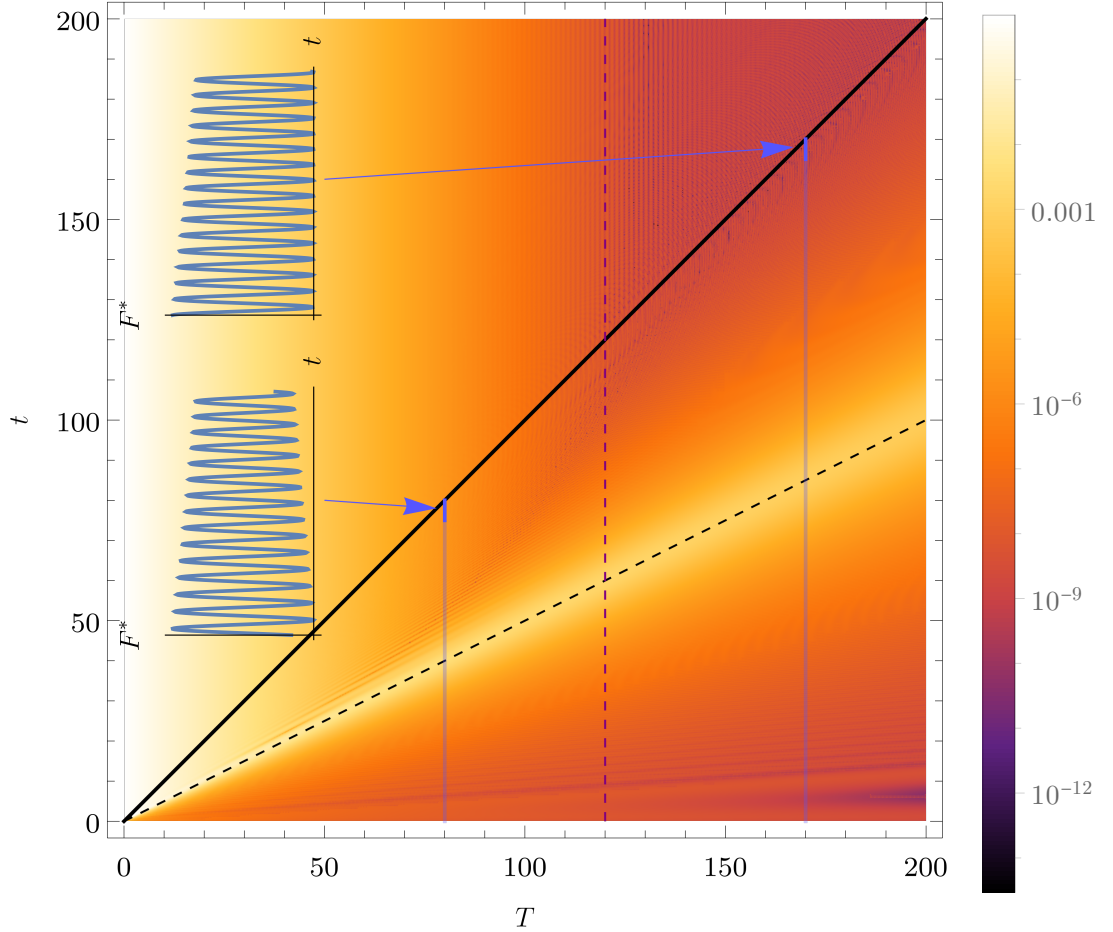


Figure 4.18: Fidelity dependence for linear driving with $\Delta = 1$. Black line marks $t = T$, dashed black line $t = T/2$ and purple dashed line is the approximate value of T_c . Blue lines marks driving from Fig. 4.15, 4.16, visualizing the final times of the driving.

4.5.4 Energy variance

Analogically to the geodesical driving, one might be interested in energy variance. In the linear driving case, the analytical formula is more complicated and only numerical result are displayed here. On Fig. 4.19 the energy variance is plotted as a function of time and final time.

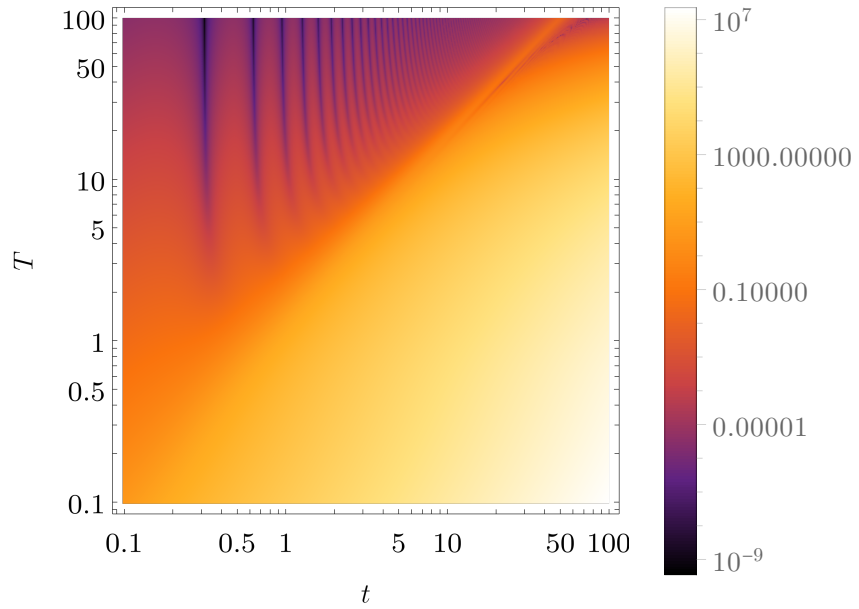


Figure 4.19: Energy variance for $\Delta_{sc} = 0.2$ for linear driving. Note that only $t < T$ has physical meaning.

5. Lipkin-Meshkov-Glick model

The Lipkin-Meshkov-Glick (LMG) model is a simple model manifesting the quantum phase transitions. It represents a many-body fermion system. The aim of this chapter is to understand the properties of the ground state and observe its influence on different driving protocols.

The model is defined by Hamiltonian

$$\hat{H}(\lambda, \chi) = \hat{J}_3 + \lambda \hat{V}_1 + \chi \hat{V}_2 + \chi^2 \hat{V}_3, \quad (5.1)$$

where

$$\hat{V}_1 := -\frac{1}{2j} \hat{J}_1^2 \quad (5.2)$$

$$\hat{V}_2 := -\frac{1}{2j} [\hat{J}_1(\hat{J}_3 + j\mathbb{1}) + (\hat{J}_3 + j\mathbb{1})\hat{J}_1] \quad (5.3)$$

$$\hat{V}_3 := -\frac{1}{2j} (\hat{J}_3 + j\mathbb{1})^2. \quad (5.4)$$

Parametric space here is $\boldsymbol{\lambda} \equiv (\lambda; \chi) \in \mathcal{U} := \mathbb{R}^2$ and Hamiltonian is real-valued.

Using the Spherical harmonics¹ basis $\{|j, m\rangle\}$ for quantum numbers j as the angular momentum and m its projection to the direction of \hat{J}_3 . Defining

$$\hat{J}_{\pm} := \frac{1}{2} (\hat{J}_1 \pm i\hat{J}_2), \quad (5.5)$$

we get matrix elements

$$\langle j'm' | \hat{J}^2 | jm \rangle = j(j+1)\delta_{j'j}\delta_{m'm} \quad (5.6)$$

$$\langle j'm' | \hat{J}_3 | jm \rangle = m\delta_{j'j}\delta_{m'm} \quad (5.7)$$

$$\langle j'm' | \hat{J}_{\pm} | jm \rangle = \sqrt{(j \mp m)(j \pm m + 1)} \delta_{j'j}\delta_{m'm \pm 1}, \quad (5.8)$$

where $\delta_{a'b}$ is Kronecker delta. The Hamiltonian in Eq. 5.1 can be written as

$$\begin{aligned} \hat{H} = & J_3 - \frac{\lambda}{8j} (J_+ + J_-)^2 - \frac{\chi}{4j} [(J_+ + J_-)(J_3 + j\mathbb{1}) + (J_3 + j\mathbb{1})(J_+ + J_-)] \\ & - \frac{\chi^2}{2j} (J_3 + j\mathbb{1})^2, \end{aligned} \quad (5.9)$$

which has pentadiagonal matrix representation. During the whole chapter, $j = N/2$ is used.

5.1 Geometry for fixed dimension

Because of pentadiagonal form of the Hamiltonian, the discussion starts at $N = 3$, followed by $N = 5$. Then the limit $N \rightarrow \infty$ is taken along with the generalization of some characteristics to an arbitrary dimension.

Due to the complexity of our Hamiltonian, it is not possible to prove every statement analytically. Some numerical methods, supported by mathematical theorems, are therefore used.

¹<https://mathworld.wolfram.com/SphericalHarmonic.html>

5.1.1 3-dimensional Hamiltonian

The lowest dimension behaving similarly to higher N is 3. The matrix represented Hamiltonian is

$$\hat{H} = \begin{pmatrix} -\frac{\lambda+6}{4} & -\frac{\chi}{2\sqrt{3}} & -\frac{\lambda}{2\sqrt{3}} & 0 \\ -\frac{\chi}{2\sqrt{3}} & \frac{(-7\lambda-4\chi^2-6)}{12} & -\chi & -\frac{\lambda}{2\sqrt{3}} \\ -\frac{\lambda}{2\sqrt{3}} & -\chi & \frac{(-7\lambda-16\chi^2+6)}{12} & -\frac{5\chi}{2\sqrt{3}} \\ 0 & -\frac{\lambda}{2\sqrt{3}} & -\frac{5\chi}{2\sqrt{3}} & -\frac{\lambda}{4} - 3\chi^2 + \frac{3}{2} \end{pmatrix}. \quad (5.10)$$

The spectrum of this Hamiltonian can be calculated analytically using some complex functions $D, E, F, G : \mathbb{C} \rightarrow \mathbb{C}$, see Appendix B, as

$$E_0 = \frac{1}{12} \left(G - F - \frac{\sqrt{D - E}}{2} \right) \quad (5.11)$$

$$E_1 = \frac{1}{12} \left(G - F + \frac{\sqrt{D - E}}{2} \right) \quad (5.12)$$

$$E_2 = \frac{1}{12} \left(G + F - \frac{\sqrt{D + E}}{2} \right) \quad (5.13)$$

$$E_3 = \frac{1}{12} \left(G + F + \frac{\sqrt{D + E}}{2} \right). \quad (5.14)$$

Eigenvectors can also be expressed analytically, but due to their complexity only analytical results are presented here. On sections $\lambda = 1$ and $\chi = 1$ (see energy spectrum on Figures 5.1 and 5.2 respective), the energies get close to each other somewhere around the center of our coordinate system $(\lambda; \chi)$ and then separate monotonously to never meet again. In addition, the spectrum has $\chi \leftrightarrow -\chi$ symmetry.

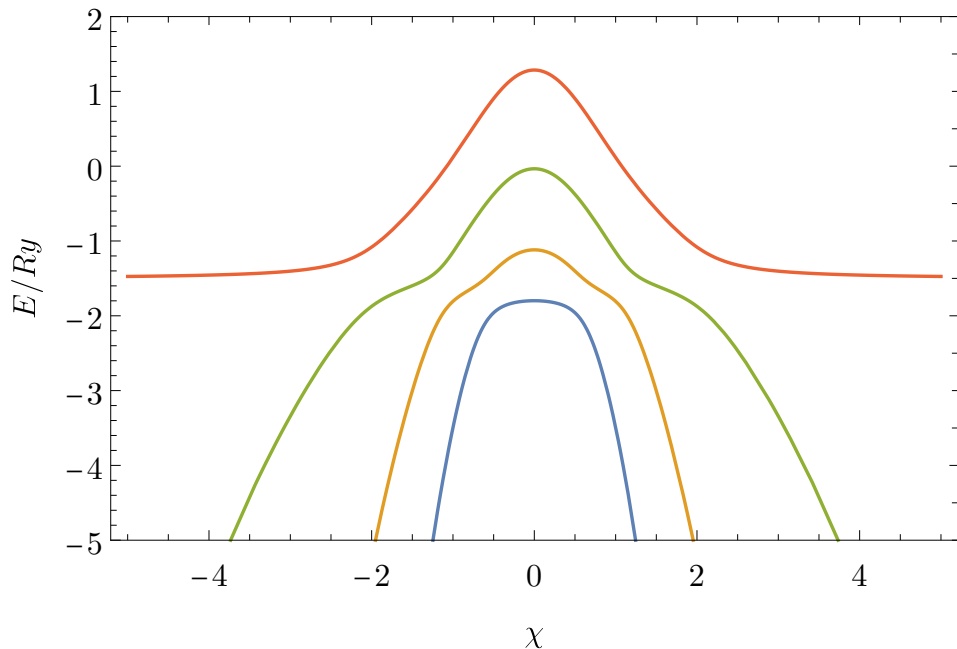


Figure 5.1: Energy spectrum for $N = 3$, section $\lambda = 1$

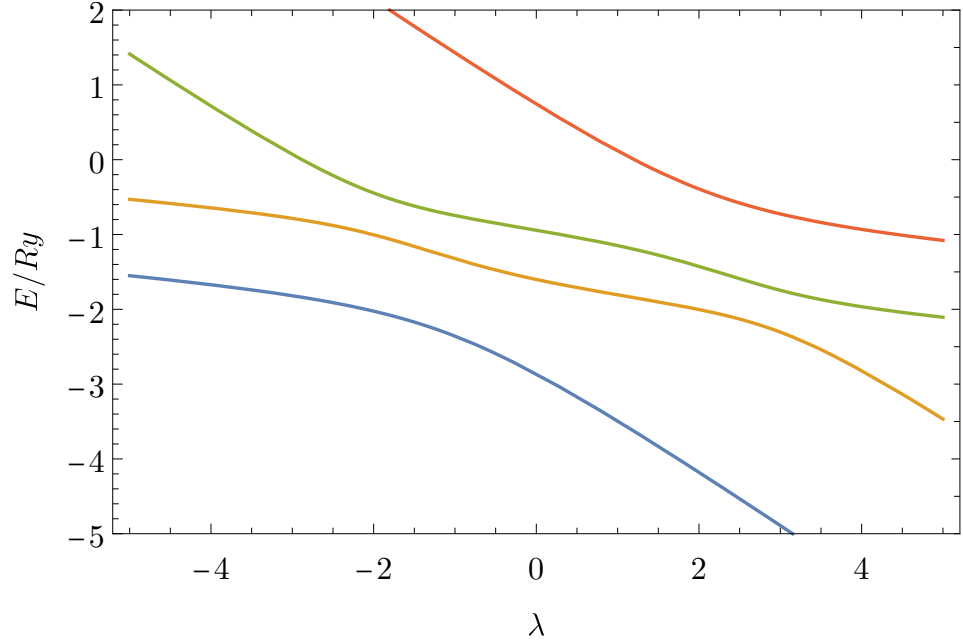


Figure 5.2: Energy spectrum for $N = 3$, section $\chi = 1$

From Eq. 5.11, 5.12 can be seen the possible existence of spectrum degeneracies between every two neighboring energy levels². Degeneracy $E_0 = E_1$ holds for $D = E$, which for real values λ , χ has two solutions

$$(\lambda_d, \pm\chi_d) = \left(-\frac{1}{2}; \sqrt{\frac{3}{5}} \right).$$

According to Theorem 1, Hamiltonian driven by two real parameters can be degenerated only on 0-dimensional manifolds. This means that degeneracies can be only separated points in the parametric space.

If the energy spectrum is degenerate and the metric tensor diverges, see individual elements in Fig. 5.3, its determinant also diverges, as shown in Fig. 5.4, along with Christoffel symbols in Fig. 5.5. Note that the metric tensor determinant is positive definite, thus the manifold is Riemannian. Further on, it reflects the symmetry $\chi \leftrightarrow -\chi$, except for elements g_{12} , Γ_{121} , Γ_{211} , and Γ_{222} , which switch their sign.

²If the functions D, E, F, G were into real numbers, degeneracies would exist between every two neighboring energy levels. Because they are complex, the solution $E_i = E_j$ might not exist. From numerical results, degeneracies exist between every two neighboring energy levels.

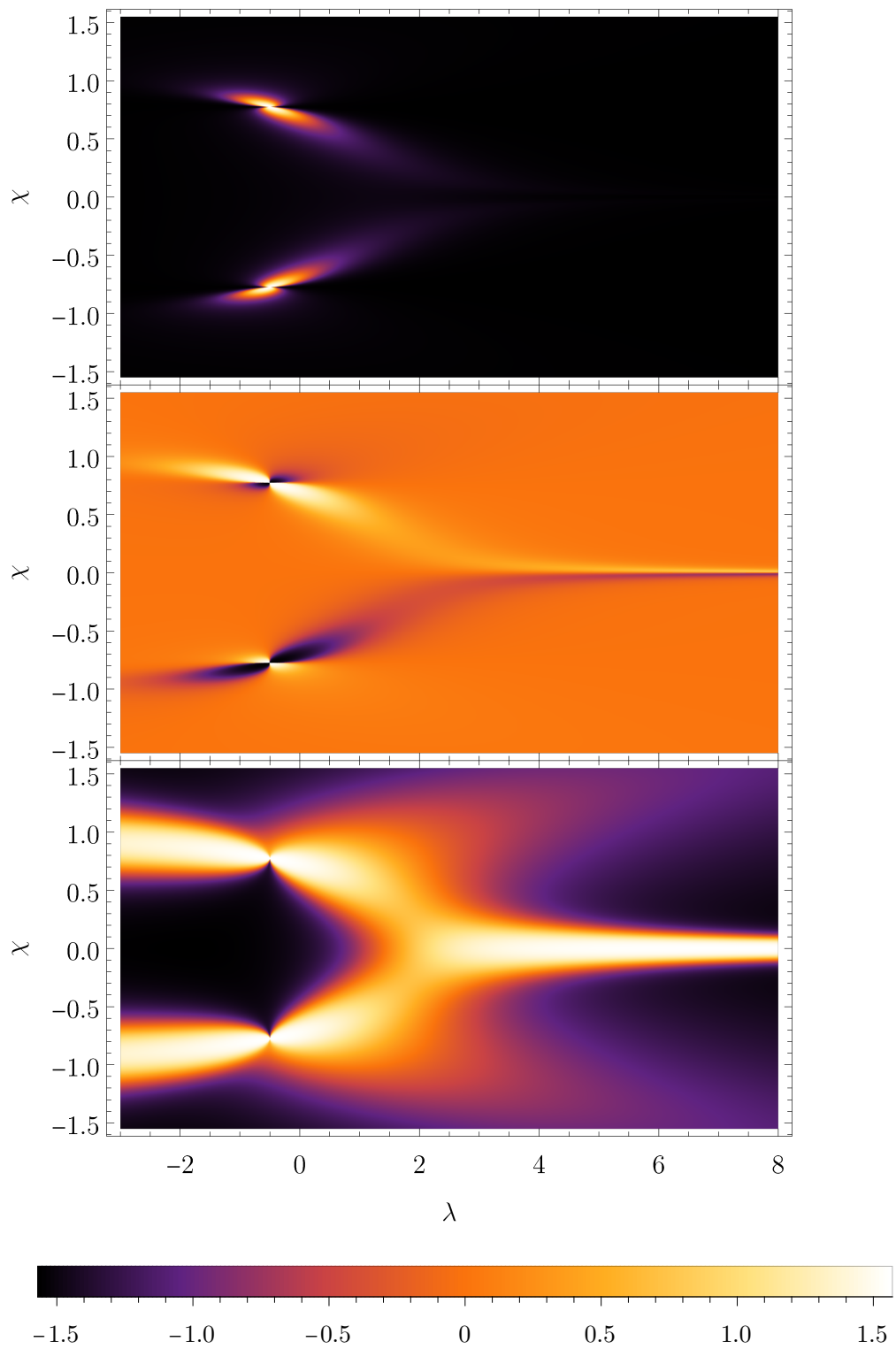


Figure 5.3: Arctangent of the metric tensor elements for $N = 3$ in the parametric space. From the top: $\arctan(g_{11})$, $\arctan(g_{12}) = \arctan(g_{21})$, $\arctan(g_{22})$

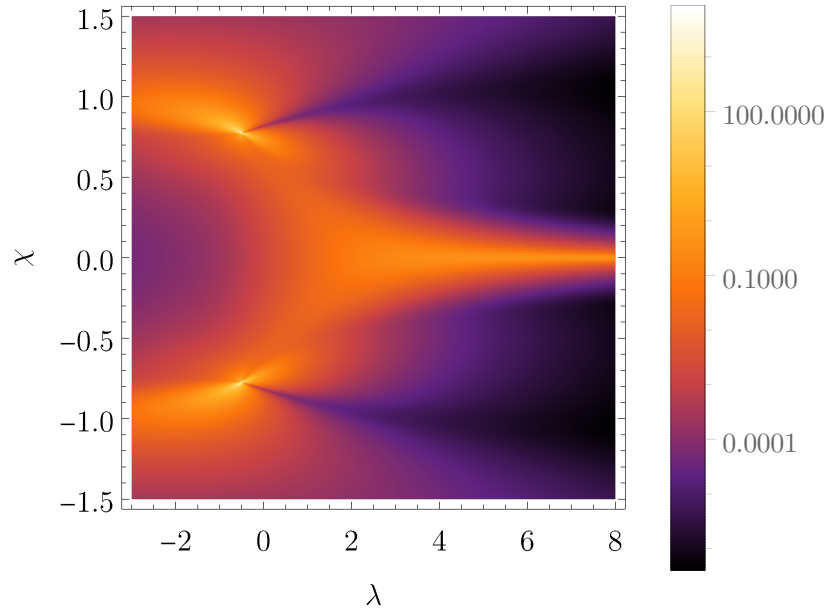


Figure 5.4: Ground state metric tensor determinant in a parametric space for $N = 3$.

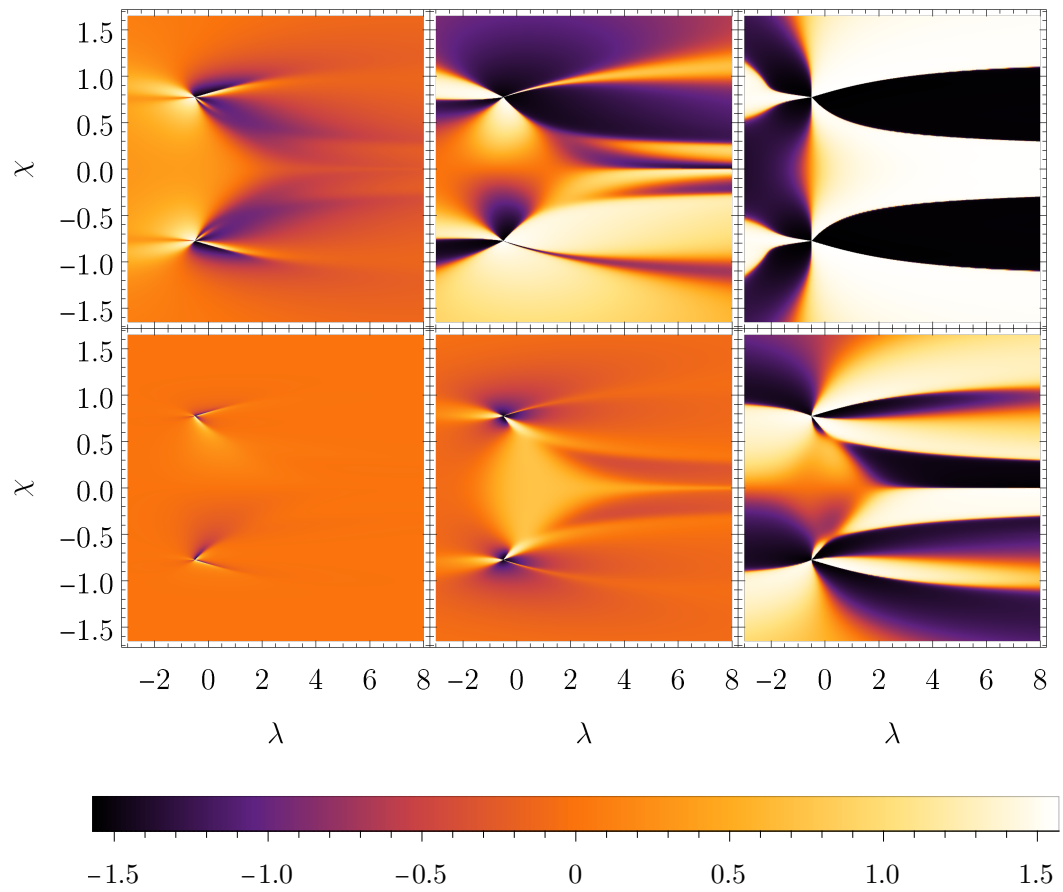


Figure 5.5: Arctangent of the ground state Christoffel symbols for $N = 3$. First row from left: $\arctan(\Gamma_{111})$, $\arctan(\Gamma_{121})$, $\arctan(\Gamma_{122})$. Second row from left: $\arctan(\Gamma_{211})$, $\arctan(\Gamma_{221})$, $\arctan(\Gamma_{222})$.

Due to the metric tensor degeneracy, the space is not geodesically maximal. To see that the singularity is not only *coordinate one*³, the Ricci scalar can be calculated, see Fig. 5.6. Divergent Ricci scalar implies the singularity is physical. This can be seen from sections in χ -direction drawn in Fig. 5.7, which at coordinate $(\lambda_d; \chi_d)$ diverges. This implies the singularity is *physical*.

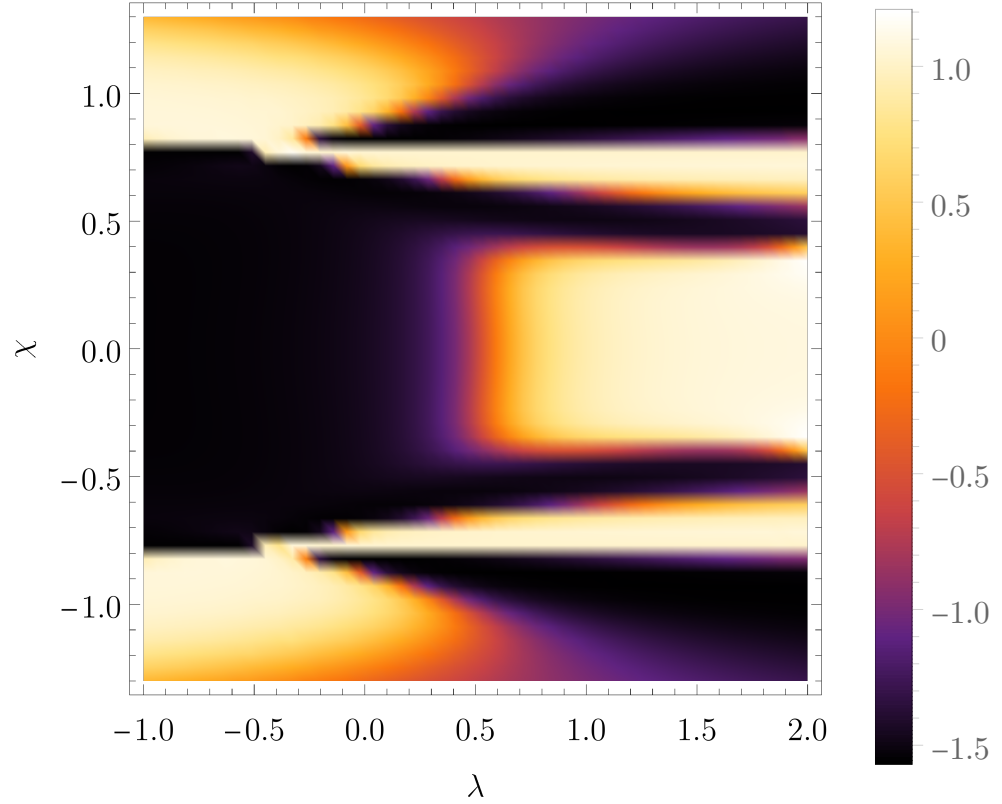


Figure 5.6: Arctangent of Ricci curvature for the case $N = 3$.

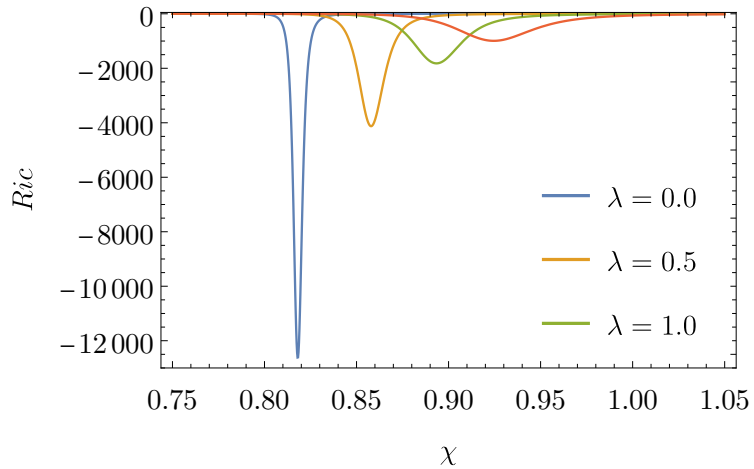


Figure 5.7: Ricci's curvature sections for three different λ . $N = 3$.

³Coordinate singularity is present only in some coordinates. This is different from so-called *physical singularity*, which is present in every choice of the coordinate system.

Geodesics

The importance of geodesics was described in Chapter 3.2. In addition, they give a tool for observing some system characteristics, such as singularities, or curvature in general. *Initial valued Geodesics* are solutions to

$$(\lambda(0); \chi(0)) =: (\lambda_i; \chi_i)$$

$$\left. \left(\frac{d\lambda(t)}{dt}; \frac{d\chi(t)}{dt} \right) \right|_{T_i} =: (\lambda'_i; \chi'_i),$$

where zero was set as initial time.

We might also choose *boundary valued geodesics* with fixed initial $(\lambda(0); \chi(0))$ and final position $(\lambda(T); \chi(T))$. Because the shape of geodesics in parametric space does not depend on the initial derivative, it does not depend on the speed of driving in the parametric space. Initial valued geodesics are therefore more advantageous to calculate, because they have only three free parameters — the initial coordinates $(\lambda; \chi)$ and ratio λ'/χ' . Another reason is purely numeric, which is the boundary valued geodesics are calculated by numerous evolutions of initial valued geodesics with *response initial parameter tweaking*. This makes the calculations slower (in our case the calculation time was 10 to 100 times longer).

Results for geodesics starting at $(\lambda_i; \chi_i) = (0; 0)$, $(\lambda', \chi') = (\cos \theta; \sin \theta)$ can be seen in Fig. 5.8. Other values θ result in a close approach of the geodesics to the singularity, making the calculations numerically unstable. The fact that geodesics lean towards singularities is well known from the theory of General Relativity (GR). The main difference here is that our “test particle” seems to be partially repulsed by the singularity. The analogy with GR would therefore fail because of the nonexistence of negative mass and gravitational dipoles. The better analogy is electromagnetism, which has a downside in the fact that the geometrical formalism is not used so much in this theory. Comparison of these two intuitive examples can be seen in Fig. 5.9. The geodesic behavior is not caused only by the singularity but also by a large Ricci curvature leaning to the right from it. This means the distance across this *unreachable gap*, marked by *blue line* in Fig. 5.8, is also large. This leads to strong tendency of geodesics to go around the singularity rather than crossing it. The presence of singularities means that our ground state manifold is geodesically incomplete and according to Theorem 3 there exist some geodesically unreachable coordinates. From this goes the term *unreachable gap*.

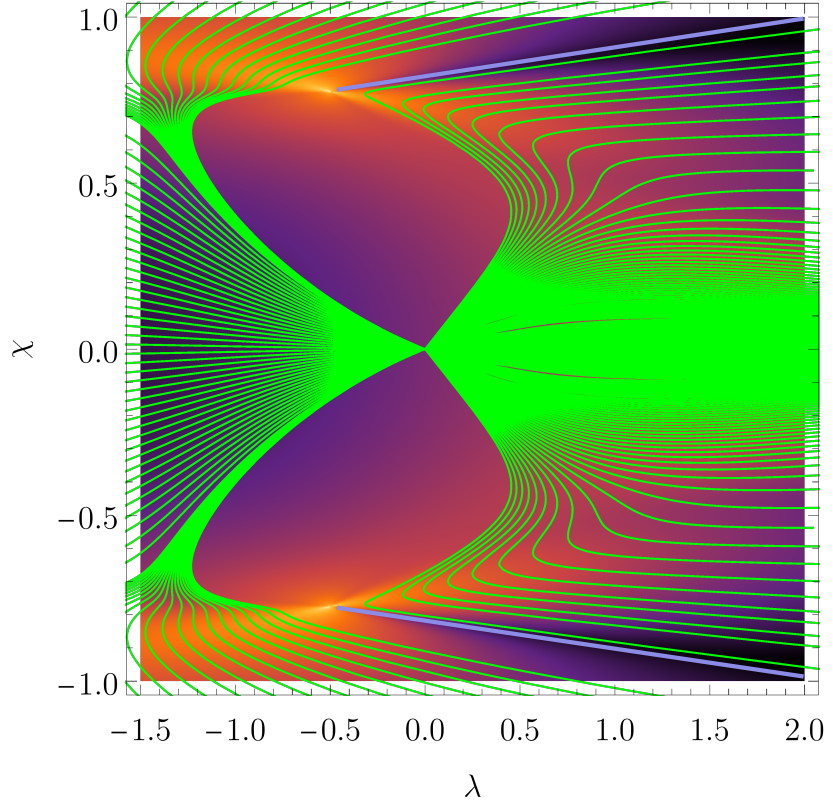


Figure 5.8: Geodesics for $N = 3$ starting from $(\lambda_i; \chi_i) = (0; 0)$ with $(\lambda'_i; \chi'_i) = (\cos \theta; \sin \theta)$, parametrized by angle $\theta \in [-0.63; 0.63]$, $\theta \in [\pi - 0.225; \pi + 0.225]$, with step $\Delta\theta = 0.01$. Blue line marks the (high Ricci curvature) unreachable gap.

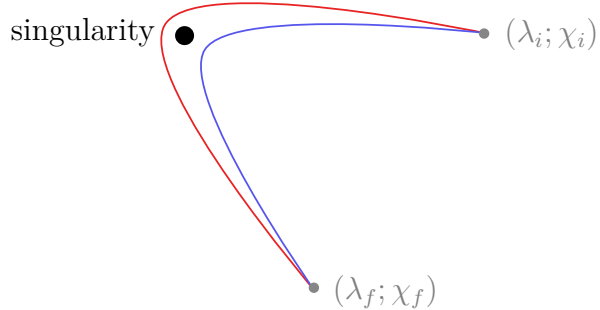


Figure 5.9: Comparing boundary valued geodesics with repulsing (inner line) and attracting (outer line) metric tensor divergence in the spherically symmetrical space.

5.1.2 5-dimensional Hamiltonian

Another special case is $N = 5$. From analysis of the energy levels, we see that there are more degeneracies, see Fig. 5.10. One can see that only $E_0 = E_1$ degeneracy lies on the separatrix and the other singularities are distributed around. The $\chi \leftrightarrow -\chi$ symmetry holds for all of them.

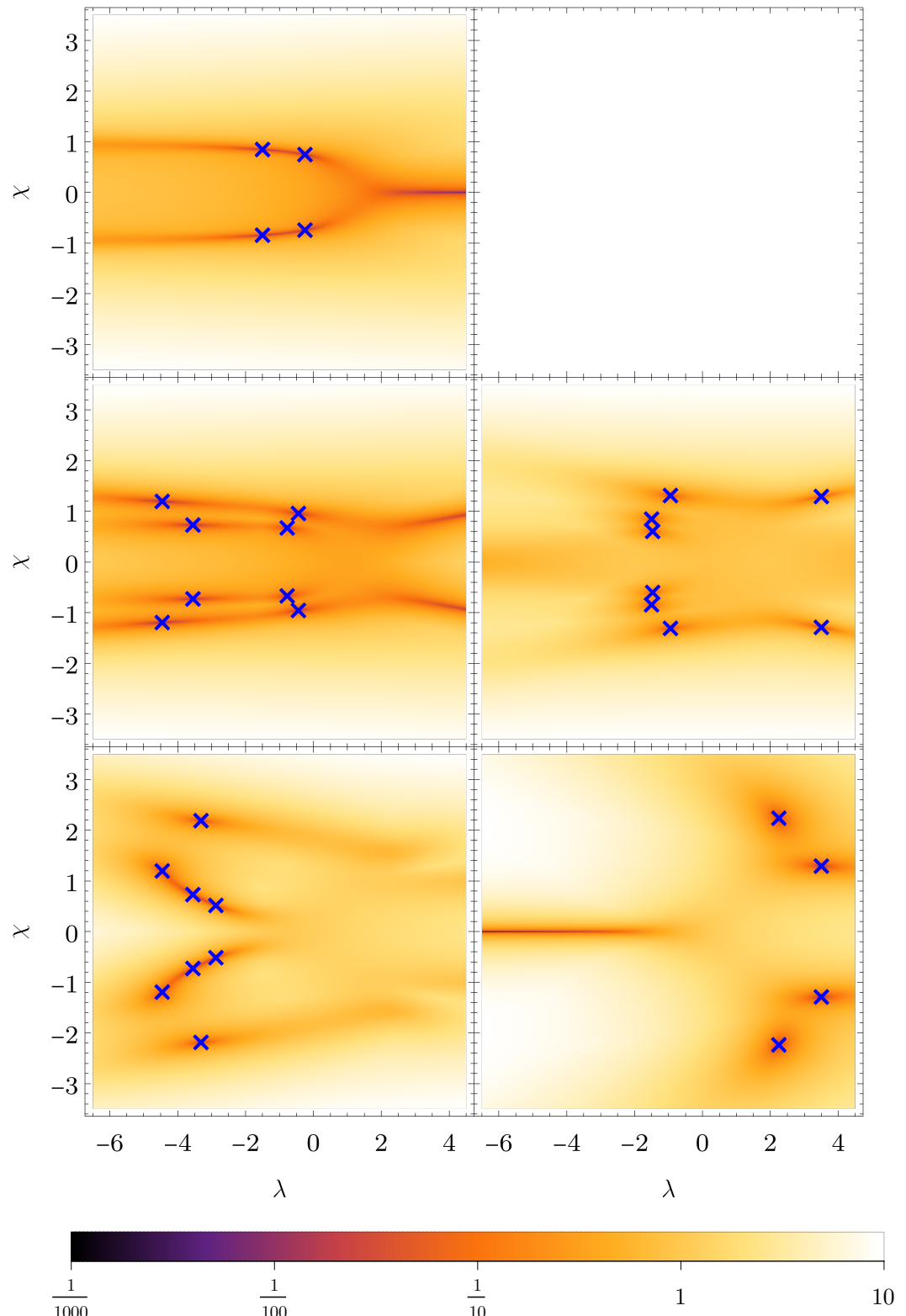


Figure 5.10: Energy differences between neighboring energy levels for $N = 5$. First row: $E_1 - E_0$, second row from left: $E_2 - E_1$, $E_3 - E_2$, third row from left: $E_4 - E_3$, $E_5 - E_4$. Spectra degeneracies are marked with blue cross.

The ground state manifold can be understood from the metric tensor determinant, see Fig. 5.11. Here we see the spectrum degeneracy causes high positive values of metric tensor determinant and the [unreachable gap](#) is characterized by small determinant values.

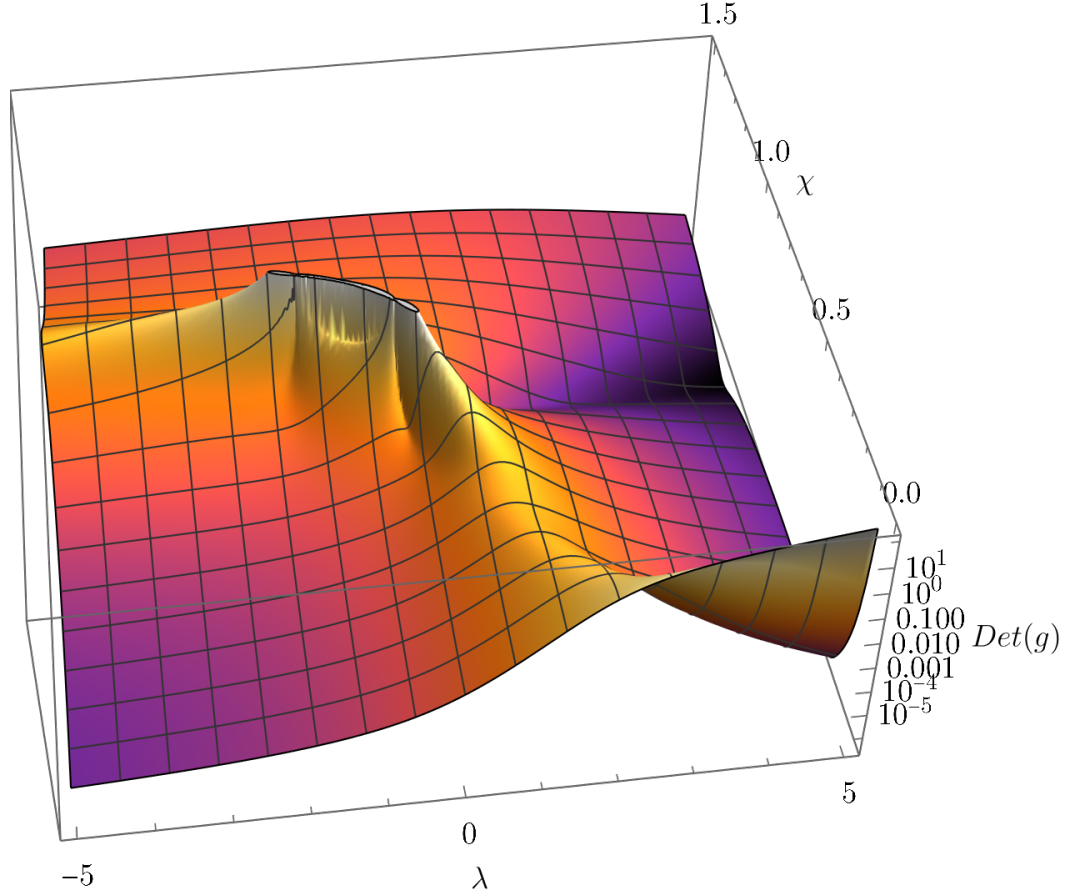


Figure 5.11: Metric tensor determinant for the case $N = 5$.

Geodesics for case $N = 5$ starting at $(\lambda; \chi) = (0; 0)$ have the characteristics already seen in the case $N = 3$. However, when starting at $(1; 0)$, the behavior around the singularity is not the only interesting thing happening. As can be seen in Fig. 5.12, the geodesics tend to deflect themselves from the area with high curvature around the axis $\chi = 0$, which happens even for other initial conditions, just that for $(0; 0)$ it is not so apparent. Small irregularity can be seen in Fig. 5.8 around $(0.5; 0.1)$. This implies that the geodesic equation might have at least two solutions as candidates for the globally shortest path between two points.⁴

⁴One might recall the effect of gravitational lensing here. In the presence of any mass in the spacetime, there exist more possible light paths (solutions to the geodesic equation) between two points, differing by the initial condition.

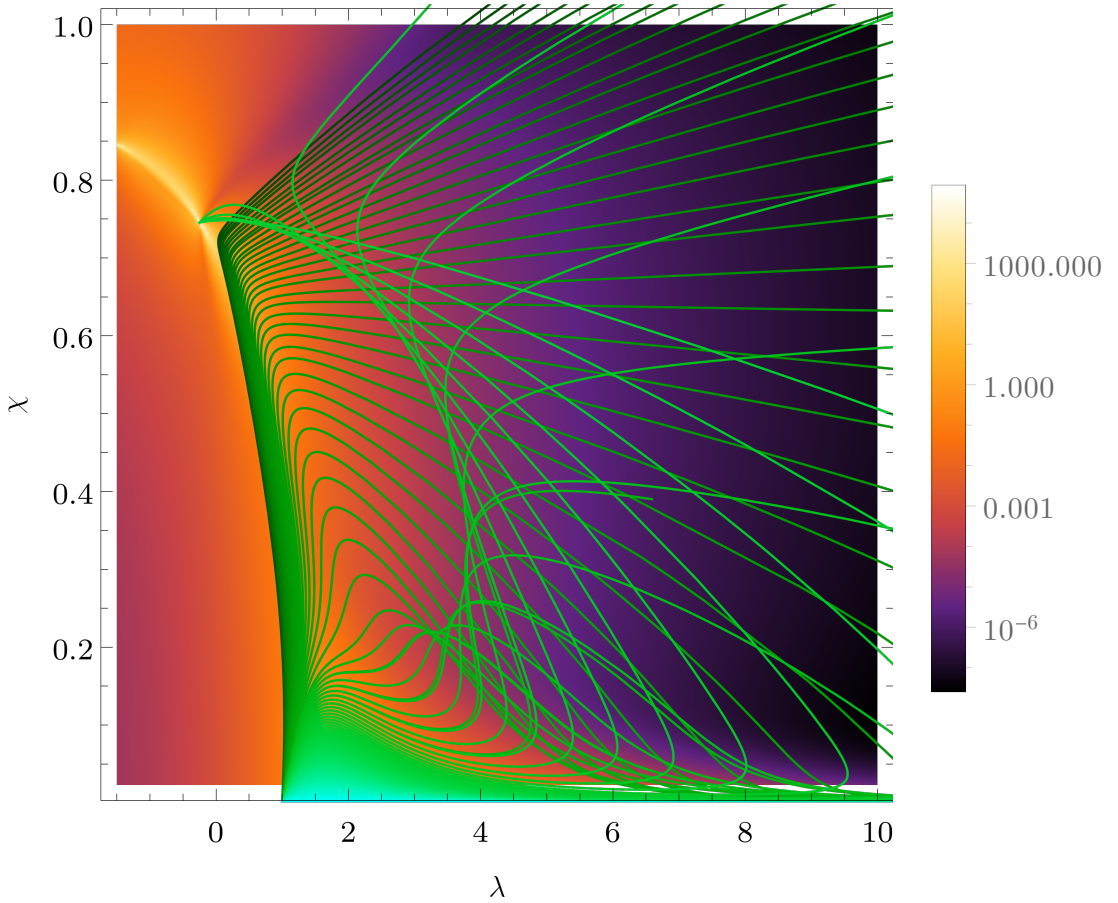


Figure 5.12: Geodesics for the case $N = 5$, starting at $(1; 0)$. *The numerics for geodesics passing close to singularity can be observed to break down.*

5.1.3 Infinite dimension limit

The limit $N \rightarrow \infty$ can be taken from Hamiltonian in Eq. 5.1 using Holstein-Primakoff mapping [Holstein and Primakoff, 1940] for bosonic operators

$$\mathcal{H} := \lim_{j \rightarrow \infty} \frac{\hat{H}}{2j}, \quad (5.15)$$

resulting in classical Hamiltonian

$$\begin{aligned} \mathcal{H}(x, p) = & -\frac{1}{2} + \frac{1-\lambda}{2}x^2 + \frac{\lambda-\chi^2}{4}x^4 - \frac{\chi x^3}{2}\sqrt{2-x^2-p^2} - \frac{\chi^2}{4}p^4 \\ & + \frac{p^2}{4} \left[2 + (\lambda - 2\chi^2)x^2 - 2\chi x\sqrt{2-x^2-p^2} \right]. \end{aligned} \quad (5.16)$$

Finding derivatives minima the *separatrix*

$$\chi^2 = \frac{\lambda-1}{\lambda-2} \quad (5.17)$$

is obtained. The separatrix represents phase transition in the limit $N \rightarrow \infty$. In case of LMG model, the transition is of first order everywhere, except in $(\lambda; \chi) = (1; 0)$, where it has order two. The separatrix is shown in Fig. 5.13

compared to minimum of $E_1 - E_0$ function, i.e., between the ground state and the first excited state for $N = 3$ case. With increasing N it converges to the separatrix line.

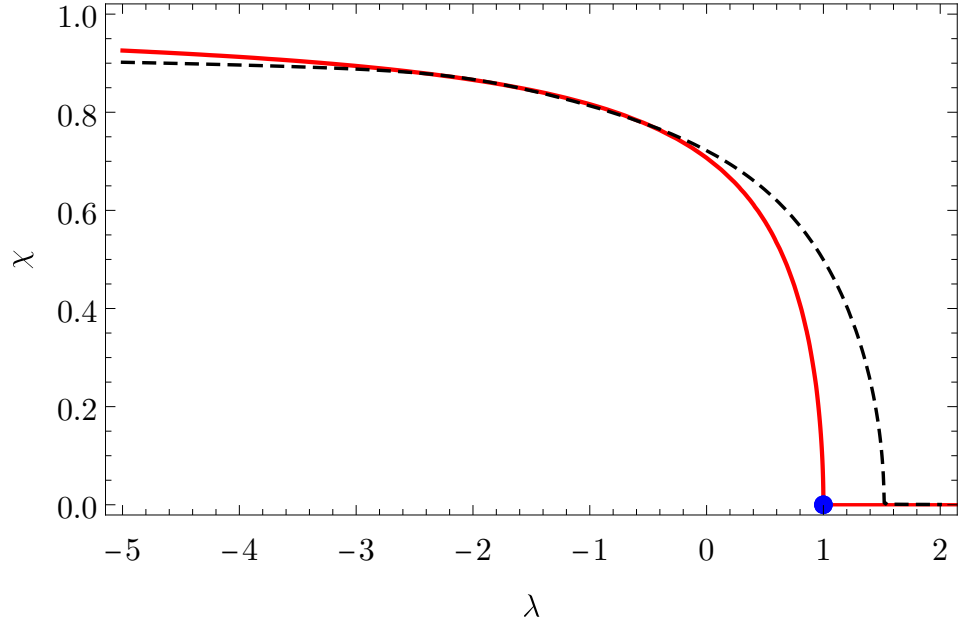


Figure 5.13: First order phase transition, the Separatrix (red), second order transition (blue point) compared to minimum between the ground state and first excited state in $N=3$ case (black, dashed).

5.2 General spectrum behavior

For higher dimensions we see the same characteristic behaviour in the energy spectrum sections, see the example in Fig. 5.14, 5.15 for $N = 10$ case. It is not yet clear if there is degeneracy between every two neighboring energy levels. From numerical observation on $N < 10$ goes that there are $N - 2$ crossings for N odd and $N - 3$ for N even. Proving this generally is not an easy task, because the singularities might not exist on the real axis and analytical proof is needed.

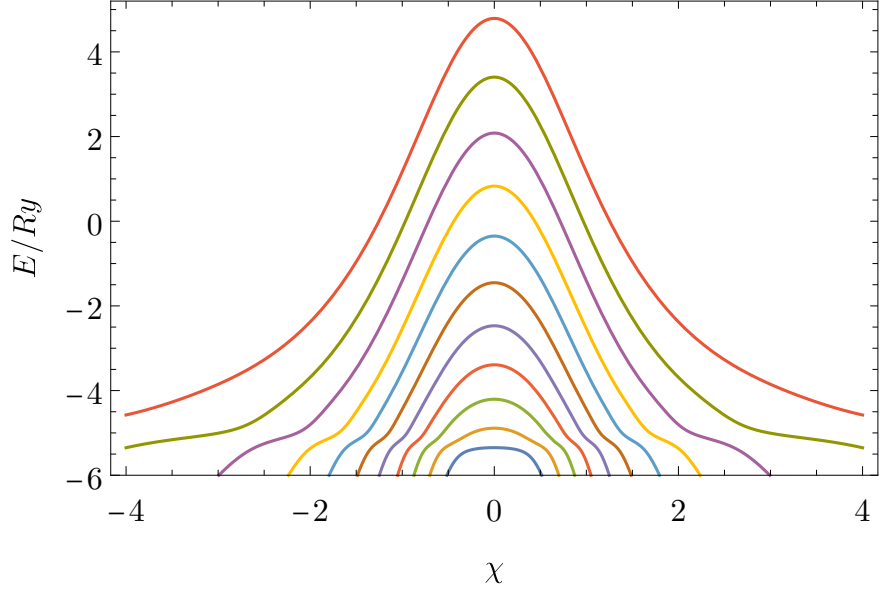


Figure 5.14: Energy spectrum as function of χ . $\lambda = 1$ and $N = 10$.

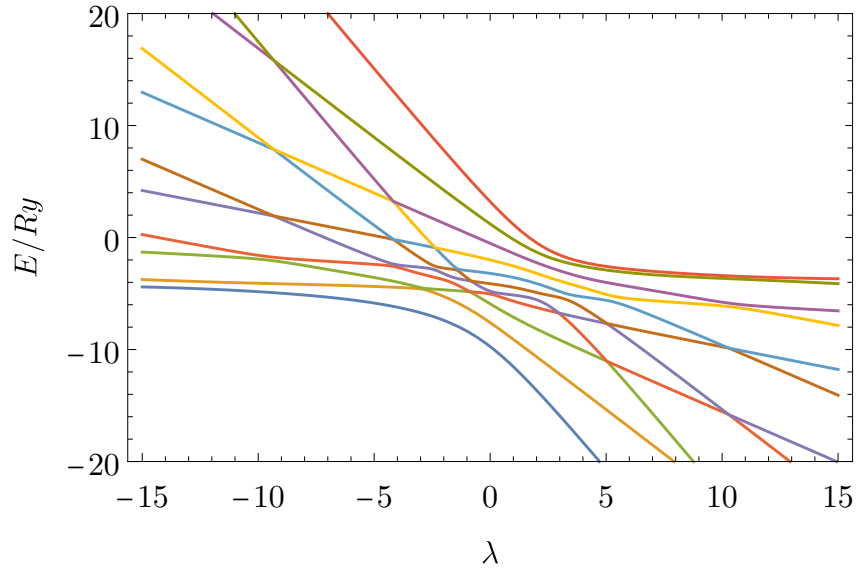


Figure 5.15: Energy spectrum as function of λ ,. $\chi = 1$ and $N = 10$.

Special attention was given to the spectrum degeneracies between zeroth and first energy level, because those influence the metric tensor and ground state manifold geodesics the most. Their exact calculation is numerically expensive, and only the first few cases, namely, $N \in \{3, 4, 5, 6, 7\}$, were calculated, see Tab. 5.1.

N	$(\lambda_l; \pm \chi_l)$	$(\lambda_2; \pm \chi_2)$	$(\lambda_r; \pm \chi_r)$
3	$(-\frac{1}{2}; \sqrt{\frac{3}{5}})$		
4	$(-3; \sqrt{\frac{4}{5}})$		$(-\frac{1}{3}; \sqrt{\frac{4}{7}})$
5	$(-\frac{3}{2}; \sqrt{\frac{5}{7}})$		$(-\frac{1}{4}; \sqrt{\frac{5}{9}})$
6	$(-5; \sqrt{\frac{6}{7}})$	$(-1; \sqrt{\frac{2}{3}})$	$(-\frac{1}{5}; \sqrt{\frac{6}{11}})$
7	$(-\frac{5}{2}; \sqrt{\frac{7}{9}})$	$(-\frac{3}{4}; \sqrt{\frac{7}{11}})$	$(-\frac{1}{6}; \sqrt{\frac{7}{13}})$

Table 5.1: Singularities between the zeroth and first energy levels for dimensions 3–7. Subscript $l(r)$ means the most *left(right)-wise* positioned coordinates in the (λ, χ) -plot.

From singularity behavior in low dimensions, one might see the pattern for (λ_l, χ_l) and (λ_r, χ_r) , i.e., those with minimal, resp maximal λ coordinate

$$(\lambda_l; \pm \chi_l) = \begin{cases} \left(1 - \frac{N}{2}; \sqrt{\frac{N}{N+2}}\right) & , N \geq 3, N \text{ is odd} \\ \left(1 - N; \sqrt{\frac{N}{N+1}}\right) & , N \geq 3, N \text{ is even} \end{cases} \quad (5.18)$$

$$(\lambda_r; \pm \chi_r) = \left(\frac{1}{1-N}; \sqrt{\frac{N}{2N-1}} \right) \quad , N \geq 3. \quad (5.19)$$

These were numerically proven to be singularities for cases up to $N = 1000$.

Dimensions 3 to 10 are shown in Fig. 5.16. In addition, the degeneracies between zeroth and first energy levels belong to the separatrix described by Eq. 5.17. Due to this, the position of singularities is constrained to the *second order phase transition line* between po ints $(\lambda_l, \pm \chi_l)$ and $(\lambda_r, \pm \chi_r)$.

In the limit $N \rightarrow \infty$ they converge to

$$\lim_{N \rightarrow \infty} (\lambda_l; \pm \chi_l) = (-\infty, 1)$$

$$\lim_{N \rightarrow \infty} (\lambda_r; \pm \chi_r) = \left(0, \frac{1}{\sqrt{2}}\right).$$

This means that for $N \rightarrow \infty$, the separatrix is covered by singularities on $\lambda < 0$.

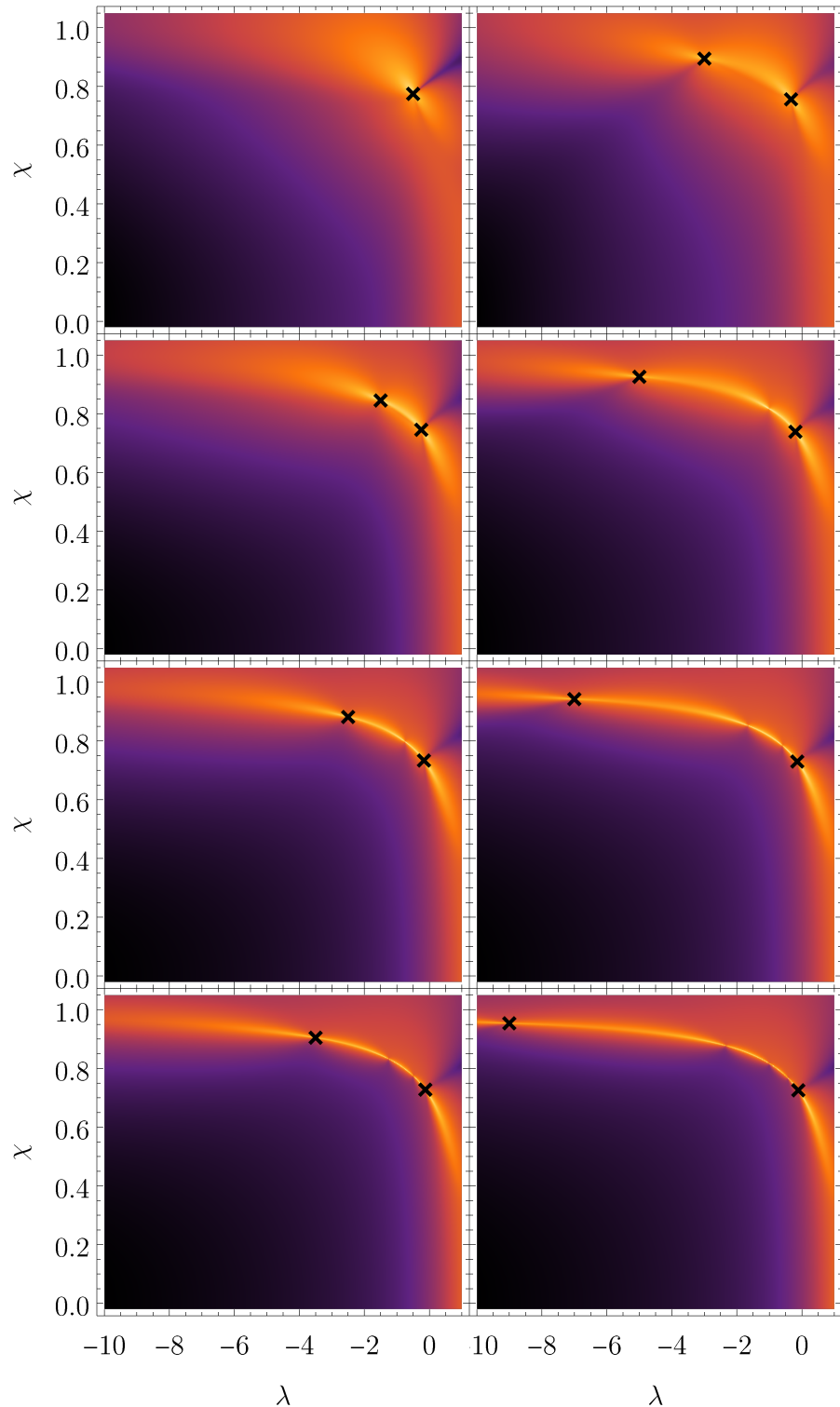


Figure 5.16: Spectrum degeneracies between E_0 and E_1 . Hamiltonian dimensions are 1,3,5,7 in the first column and 2,4,6,8 in the second column. Black crosses mark most left-wise and right-wise singularity and the background corresponds to the metric tensor determinant. Other singularities are also well visible in the determinant as defects on the *high determinant value line*.

Transport using quenches

In Chapter 3.2, the transport using quenches was introduced. This transport also resembles some ground state manifold characteristics. Performing quench from $(\lambda_i; \chi_i) = (0; 0)$ to $(\lambda; \chi)$, the fidelity is small for final coordinates below separatrix. When crossing the *quantum phase transition* line, the fidelity increases dramatically, as can be seen on Fig. 5.17.

Transport using quenches can be observed on Fig. 5.18. The quenches are performed around paths with $\int_a^b ds = \text{const}$ between every two neighboring points on ground state manifold geodesic. One can see that if the system is measured periodically, the quenches jump smaller distances when closer to a point of degeneracy. Decreasing time step Δt has no effect on the relative fidelity of quenches during the evolution but has an effect on their absolute fidelity. As one would expect that for $\Delta t \rightarrow 0$ transport becomes adiabatic, and the fidelity at any time will become 1. See that the shape of the curves looks similar in the columns, but their magnitude decreases.

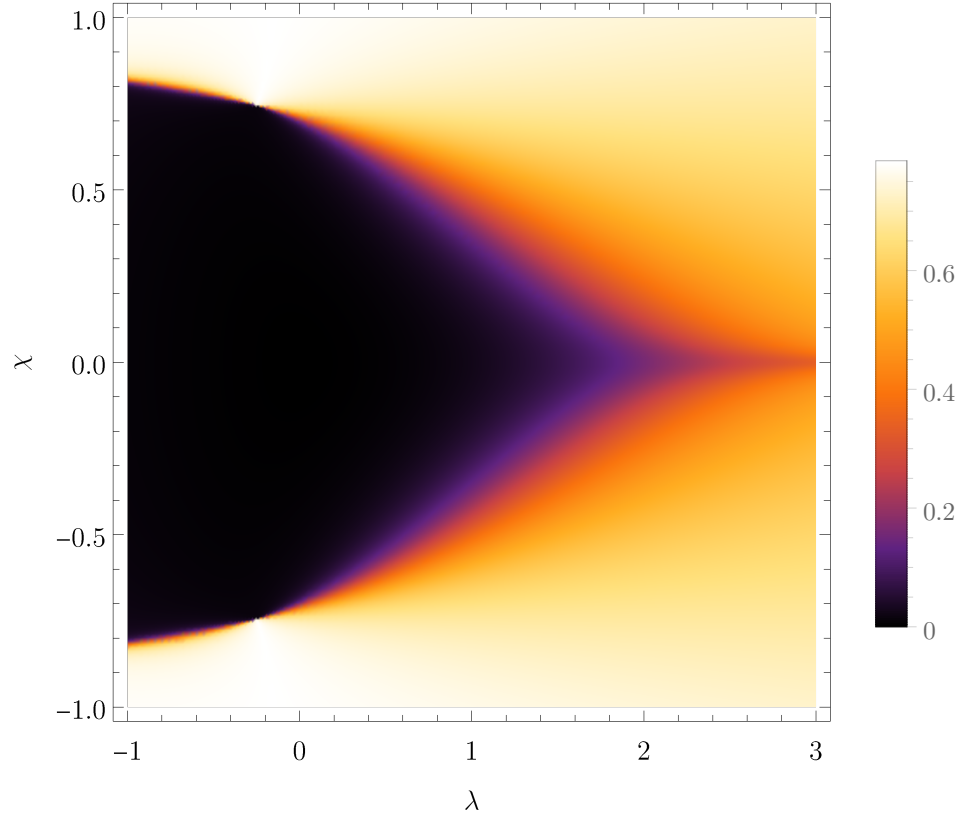


Figure 5.17: Arctangent of the fidelity of quench from $(\lambda_i; \chi_i) = (0; 0)$ to the coordinate $(\lambda; \chi)$.

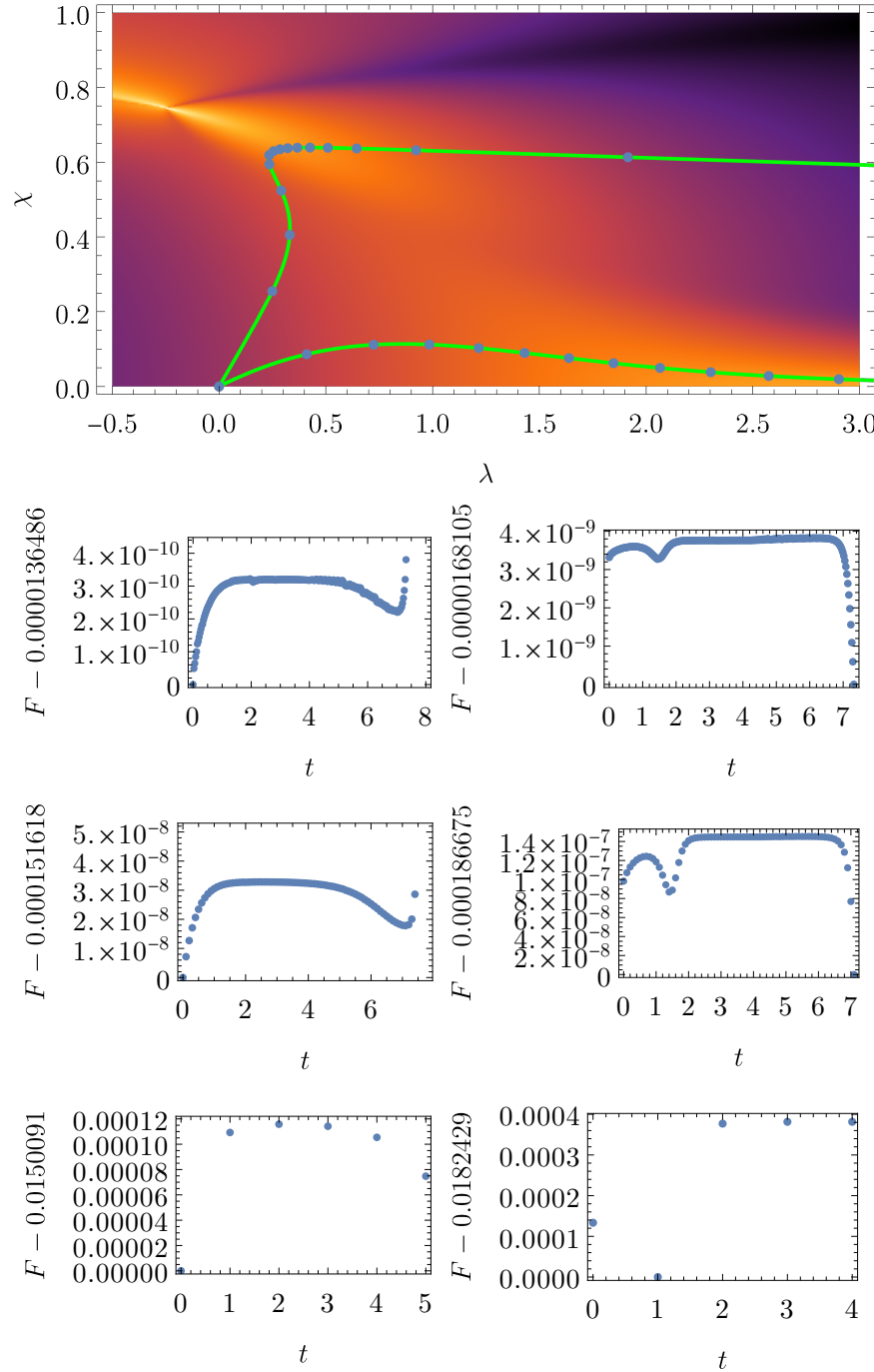


Figure 5.18: Fidelity for sequential quenches along geodesics (see green lines on top). Left (right) column corresponds to lower (upper) geodesic. Time steps from top are $\Delta t \in \{0.03, 0.1, 0.5\}$. Time difference between points in the plot on top is $\Delta t = 0.5$.

Conclusion

In this thesis, the mathematical reformulation of quantum state driving theory of finite Hamiltonian systems is presented. The playground in a form of fiber space is constructed and geometry of energy states reformulated on it. Some theorems are proposed, based on previous knowledge from the area of physics concerning quantum state driving and clear definitions of generally used terms is presented.

From a simple two level system, the correspondence to a damped harmonic oscillator in the fidelity behavior is shown. In a case of geodesic driving, the fidelity oscillates with constant frequency and periodically becomes one. For linear driving, the fidelity has essentially two regimes — fast transport regime, described by semiclassical Landau-Zener formula, and close adiabatic regime, described by APT. In both models, the fidelity is excited when energy levels get close to each other, especially in a presence of diabolic points. These excitations lead to damped oscillations.

In LMG model, the ground state manifold is analyzed. The Riemannian manifold characteristics were calculated along with its implications. These are ground state manifold geodesics and coordinates of diabolic points in parametric space, dependent on Hamiltonian dimension. In three dimensions, this was done analytically, proving the existence of diabolic points. For higher dimensions, numerical methods were used. In the end, the transport using quenches was numerically demonstrated, showing the transformation to adiabatic transport by shortening the quenches.

Many questions still lay unsolved and some were newly opened. For example: “What are the possibilities for quantum quench transport?”. “What is the correspondence of energy variance and driving fidelity?”. Further on, from the LMG model, the proposed analytical formula for diabolic points coordinates remains to be proven analytically, along with the number of these points.

This thesis provides a great amount of numerical analysis on two quantum models, which will hopefully serve for future discoveries in this area of physics. The state manifold analyses might lead the finding of better fidelity protocols, or maybe the geodesics will be found to be somewhat “most stable protocols” for counter-diabatic driving. Either way, the possibilities are yet open and not known.

Bibliography

- A. Ashtekar and T. A. Schilling. Geometry of quantum mechanics. In *AIP Conference Proceedings*, volume 342, pages 471–478, Cancun (Mexico), 1995. AIP. URL <http://aip.scitation.org/doi/abs/10.1063/1.48786>. ISSN: 0094243X.
- A. Ashtekar and T. A. Schilling. Geometrical Formulation of Quantum Mechanics. *arXiv:gr-qc/9706069*, 1997. URL <http://arxiv.org/abs/gr-qc/9706069>. arXiv: gr-qc/9706069.
- M. V. Berry. Quantal phase factors accompanying adiabatic changes. *Proc. R. Soc. Lond. A*, 392(1802):45–57, 1984. URL <http://rspa.royalsocietypublishing.org/content/392/1802/45>.
- M. V. Berry. The quantum phase, five years after' in ‘geometric phases in physics’. *A Shapere, F Wilczek. (World Scientific) 7-28*, 1989.
- M. V. Berry. Transitionless quantum driving. *Journal of Physics A: Mathematical and Theoretical*, 42(36), 2009. URL <https://doi.org/10.1088/1751-8113/42/36/365303>.
- M. Bukov, D. Sels, and A. Polkovnikov. Geometric Speed Limit of Accessible Many-Body State Preparation. *Physical Review X*, 9(1):011034, 2019. ISSN 2160-3308. URL <https://doi.org/10.1103/PhysRevX.9.011034><https://link.aps.org/doi/10.1103/PhysRevX.9.011034>.
- R. Cheng. Quantum Geometric Tensor (Fubini-Study Metric) in Simple Quantum System: A pedagogical Introduction. *arXiv:1012.1337 [math-ph, physics:quant-ph]*, 2013. URL <http://arxiv.org/abs/1012.1337>.
- M. Fecko. *Differential Geometry and Lie Groups for Physicists*. Cambridge University Press, 2006. doi: 10.1017/CBO9780511755590.
- C. Gorodski. *An introduction to Riemannian geometry*. unpublished, 2012. URL <https://www.ime.usp.br/~gorodski/teaching/mat5771-2016/gorodski-riem-geom-2012.pdf>. Preliminary version.
- D. Gutiérrez-Ruiz, D. Gonzalez, J. Chávez-Carlos, J. G. Hirsch, and J. D. Vergara. Quantum geometric tensor and quantum phase transitions in the lipkin-meshkov-glick model. *Phys. Rev. B*, 103, May 2021. URL <https://link.aps.org/doi/10.1103/PhysRevB.103.174104>.
- T. Holstein and H. Primakoff. Field dependence of the intrinsic domain magnetization of a ferromagnet. *Phys. Rev.*, 58:1098–1113, Dec 1940. doi: 10.1103/PhysRev.58.1098.
- M. Kolodrubetz, P. Mehta, and A. Polkovnikov. Geometry and non-adiabatic response in quantum and classical systems. *Physics Reports*, 697:1–87, 2017. ISSN 0370-1573. URL <https://www.sciencedirect.com/science/article/pii/S0370157317301989>. Geometry and non-adiabatic response in quantum and classical systems.

P. Krtouš. Geometrické metody ve fyzice, studijní text k přednáškám geometrické metody fyziky i a ii. 2013.

L. D. Landau and L. M. Lifshitz. *Quantum Mechanics Non-Relativistic Theory, Third Edition: Volume 3*. Butterworth-Heinemann, 3 edition, 1981. ISBN 0750635398. URL <http://www.worldcat.org/isbn/0750635398>.

W. Tu Loring. *Differential Geometry*. Springer International Publishing, 2017. doi: 10.1007/978-3-319-55084-8.

D. Loss and D. P. DiVincenzo. Quantum computation with quantum dots. *Phys. Rev. A*, 57:120–126, Jan 1998. doi: 10.1103/PhysRevA.57.120. URL <https://link.aps.org/doi/10.1103/PhysRevA.57.120>.

Y. Makhlin, G. Schön, and A. Shnirman. Josephson junction based quantum computing. *AAECC 10*, page 375–382, 2000. doi: <https://doi.org/10.1007/s002000050136>.

F. Matus, P. Cejnar, P. Stránský, and J. Střeleček. unpublished. *MFF UK*, 2022.

M. Molitor. Exponential families, Kahler geometry and quantum mechanics. *Journal of Geometry and Physics*, 70:54–80, 2013. ISSN 03930440. doi: 10.1016/j.geomphys.2013.03.015. URL <http://arxiv.org/abs/1203.2056>. arXiv: 1203.2056.

H. Nakamura. *Nonadiabatic transition: concepts, basic theories and applications*. World Scientific, Hackensack, New Jersey, second edition edition, 2012. ISBN 978-981-4329-77-4.

P. Petersen. *Riemannian Geometry*. Springer Verlag, 1998. ISBN 978-0-387-29403-2.

G. Rigolin and G. Ortiz. Beyond the quantum adiabatic approximation: Adiabatic perturbation theory. *Physical Review A* 78, no. 5 (November 18, 2008): 052508, 2008. URL <https://doi.org/10.1103/PhysRevA.78.052508>.

J. J. Sakurai and Jim Napolitano. *Modern Quantum Mechanics*. Cambridge University Press, 3 edition, 2020. doi: 10.1017/9781108587280.

J. R. R. Tolkien. *The Lord of the Rings*. Folio Society, 1977. ISBN 978-0458907502.

A. Uhlmann. The “transition probability” in the state space of a $*$ -algebra. *Reports on Mathematical Physics*, 9(2):273–279, 1976. ISSN 0034-4877. URL <https://www.sciencedirect.com/science/article/pii/0034487776900604>.

List of Figures

1	Visualization of the state adiabatic transport compared to transport with excitation in a system with time varying energy eigenstates.	5
2.1	Base manifold $\mathcal{U} \subset \mathbb{R}^N$ is visualized as a line. For every point $\lambda \in \mathcal{U}$ one Hilbert space $\mathcal{H}(\lambda)$ (blue disk) is constructed as a fiber. The union of all these fibers creates the full Hilbert space \mathcal{H}_{full} (hollow cylinder) and from every Hilbert space there exist projection π onto the base manifold.	14
2.2	For every λ we have the projective Hilbert space $\mathcal{PH}(\lambda)$ containing physical states $ \psi(\lambda)\rangle$ corresponding to density matrix $\rho \equiv \psi(\lambda)\rangle\langle\psi(\lambda) $. Every state can be multiplied by phase factor $e^{i\varphi}$, extending it to Hilbert space $\mathcal{H}(\lambda)$.	14
2.3	From the full Hilbert space \mathcal{H}_{full} (the biggest hollow cylinder) we identified eigenstates and unified them into state manifolds M_s . These are drawn as inner cylinders of \mathcal{H}_{full} , especially see the ground state manifold M_0 as the inner cylinder. The phase φ introduces gauge symmetry $e^{i\varphi}$. If it is fixed, we get projective state manifolds \mathcal{PM}_s , especially see \mathcal{PM}_0 . Projective state manifolds are isomorphic to the base manifold \mathcal{U} .	16
2.4	The cylinders from Fig. 2.3 are now displayed as two-dimensional sheets. The transport of states on state manifolds M_s along the path $\mathcal{J}(t)$. The information about gauge phase φ is represented by color (see the changing color on the paths in M_s).	17
4.1	Driving along the geodesic. $\lambda_i \equiv (\Omega_i, \Delta_i)$ and $\lambda_f \equiv (\Omega_f, \Delta_f)$ are initial and final parameters respective. Density plot shows the difference between Hamiltonian eigenvalues.	36
4.2	Infidelity in time for final time $T = 1$ for geodesical driving.	38
4.3	Final infidelity dependence on final time T for geodesical driving.	38
4.4	Infidelity dependence on final time in logarithmic scale. The difference in numerical precision of both methods can be seen in the spikes height. As it will be shown later, the spikes should go to zero, thus analytical formula has higher numerical precision.	38
4.5	Rescaled final infidelity $T_s := 2sT$ dependence on final time. Red points mark the condition $F = 1$.	39
4.6	Fidelity dependence on time and final time in log-log scale. Note that only $t < T$ has physical meaning.	39
4.7	Energy variance for geodesical driving protocol, dependent on time t and final time T . Driving occurs only in area $t < T$.	40
4.8	Driving along the linear path. $\lambda_i := (-10; 1)$ and $\lambda_f := (10; 1)$ are initial and final parameters respective. Density plot shows the difference between Hamiltonian eigenvalues.	41
4.9	Infidelity in time for three final times $T \in \{1, 5, 20\}$ for the linear driving defined in 4.36.	42
4.10	Value of first element of the ground state vector $\alpha \equiv 0(t)\rangle^1$ during linear driving.	43

4.11	Final infidelity as a function of T with zoom on the transitional part.	43
4.12	Final infidelity as a function of T in log-log scale wit linear scaled plot inserted.	44
4.13	Final infidelity as a function of Δ and T and its three regimes. Zoomed boundary between them can be seen on 4.14.	45
4.14	Fine structure of the boundary between fast-driving and adiabatic regimes of final infidelity.	45
4.15	Infidelity as function of time for fast-driving regime, $T = 80 < T_c$	46
4.16	Infidelity as function of time for close-adiabatic regime. $T = 170 > T_c$	46
4.17	Fidelity as a function of driving final time, approximated by the sum (green) of Landau-Zener (red, dashed) and APT (purple, dashed)	47
4.18	Fidelity dependence for linear driving with $\Delta = 1$. Black line marks $t = T$, dashed black line $t = T/2$ and purple dashed line is the approximate value of T_c . Blue lines marks driving from Fig. 4.15, 4.16, visualizing the final times of the driving.	48
4.19	Energy variance for $\Delta_{sc} = 0.2$ for linear driving. Note that only $t < T$ has physical meaning.	49
5.1	Energy spectrum for $N = 3$, section $\lambda = 1$	51
5.2	Energy spectrum for $N = 3$, section $\chi = 1$	52
5.3	Arctangent of the metric tensor elements for $N = 3$ in the parametric space. From the top: $\arctan(g_{11})$, $\arctan(g_{12}) = \arctan(g_{21})$, $\arctan(g_{22})$	53
5.4	Ground state metric tensor determinant in a parametric space for $N = 3$	54
5.5	Arctangent of the ground state Christoffel symbols for $N = 3$. First row from left: $\arctan(\Gamma_{111})$, $\arctan(\Gamma_{121})$, $\arctan(\Gamma_{122})$. Second row from left: $\arctan(\Gamma_{211})$, $\arctan(\Gamma_{221})$, $\arctan(\Gamma_{222})$	54
5.6	Arctangent of Ricci curvature for the case $N = 3$	55
5.7	Ricci's curvature sections for three different λ . $N = 3$	55
5.8	Geodesics for $N = 3$ starting from $(\lambda_i; \chi_i) = (0; 0)$ with $(\lambda'_i; \chi'_i) = (\cos \theta; \sin \theta)$, parametrized by angle $\theta \in [-0.63; 0.63]$, $\theta \in [\pi - 0.225; \pi + 0.225]$, with step $\Delta\theta = 0.01$. Blue line marks the (high Ricci curvature) unreachable gap.	57
5.9	Comparing boundary valued geodesics with repulsing (inner line) and attracting (outer line) metric tensor divergence in the spherically symmetrical space.	57
5.10	Energy differences between neighboring energy levels for $N = 5$. First row: $E_1 - E_0$, second row from left: $E_2 - E_1$, $E_3 - E_2$, third row from left: $E_4 - E_3$, $E_5 - E_4$. Spectra degeneracies are marked with blue cross.	58
5.11	Metric tensor determinant for the case $N = 5$	59
5.12	Geodesics for the case $N = 5$, starting at $(1; 0)$. The numerics for geodesics passing close to singularity can be observed to break down.	60

5.13 First order phase transition, the Separatrix (red), second order transition (blue point) compared to <i>minimum between the ground state and first excited state in N=3 case</i> (black, dashed).	61
5.14 Energy spectrum as function of χ . $\lambda = 1$ and $N = 10$	62
5.15 Energy spectrum as function of λ ,. $\chi = 1$ and $N = 10$	62
5.16 Spectrum degeneracies between E_0 and E_1 . Hamiltonian dimensions are 1,3,5,7 in the first column and 2,4,6,8 in the second column. Black crosses mark most left-wise and right-wise singularity and the background corresponds to the metric tensor determinant. Other singularities are also well visible in the determinant as defects on the <i>high determinant value line</i>	64
5.17 Arctangent of the fidelity of quench from $(\lambda_i; \chi_i) = (0; 0)$ to the coordinate $(\lambda; \chi)$	65
5.18 Fidelity for sequential quenches along geodesics (see green lines on top). Left (right) column corresponds to lower (upper) geodesic. Time steps from top are $\Delta t \in \{0.03, 0.1, 0.5\}$. Time difference between points in the plot on top is $\Delta t = 0.5$	66

A. Geometrization of quantum mechanics

Differential geometry is believed to be the modern language of physics and there is a strong urge to reformulate theories in this language. As introduction to the problem, see Ashtekar and Schilling [1997], Ashtekar and Schilling [1995], or more mathematical work by Molitor [2013].

In the whole thesis, classical formulation of quantum mechanics with some parts described using differential geometry is used. Here, the complete reformulation of quantum mechanics and the bridge between this theory and the one already formulated is introduced. Reformulating the whole theory of quantum driving into the language of differential geometry might give some new insights, but it is beyond the scope of this thesis.

A.1 From the projective Hilbert space to state manifolds

Consider the Hilbert space \mathcal{H} to be a space of *bare states* and \mathcal{S} to be the space of *normalized bare states*. Physical observables are related to the *space of rays*, defined as $\mathcal{PH} := \mathcal{H}/U(1)$, for the factorization by elements of one-dimensional unitary group $U(1)$. This group consists of unitary transformations $e^{i\varphi}$ for $\varphi \in \mathbb{R}$, defining gauge symmetry between quantum states. \mathcal{PH} is then considered to be the *space of pure states*. We will consider the states to be normalized, leading to the *space of normalized pure physical states*.

It can be shown, that \mathcal{PH} is of Kähler structure, meaning it has two non-degenerate sesquilinear¹ 2-forms embedded along with complex unit operator J , defining structure

$$(J, G, \Omega),$$

such that

$$J^2 = \mathbb{1}. \quad (\text{A.1})$$

Any bracket of $|\psi_1\rangle, |\psi_2\rangle \in \mathcal{PH}$ can be decomposed into real and imaginary part[Ashtekar and Schilling, 1997]

$$\langle \psi_1 | \psi_2 \rangle \equiv Q(\psi_1, \psi_2) = \frac{1}{2}G(\psi_1, \psi_2) - \frac{i}{2}\Omega(\psi_1, \psi_2). \quad (\text{A.2})$$

From bracket sesquilinearity goes that G is symmetric and Ω antisymmetric form, thus they can be uniquely written into one 2-form called *Fubini-Study metric* with property

$$G = \text{Re}Q; \quad \Omega = \text{Im}Q. \quad (\text{A.3})$$

Because $|\langle \psi_1 | \psi_2 \rangle| \in [0, 1]$ we say, that the *metric is measuring the geodesic distance on the Bloch sphere*. Here if we define

$$|\langle \psi_1 | \psi_2 \rangle| = \cos^2 \frac{\theta}{2}, \quad (\text{A.4})$$

¹Complex conjugated is the first input of the 2-form.

we get $d\theta = 2ds = 2\sqrt{|g_{\mu\nu}d\lambda^\mu d\lambda^\nu|}$, see Cheng [2013].

To write the metric in a standard form, we need to realize how our space looks like. For finite $(N + 1)$ -dimensional Hilbert space, one dimension is lost in the gauge transformation, leaving us with N -dimensional \mathcal{PH} . Another dimension is lost due to normalization, which is usually done by mapping to an n -dimensional complex sphere

$$CP^N = \left\{ \mathbf{Z} = (Z_0, Z_1, \dots, Z_N) \in \mathbb{C}^{N+1}/\{0\} \right\} / \{\mathbf{Z} \sim c\mathbf{Z} \text{ for } c \in \mathbb{C}\}.$$

Natural property of such complex spaces is splitting of its tangent space to holonomic and anholonomic part²

$$\mathcal{T}_0^1 \mathcal{M} = \text{Span} \left\{ \frac{\partial}{\partial Z_i} \right\}; \quad \mathcal{T}_1^0 \mathcal{M} = \text{Span} \left\{ \frac{\partial}{\partial Z_{\bar{i}}} \right\}.$$

For suitable distance dZ , this can be used to define distance on state manifolds.

Distance on \mathbb{C}^{n+1} is usually defined using Hermitian metric³

$$ds^2 = d\bar{Z} \otimes dZ. \quad (\text{A.5})$$

A.2 Restriction to eigenstate manifolds

In quantum mechanics, one can examine a Hamiltonian $\hat{H}(\boldsymbol{\lambda})$, for some parameter $\boldsymbol{\lambda} \in \mathcal{U} \subset \mathbb{R}^n$. At every point $\boldsymbol{\lambda}$ we get projective Hilbert space $\mathcal{PH}(\boldsymbol{\lambda})$. This creates a fiber structure space, in which there are some sections with interesting physical applications. Some of these sections are *eigenstate manifolds*, defined by setting only one non-zero coefficient Z_k in eigenbasis $|\psi\rangle = \sum_{k=0}^n Z_k |k\rangle$. From normalization goes automatically $Z_k = 1$. The distance on these manifolds is, as derived in Eq. 2.27,

$$\begin{aligned} ds^2 &= 1 - \langle k + \delta k | k \rangle \langle k | k + \delta k \rangle = 1 - \langle k + \delta k | \left(\mathbb{I} - \sum_{j \neq k} |j\rangle \langle j| \right) |k + \delta k \rangle \\ &= \sum_{j \neq k} \langle k + \delta k | j \rangle \langle j | k + \delta k \rangle. \end{aligned} \quad (\text{A.6})$$

Using the Schrödinger equation $\hat{H}|k\rangle = \textcolor{teal}{E}_k|k\rangle$, distributivity of derivative and projection to some state $|j\rangle$, we get

$$\begin{aligned} \hat{H}|k\rangle &= \textcolor{teal}{E}_k|k\rangle \\ (\delta \hat{H})|k\rangle + \hat{H}|k + \delta k\rangle &= (\delta \textcolor{teal}{E}_k)|k\rangle + \textcolor{teal}{E}_k|k + \delta k\rangle \\ \langle j | (\delta \hat{H} - \delta \textcolor{teal}{E}_k) |k\rangle &= \langle j | (\textcolor{teal}{E}_k - \hat{H}) |k + \delta k\rangle = \langle j | (\textcolor{teal}{E}_k - \textcolor{blue}{E}_j) |k + \delta k\rangle. \end{aligned} \quad (\text{A.7})$$

We can set $\delta \textcolor{blue}{E}_k = 0$, leading for $j \neq k$ to

$$\frac{\langle j | \delta \hat{H} | k \rangle}{(\textcolor{teal}{E}_k - \textcolor{blue}{E}_j)^2} = \langle j | k + \delta k \rangle. \quad (\text{A.8})$$

²The line over index means complex conjugation.

³Hermitian metric is by definition sesquilinear, as one would expect in quantum mechanics later on.

Plugging to Equation A.6 and considering $\hat{H} = \hat{H}(\boldsymbol{\lambda})$, we get metric on a ground state manifold

$$ds^2 = \operatorname{Re} \sum_{j \neq k} \frac{\langle 0 | \partial_\mu \hat{H} | j \rangle \langle j | \partial_\nu \hat{H} | 0 \rangle}{(\textcolor{teal}{E}_k - \textcolor{blue}{E}_j)^2} d\boldsymbol{\lambda}^\mu d\boldsymbol{\lambda}^\nu \quad (\text{A.9})$$

Definition of the k -state manifold is then

$$g_{\mu\nu}^{(k)} = \operatorname{Re} \sum_{j \neq k} \frac{\langle k | \frac{\partial \hat{H}(\boldsymbol{\lambda})}{\partial \lambda^\mu} | j \rangle \langle j | \frac{\partial \hat{H}(\boldsymbol{\lambda})}{\partial \lambda^\nu} | k \rangle}{(E_k - E_j)^2}. \quad (\text{A.10})$$

The Fubini-Study metric on the eigenstate manifold is sometimes called *Geometric tensor*.

B. Eigenvalues for Lipkin-Meshkov Glick model

Eigenvalues for $N = 3$ case of Lipkin-Meshkov Glick model are

$$E_0 = \frac{1}{12} \left(G - F - \frac{\sqrt{D - E}}{2} \right) \quad (\text{B.1})$$

$$E_1 = \frac{1}{12} \left(G - F + \frac{\sqrt{D - E}}{2} \right) \quad (\text{B.2})$$

$$E_2 = \frac{1}{12} \left(G + F - \frac{\sqrt{D + E}}{2} \right) \quad (\text{B.3})$$

$$E_3 = \frac{1}{12} \left(G + F + \frac{\sqrt{D + E}}{2} \right), \quad (\text{B.4})$$

for

$$\begin{aligned} A = & 16\sqrt[3]{2} \left(64\lambda^6 - 192\lambda^5\chi^2 + 24\lambda^4 (52\chi^4 - 93\chi^2 + 36) \right. \\ & - 8\lambda^3 (29\chi^4 + 414\chi^2 - 513)\chi^2 \\ & + 6\lambda^2 (1225\chi^8 - 10053\chi^6 + 17595\chi^4 - 10557\chi^2 + 1377) \\ & + \left((64\lambda^6 + 864\lambda^4 + 8262\lambda^2 + 3(818\lambda - 27285)\chi^{10} \right. \\ & + 6(\lambda(1225\lambda - 3198) + 27108)\chi^8 \\ & - (2\lambda(\lambda(116\lambda + 30159) - 89073) + 326727)\chi^6 \\ & + 6(\lambda(\lambda(8\lambda(26\lambda - 69) + 17595) - 42660) + 51516)\chi^4 \\ & - 3(2\lambda(\lambda(4\lambda(\lambda(8\lambda + 93) - 171) + 10557) - 16119) + 36207)\chi^2 \quad (\text{B.5}) \\ & \left. + 24013\chi^{12} + 25515 \right)^2 \\ & - \left(16\lambda^4 + 144\lambda^2 + 2(74\lambda - 1185)\chi^6 + 3(4\lambda(16\lambda - 77) + 1329)\chi^4 \right. \\ & \left. - 2(2\lambda(\lambda(8\lambda + 93) - 207) + 1161)\chi^2 + 889\chi^8 + 1053 \right)^{1/2} \\ & + 6\lambda(409\chi^8 - 3198\chi^6 + 29691\chi^4 - 42660\chi^2 + 16119)\chi^2 + 24013\chi^{12} \\ & - 81855\chi^{10} + 162648\chi^8 - 326727\chi^6 + 309096\chi^4 \\ & \left. - 108621\chi^2 + 25515 \right)^{1/3} \end{aligned}$$

$$\begin{aligned} B = & \frac{256\sqrt[3]{2}}{3A} \left(16\lambda^4 + 144\lambda^2 + 2(74\lambda - 1185)\chi^6 + 3(4\lambda(16\lambda - 77) \right. \\ & \left. + 1329)\chi^4 - 2(2\lambda(\lambda(8\lambda + 93) - 207) + 1161)\chi^2 + 889\chi^8 + 1053 \right) \quad (\text{B.6}) \end{aligned}$$

$$C = 4\sqrt{\frac{A}{3\sqrt[3]{2}} + B + \frac{16}{3}(4\lambda^2 - (4\lambda + 33)\chi^2 + 49\chi^4 + 45)} \quad (\text{B.7})$$

$$D = -\frac{A}{3\sqrt[3]{2}} - B - \frac{8}{3} \left(59\lambda^2 + 436\lambda\chi^2 + 392\chi^4 + 132\chi^2 - 180 \right) \\ + 8 \left(5\lambda + 14\chi^2 \right)^2 \quad (B.8)$$

$$E = \frac{9216}{C} \left((\lambda - 1)\chi^4 - 4(\lambda - 1)\chi^2 + \lambda - 2\chi^6 \right) \\ F = \frac{1}{2} \sqrt{\frac{A}{3\sqrt[3]{2}} + B + \frac{16}{3} (4\lambda^2 - (4\lambda + 33)\chi^2 + 49\chi^4 + 45)} \quad (B.9) \\ G = -5\lambda - 14\chi^2$$

C. Attachments

C.1 Computing the metric tensor

Mathematica code for metric tensor and geodesics??

C.2 Computing the Geodesics

C.3 Computing the driving fidelity